Phase diagram of QCD in a magnetic field

Jens O. Andersen and William R. Naylor

Department of Physics, Norwegian University of Science and Technology, Høgskoleringen 5, N-7491 Trondheim, Norway

Anders Tranberg

Faculty of Science and Technology, University of Stavanger, N-4036 Stavanger, Norway

(published 8 April 2016)

Recent advances in our understanding of the phase structure and the phase transitions of hadronic matter in strong magnetic fields B and zero quark chemical potentials μ_f are reviewed in detail. Many aspects of QCD are described using low-energy effective theories and models such as the bag model, the hadron resonance gas model, chiral perturbation theory (χPT), the Nambu–Jona-Lasinio (NJL) model, the quark-meson (QM) model, and Polyakov-loop extended versions of the NJL and QM models. Their properties and applications are critically examined. This includes mean-field calculations as well as approaches beyond the mean-field approximation such as the functional renormalization group. Renormalization issues are discussed and the influence of the vacuum fluctuations on the chiral phase transition is pointed out. At $T = 0$, model calculations and lattice simulations predict magnetic catalysis: The quark condensate increases as a function of the magnetic field. This is covered in detail. Recent lattice results for the thermodynamics of non-Abelian gauge theories with emphasis on $\mathrm{SU}(2)_c$ and $\mathrm{SU}(3)_c$ are also discussed. In particular, inverse magnetic catalysis around the transition temperature T_c as a competition between contributions from valence quarks and sea quarks resulting in a decrease of T_c as a function of B is focused on. Finally, recent efforts to modify models in order to reproduce the behavior observed on the lattice are discussed.

DOI: 10.1103/RevModPhys.88.025001

CONTENTS

I. INTRODUCTION

The phase structure of QCD is usually displayed in a phase diagram spanned by the temperature T and the baryon chemical potential μ_B. The first phase diagram was conjectured already in the 1970s suggesting a confined low-temperature phase of hadrons and a deconfined high-temperature phase of quarks and gluons. Since the appearance of this phase diagram, large efforts have been made to map it out in detail. It turns out that the phase diagram of QCD is surprisingly rich, for example, there may be several color superconducting phases at low temperature depending on the baryon chemical potential μ_B (Alford, Berges, and Rajagopal, 2000; Hsu and Schwetz, 2000; Rajagopal and Wilczek, 2001; Alford, Schmitt, and Rajagopal, 2008; Fukushima and Hatsuda, 2011). Furthermore, the phase diagram can be generalized in a variety of ways. For example, instead of using a baryon chemical potential μ_B, i.e., the same chemical potential for each quark flavor, one can introduce an independent chemical potential μ_f for each flavor. Equivalently (for two quark flavors), one can use a chemical potential $\mu = \mu_u + \mu_d$ and an isospin chemical potential $\mu_I = \mu_u - \mu_d$. A nonzero isospin chemical potential allows for new phases with pion condensation once it exceeds the pion mass $\mu_I \geq m_\pi$

(Son and Stephanov, 2001). One can also add one new axis for each quark mass m_f. It turns out that the nature of the chiral transition depends on the number of flavors and on their masses (Pisarski and Wilczek, 1984; Stephanov, 2006), and this information has been conveniently displayed in the so-called Columbia plot. Finally, there are external parameters, such as an external magnetic field B, that can be varied and are of phenomenological interest.

There are at least three areas of high-energy physics where strong magnetic fields play an important role:

(1) noncentral heavy-ion collisions,
(2) compact stars, and
(3) the early Universe.

In noncentral heavy-ion collisions, very strong and time-dependent magnetic fields are created. The basic mechanism is simple. In the center-of-mass frame, the two nuclei represent electric currents in opposite directions and, according to Maxwell's equations, they produce a magnetic field B. The magnetic field depends on the energy of the ions, the impact parameter b, and position as well as time. Detailed calculations of these magnetic fields depend on a number of assumptions. For example, it is common to ignore the contribution to the magnetic field from the particles produced in the collision as the expansion of these is almost spherical. It is then sufficient to take into account only the colliding particles. (Kharzeev, McLerran, and Warringa, 2008). The strengths of these short-lived fields have been estimated to be up to the order of $B \sim 10^{19}$ G or $|qB| \sim 6m_\pi^2$, where q is the electric charge of the pion ($1\ \mathrm{T} = 10^4$ G and $1\ \mathrm{T} = 694.44\ \mathrm{eV}^2$).

Detailed calculations have been carried out by Kharzeev, McLerran, and Warringa (2008), Skokov, Illarionov, and Toneev (2009), and Bzdak and Skokov (2012). The result of such a calculation is displayed in Fig. 1, where the curves show the magnetic field as a function of proper time τ for three different impact parameters.

There is a certain class of neutron stars, called magnetars, that is characterized by very high magnetic fields and relatively low rotation frequencies as compared to a typical neutron star (Duncan and Thompson, 1992). The strengths of the magnetic fields on the surface of such stars are believed to be on the order of 10^{14}–10^{15} G. The magnetic field strength depends on the density and is highest in the core of the star. In the interior one expects magnetic fields on the order of 10^{16}–10^{19} G. This implies that in order to calculate the mass-radius relation for magnetars, detailed knowledge of the equation of state of strongly interacting matter in a large range of magnetic field strengths is required. If the density in the core of the star is sufficiently large to allow for quark matter, one must match the equation of state for hadronic matter to that of deconfined quark matter. The latter may again be color superconducting and perhaps even inhomogeneous depending on the values of the relevant parameters (Ferrer, de la Incera, and Manuel, 2005, 2006; Ferrer and de la Incera, 2007; Noronha and Shovkovy, 2007, 2012; Fukushima and Warringa, 2008).

The situation is further complicated by the fact that a star is (globally) electrically neutral as well as the fact that the magnetic field breaks spherical symmetry. The magnetic field

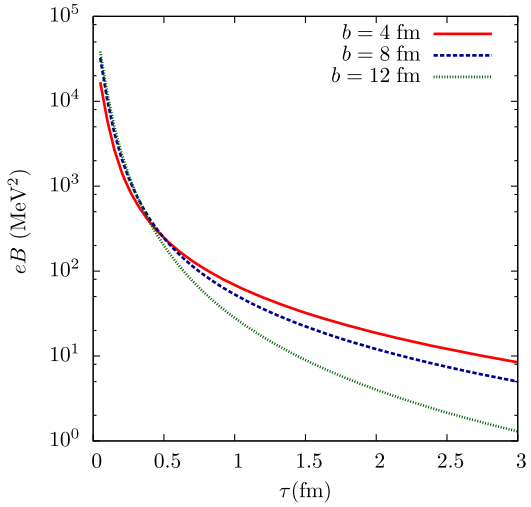

FIG. 1. Magnetic field as a function of proper time τ for three different values of the impact parameter b. From Kharzeev, McLerran, and Warringa, 2008.

then gives rise to an anisotropic pressure $\mathcal{P}$ whose components $\mathcal{P}_{ij}$ can be expressed in terms of the components of the energy-momentum tensor $\mathcal{T}_{ij}$ that enter on the right-hand side of Einstein's field equations (Strickland, Dexheimer, and Menenez, 2012).

In the absence of a magnetic field, the minimal standard model has a first-order transition for low Higgs masses m_H (Kajantie *et al.*, 1997). With increasing m_H the first-order transition becomes weaker (Kajantie *et al.*, 1996) and the first-order line eventually ends at a second-order point for a critical value $m_H^c \approx 72$ GeV (Rummukainen *et al.*, 1998). The universality class of the critical end point is that of the three-dimensional Ising model. For larger Higgs masses, there is only a crossover. In the presence of a (hyper)magnetic field, the transition becomes somewhat stronger (Giovannini and Shaposhnikov, 1998). Allowing for a primordial hypermagnetic field of arbitrary magnitude, it is possible that even at the physical Higgs mass, the electroweak phase transition may be first order. If the magnetic fields are generated from bubble collisions during the electroweak transition, they will typically be of the order of $B/T^2 \lesssim 0.5$ (Baym, Bödeker, and McLerran, 1996), in which case nonperturbative numerical simulations suggest that the transition is still not first order at the physical Higgs mass (Kajantie *et al.*, 1999). Moreover, such magnetic fields could have other implications relevant for baryogenesis, for instance, through its effect on sphaleron processes (De Simone *et al.*, 2011). In the minimal supersymmetric standard model, the transition is stronger than in the standard model, and even moderate magnetic fields may allow for a first-order transition at the physical Higgs mass.

There is now a large body of literature on QCD in a magnetic background and we think that a review on the subject is timely. In order to restrict the topics covered, we focus on the phase structure in the B-T plane and the chiral and deconfinement phase transitions at zero chemical potentials $\mu_f = 0$. After the submission of our paper, two related reviews appeared (Kharzeev, 2015; Miransky and Shovkovy, 2015). The first is focusing on heavy-ion collisions and the

chiral magnetic effect, while the second has a much broader scope, ranging from QCD to graphene. The three reviews are complementary and together they cover many aspects of matter in magnetic fields.

For the convenience of the reader, we summarize the most important conclusions:

- (•) Magnetic catalysis at $T = 0$: Model calculations and lattice simulations predict that the quark condensate is an increasing function of the magnetic field B. This is magnetic catalysis.
- (•) Vacuum fluctuations: The critical temperature and the order of the phase depend on how the vacuum fluctuations are treated.
- (•) Critical temperature: Naive calculations using chiral models predict that the critical temperature for the chiral transition is an increasing function of the magnetic field B. The deconfinement and chiral transitions split.
- (•) Critical temperature: Lattice calculations for three-color QCD with realistic quark masses predict that the critical temperature is a decreasing function of the magnetic field B. This is inverse magnetic catalysis. The critical temperatures for the deconfinement and chiral transition are the same.

It is the aim of this review to critically discuss the basis for these conclusions and provide enough details for the reader to appreciate the progress that has been made in recent years.

Finally, a word of caution. Writing a review is a challenge in terms of notation. We have tried to consistently use the same notation for a given quantity, but once in a while we have changed the notation so as not to be in conflict with the notation for other quantities. Hopefully, it is clear from the context which is which. The review is organized as follows. In Sec. II, we briefly discuss the solutions to the Dirac equation in a constant magnetic field and explain that there is no sign problem in lattice QCD in a finite magnetic field. In Sec. III, we calculate the one-loop free energy densities for fermions and bosons in a constant magnetic field using dimensional regularization and ζ-function regularization. In Sec. IV, we discuss Schwinger's classic results for the vacuum energy of bosons and fermions in a constant magnetic background B. In Sec. V, we discuss various low-energy models and theories that are being used to study the behavior of hadronic systems at finite T and B. These include the Massachusetts Institute of Technology (MIT) bag model, chiral perturbation theory (χPT), the Nambu–Jona-Lasinio (NJL) model, the quark-meson (QM) model, and the hadron resonance gas model. The Polyakov-loop extended versions of the NJL and QM models (PNJL and PQM models) are discussed in Sec. VI. In Sec. VII, we review the functional renormalization group and its application to hadronic matter at finite B. In Sec. VIII, we discuss magnetic catalysis at zero temperature and compare models with Dyson-Schwinger (DS) and lattice calculations. In Sec. IX, lattice results for $\mathrm{SU}(3)_c$ and $\mathrm{SU}(2)_c$ at finite temperature are reviewed, focusing on the mechanisms behind (inverse) magnetic catalysis. In Sec. X, we analyze recent efforts to incorporate inverse magnetic catalysis in model calculations. Finally, in Sec. XI, we conclude and briefly discuss directions for future studies. The appendixes provide our conventions and notation, a list of sum integrals needed in the calculations, series expansions of some special functions, and some explicit calculations.

II. ENERGY SPECTRA FOR CHARGED PARTICLES IN A CONSTANT MAGNETIC FIELD AND THEIR PROPAGATORS

In this section, we briefly discuss the spectra of fermions and bosons in a constant magnetic background B. We first consider fermions. The Dirac equation for a single fermion of mass m_f in a background electromagnetic gauge field A_μ^{EM} is given by

$$(i\not{D} - m_f)\psi = 0, \tag{1}$$

where $\not{D} = \gamma^\mu D_\mu$, γ^μ are the γ matrices in Minkowski space, $D_\mu = \partial_\mu + iq_f A_\mu^{\mathrm{EM}}$ is the covariant derivative, and q_f is the electric charge. In the case where the zeroth component of the gauge field vanishes, $A_0^{\mathrm{EM}} = 0$, the stationary solutions can be written as

$$\psi = e^{-iEt}\begin{pmatrix}\phi\\ \chi\end{pmatrix}, \tag{2}$$

where ϕ and χ are two-component spinors. Inserting Eq. (2) into Eq. (1) and using the Dirac representation of the γ matrices, we obtain the coupled equations

$$(E - m_f)\phi = -i(\boldsymbol{\sigma}\cdot\boldsymbol{D})\chi, \tag{3}$$

$$(E + m_f)\chi = -i(\boldsymbol{\sigma}\cdot\boldsymbol{D})\phi. \tag{4}$$

Eliminating χ from Eqs. (3) and (4), we find an equation for ϕ:

$$(E^2 - m_f^2)\phi = -(\boldsymbol{\sigma}\cdot\boldsymbol{D})^2\phi. \tag{5}$$

Specializing to a constant magnetic field, we choose the Landau gauge $A_\mu^{\mathrm{EM}} = (0, 0, -Bx, 0)$.[1] Using $(\boldsymbol{\sigma}\cdot\mathbf{A})(\boldsymbol{\sigma}\cdot\mathbf{B}) = \mathbf{A}\cdot\mathbf{B} + i\boldsymbol{\sigma}\cdot(\mathbf{A}\times\mathbf{B})$, Eq. (5) becomes

$$\left[E^2 - m_f^2 + \frac{\partial^2}{\partial x^2} + \left(\frac{\partial}{\partial y} - iq_f Bx\right)^2 + \frac{\partial^2}{\partial z^2} + \sigma_z q_f B\right]\phi = 0. \tag{6}$$

The solution is now written as $\phi = e^{-is_\perp(q_fB)p_y y + ip_z z}f(x)$, where $s_\perp(q_fB) = \mathrm{sign}(q_fB)$. The equation for $f(x)$ then becomes

$$\left[-\frac{d^2}{dx^2} + (s_\perp p_y + q_f Bx)^2 - \sigma_z q_f B\right]f(x) = [E^2 - m_f^2 - p_z^2]f(x). \tag{7}$$

This is a 2×2 matrix equation. However, the two equations decouple and the solutions can then be written as

[1] Another common choice is the symmetric gauge $A_\mu^{\mathrm{EM}} = \frac{1}{2}(0, By, -Bx, 0)$.

$$f(x)=\begin{pmatrix} f_+(x) \\ 0 \end{pmatrix} \quad \text{and} \quad f(x)=\begin{pmatrix} 0 \\ f_-(x) \end{pmatrix}, \tag{8}$$

where the subscripts $\pm$ indicate that the solutions are eigenvectors of σ_z with eigenvalues ± 1, respectively. The equation for $f_\pm(x)$ finally becomes

$$\left[-\frac{d^2}{dx^2}+(s_\perp p_y+q_f B x)^2\right] f_\pm(x) = [E^2-m_f^2-p_z^2 \pm q_f B] f_\pm(x). \tag{9}$$

This is the equation for a harmonic oscillator with known solutions involving the Hermite polynomials $H_k(x)$. The solutions are

$$\phi = c e^{-(1/2)(x/l+p_y l)^2} H_k\left(\frac{x}{l}+p_y l\right) \times e^{-i s_\perp p_y y + i p_z z}, \tag{10}$$

where c is a normalization constant and $l=1/\sqrt{|q_f B|}$. The spectrum is

$$E_k^2 = m_f^2+p_z^2+|q_f B|(2k+1-s), \tag{11}$$

where $k=0,1,2,\ldots$, and $s=\pm 1$. The state with the lowest energy has $k=0$ and $s=1$ and is nondegenerate. All other states have a twofold degeneracy. Moreover, the energy is independent of p_y and the energy levels are therefore degenerate in this variable. The degeneracy is associated with the position of the center of the Landau levels. Assume that we use a quantization volume $V=L^3$, where L is the length of the side of the box. Since the characteristic size of a Landau level is $1/\sqrt{|q_f B|}$, the degeneracy N associated with the quantum number p_y is $N=(|q_f B|/2\pi)L^2$. The sum over states in the quantization volume V is then given by a sum over spin s, Landau levels k, and the z component of the momentum p_z multiplied by N:

$$\frac{1}{V}\frac{|q_f B|}{2\pi} L^2 \sum_{s=\pm 1}\sum_{k=0}^{\infty}\sum_{p_z}. \tag{12}$$

In the thermodynamic limit, the sum over p_z is replaced by an integral such that the expression in Eq. (12) is replaced by

$$\frac{|q_f B|}{2\pi}\sum_{s=\pm 1}\sum_{k=0}^{\infty}\int_{-\infty}^{\infty}\frac{dp_z}{2\pi}. \tag{13}$$

In the thermodynamic limit and for $B=0$, the sum over three-momenta $\boldsymbol{p}$ is replaced by an integral in the usual way

$$\frac{1}{V}\sum_{\boldsymbol{p}} \to \int \frac{d^3p}{(2\pi)^3}. \tag{14}$$

Once we found a complete set of eigenstates, we can calculate the fermion propagator. We then need the expression for the two-component spinor χ as well. The fermion propagator at $T=0$ for a fermion with electric charge q_f in Minkowski space is given by (Shovkovy, 2013)

$$S(x,x') = e^{i\Phi(\mathbf{x}_\perp,\mathbf{x}'_\perp)}\int\frac{d^4p}{(2\pi)^4} e^{-ip(x-x')}\tilde{S}(p^0,p^3,\mathbf{p}_\perp), \tag{15}$$

where $x=(t,\mathbf{x})=(t,x^1,x^2,x^3)$, $\mathbf{x}_\perp=(x^1,x^2)$, $p=(p^0,\mathbf{p})=(p^0,p^1,p^2,p^3)$, $\mathbf{p}_\perp=(p^1,p^2)$, and with $\Phi(\mathbf{x}_\perp,\mathbf{x}'_\perp)$ and $\tilde{S}(p)$ given by

$$\Phi(\mathbf{x}_\perp,\mathbf{x}'_\perp) = s_\perp\frac{(x^1+x'^1)(x^2-x'^2)}{2l^2}, \tag{16}$$

$$\tilde{S}(p^0,p^3,\mathbf{p}_\perp) = \int_0^\infty ds \exp\left\{is[p_\parallel^2-m_f^2]-i\frac{p_\perp^2}{|q_f B|}\tan(|q_f B|s)\right\} \times\{[\gamma^0 p^0-\boldsymbol{\gamma}\cdot\mathbf{p}+m+(p^1\gamma^2-p^2\gamma^1)\tan(q_f B s)][1-\gamma^1\gamma^2\tan(q_f B s)]\}, \tag{17}$$

where $\boldsymbol{\gamma}_\perp=(\gamma^1,\gamma^2)$ and $p_\parallel=(p^0,p^3)$. The prefactor $\Phi(\mathbf{x}_\perp,\mathbf{x}'_\perp)$ is the so-called Schwinger phase and the term $\tilde{S}(p^0,p^3,\mathbf{p}_\perp)$ is translationally invariant. The translationally invariant part can be decomposed into contributions from the different Landau levels

$$\tilde{S}(p^0,p^3,\mathbf{p}_\perp) = ie^{-p_\perp^2/|q_f B|}\sum_{k=0}^{\infty}\frac{(-1)^k D_k(p^0,p^3,\mathbf{p}_\perp)}{p_\parallel^2-m_f^2-2|q_f B|k}, \tag{18}$$

where

$$D_k(p^0,p^3,\mathbf{p}_\perp) = (\gamma^0 p^0-\gamma^3 p^3+m)\left[(1+is_\perp\gamma^1\gamma^2)L_k\left(2\frac{p_\perp^2}{|q_f B|}\right) -(1-is_\perp\gamma^1\gamma^2)L_{k-1}\left(2\frac{p_\perp^2}{|q_f B|}\right)\right]+4(\boldsymbol{\gamma}_\perp\cdot\mathbf{p}_\perp)L_{k-1}^1\left(2\frac{p_\perp^2}{|q_f B|}\right), \tag{19}$$

and $L_k^a(x)$ are the generalized Laguerre polynomials. Note that $L_{-1}^a(x)=0$.

The spectrum for bosons with mass m and charge q can be found using the same techniques. In this case, the differential operator does not involve the term $|q_f B|\sigma_z$ and so the resulting eigenvalue equation is easier to solve. The spectrum is obtained immediately by setting $s = 0$:

$$E_k^2 = m^2 + p_z^2 + |qB|(2k+1), \tag{20}$$

where $k = 0, 1, 2, \ldots$. The eigenfunctions are again given by Eq. (10). Once we have a complete set of eigenfunctions, we can derive the propagator. We derive the bosonic propagator in Appendix D and at $T = 0$; it reads

$$\Delta(x, x') = e^{i\Phi(\mathbf{x}_\perp, \mathbf{x}'_\perp)} \int \frac{d^4p}{(2\pi)^4} e^{-ip(x-y)} \Delta(p_\perp, p_\parallel), \tag{21}$$

where the translationally invariant part is

$$\Delta(p_\parallel, p_\perp) = \int_0^\infty \frac{ds}{\cos(|qB|s)} \times \exp\left\{ is[p_\parallel^2 - m^2] - ip_\perp^2 \frac{\tan(|qB|s)}{|qB|} \right\}. \tag{22}$$

We close this section with briefly commenting on the sign problem of QCD. It is straightforward to show that there is no sign problem in QCD in an external Abelian gauge field A_μ^{EM}. In order to show this, we go to Euclidean space. The partition function of QCD can be written as

$$\begin{aligned} \mathcal{Z} &= \int \mathcal{D}\bar{\psi}\mathcal{D}\psi\mathcal{D}A_\mu e^{-\int_0^\beta d\tau \int d^3x \bar{\psi}[(\not{D}+m_f)]\psi} e^{-S_g} \\ &= \int \mathcal{D}A_\mu e^{-S_g} \det(\not{D} + m_f), \end{aligned} \tag{23}$$

where $\beta = 1/T$, the covariant derivative is $D_\mu = \partial_\mu - iq_f A_\mu^{\mathrm{EM}} - iA_\mu$, $A_\mu = A_\mu^a T_a$, and T_a are the generators of SU(3). S_g is the Euclidean action for the gluons,

$$S_g = \frac{1}{2g^2} \int_0^\beta d\tau \int d^3x \mathrm{Tr}[G_{\mu\nu} G_{\mu\nu}], \tag{24}$$

where g is the non-Abelian coupling and $G_{\mu\nu}$ is the field strength tensor. $S_g > 0$ and the exponent can be regarded as a positive probability weight. We also have to check the sign of the fermion determinant. It is convenient to use the chiral representation of the γ matrices. The matrix $\not{D}$ can then be written as

$$\not{D} = \begin{pmatrix} 0 & iX \\ iX^\dagger & 0 \end{pmatrix}, \tag{25}$$

where $iX = D_0 + i\boldsymbol{\sigma} \cdot \boldsymbol{D}$. The fermion determinant then takes the form

$$\det(\not{D} + m_f) = \det[X^\dagger X + m_f^2], \tag{26}$$

which shows that it is manifestly positive. QCD in a magnetic field is therefore free of the sign problem and one can use standard lattice techniques based on importance sampling.

III. ONE-LOOP FREE ENERGY DENSITIES

In this review, we are often concerned with Euclidean Lagrangian densities of the form

$$\begin{aligned} \mathcal{L} = {} & \bar{\psi}_f \gamma_\mu D_\mu \psi_f + m_f \bar{\psi}_f \psi_f + (D_\mu \Phi_i)^\dagger (D_\mu \Phi_i) \\ & + m^2 \Phi^\dagger \Phi + \mathcal{L}_{\mathrm{int}}, \end{aligned} \tag{27}$$

where ψ_f is a fermion field of flavor f and Φ_i are complex scalar fields $(i = 1, 2, \ldots, N)$. Unless otherwise stated, we consider two flavors, $N_f = 2$ and $f = u, d$. Moreover, $D_\mu = \partial_\mu - iqA_\mu^{\mathrm{EM}}$ is the covariant derivative for bosons and $D_\mu = \partial_\mu - iq_f A_\mu^{\mathrm{EM}}$ is the covariant derivative for fermions. Here $q = \pm e$ is the electric charge for the charged scalars, and $q_u = 2/3e$ and $q_d = -1/3e$ are the electric charges for u quarks and d-quarks, respectively. m and m_f are the tree-level masses of the bosons and fermions. $\mathcal{L}_{\mathrm{int}}$ is the interacting part of the Lagrangian. It may contain bosonic and fermionic four-point interactions as well as Yukawa-type couplings between bosons and fermions.

In the functional approach to the imaginary-time formalism, the partition function $\mathcal{Z}$ is given by a path integral

$$\mathcal{Z} = \int \mathcal{D}\Phi^\dagger \mathcal{D}\Phi \mathcal{D}\bar{\psi}\mathcal{D}\psi e^{-S}, \tag{28}$$

where the Euclidean action is given by

$$S = \int_0^\beta d\tau \int d^dx \mathcal{L}, \tag{29}$$

and d is the number of spatial dimensions. In many cases, we approximate the free energy density $\mathcal{F} = -(T/V)\log\mathcal{Z}$ (where V is the spatial volume) of the system by a one-loop calculation. We therefore need to perform Gaussian integrals over bosonic or fermionic fields. These are given by the standard expressions. The one-loop free energy density $\mathcal{F}_1$ for a boson is

$$\mathcal{F}_1 = \frac{1}{2}\frac{1}{\beta V} \mathrm{Tr} \ln D_0^{-1}, \tag{30}$$

and for a fermion

$$\mathcal{F}_1 = -\frac{1}{\beta V} \mathrm{Tr} \ln D_0^{-1}, \tag{31}$$

where D_0^{-1} is the free inverse propagator. Here the trace is over spacetime, field indices, and Dirac indices in the case of fermions. These expressions are general as they apply whether or not the particle couples to an external magnetic field. Of course, the explicit expressions after evaluating the traces and making the substitutions (13) or (14) are different. For example, the one-loop free energy density for a neutral boson with mass m reads

$$\mathcal{F}_1 = \frac{1}{2}\sum\!\!\!\!\!\!\int_P \ln[P_0^2 + p^2 + m^2], \tag{32}$$

where the sum integral is defined in Eq. (B1) and involves a sum over Matsubara frequencies P_0 and an integral over three-momenta p. The explicit expression for this sum integral as well as others needed is listed in Appendix B. The one-loop free energy density for a boson with electric charge q and for a fermion with electric charge q_f as a function of B are given by the sum integrals

$$\mathcal{F}_1 = \frac{1}{2}\sum_P{\!\!\!\!\!\!\int}^{B} \ln[P_0^2 + p_z^2 + m^2 + |qB|(2k+1)], \tag{33}$$

$$\mathcal{F}_1 = -\sum_{\{P\}}{\!\!\!\!\!\!\int}^{B} \ln[P_0^2 + p_z^2 + m_f^2 + |q_fB|(2k+1-s)], \tag{34}$$

where the sum integrals are defined in Eqs. (B4) and (B5) and involve a sum over spin s, Landau levels k, and Matsubara frequencies P_0, as well as an integral over p_z. We next evaluate the sum integral (34) in some detail. We first sum over the Matsubara frequencies using Eq. (B19). This yields

$$\mathcal{F}_1 = -\frac{|q_fB|}{2\pi} \times \sum_{s=\pm1}\sum_{k=0}^{\infty}\int_{p_z}\left\{\sqrt{p_z^2+M_B^2} + 2T\ln\left[1+e^{-\beta\sqrt{p_z^2+M_B^2}}\right]\right\}, \tag{35}$$

where $M_B^2 = m_f^2 + |q_fB|(2k+1-s)$. Let us first consider the temperature-independent term. Using dimensional regularization in $d-2 = 1-2\epsilon$ dimensions to regulate the ultraviolet divergences, we obtain

$$\int_{p_z}\sqrt{p_z^2+M_B^2} = -\frac{M_B^2}{4\pi}\left(\frac{e^{\gamma_E}\Lambda^2}{M_B^2}\right)^{\epsilon}\Gamma(-1+\epsilon), \tag{36}$$

where Λ is the renormalization scale associated with the modified minimal subtraction scheme ($\overline{\text{MS}}$). The sum over Landau levels k involves the term $M_B^{2-2\epsilon}$ and is divergent for $\epsilon = 0$. We will regularize the sum using ζ-function regularization. The sum over spin s and Landau levels k can then be written as

$$\sum_{s=\pm1}\sum_{k=0}^{\infty} M_B^{2-2\epsilon} = 2(2|q_fB|)^{1-\epsilon}\sum_{k=0}^{\infty}\left[k+\frac{m_f^2}{2|q_fB|}\right]^{1-\epsilon} - m_f^{2-2\epsilon} = 2(2|q_fB|)^{1-\epsilon}\zeta(-1+\epsilon, x_f) - m_f^{2-2\epsilon}, \tag{37}$$

where we defined $x_f = m_f^2/2|q_fB|$ and the Hurwitz ζ function $\zeta(s,q)$ is defined by

$$\zeta(s,q) = \sum_{k=0}^{\infty}(q+k)^{-s}. \tag{38}$$

Inserting Eq. (37) into Eq. (35), the temperature-independent part of the free energy density $\mathcal{F}_1^{T=0}$ becomes

$$\mathcal{F}_1^{T=0} = \frac{8(q_fB)^2}{(4\pi)^2}\left(\frac{e^{\gamma_E}\Lambda^2}{2|q_fB|}\right)^{\epsilon}\Gamma(-1+\epsilon)\left[\zeta(-1+\epsilon,x_f) - \frac{1}{2}x_f^{1-\epsilon}\right]. \tag{39}$$

Expanding Eq. (39) in powers of ϵ through order ϵ^0 gives

$$\mathcal{F}_1^{T=0} = \frac{1}{(4\pi)^2}\left(\frac{\Lambda^2}{2|q_fB|}\right)^{\epsilon}\left[\left(\frac{2(q_fB)^2}{3}+m_f^4\right)\left(\frac{1}{\epsilon}+1\right) - 8(q_fB)^2\zeta^{(1,0)}(-1,x_f) - 2|q_fB|m_f^2\ln x_f + \mathcal{O}(\epsilon)\right], \tag{40}$$

where we defined

$$\zeta^{(1,0)}(-a,x) = \left.\frac{\partial\zeta(-a+\epsilon,x)}{\partial\epsilon}\right|_{\epsilon=0}. \tag{41}$$

Equation (40) has simple poles in ϵ. One of the divergences is proportional to $(q_fB)^2$ while the other is proportional to m_f^4. Later we show how one can eliminate these divergences by renormalization.

The temperature-dependent part of the free energy density $\mathcal{F}_1^T$ in Eq. (35) can be integrated by parts and this gives

$$\begin{aligned}\mathcal{F}_1^T &= -\frac{|q_fB|}{\pi}T\sum_{s=\pm1}\sum_{k=0}^{\infty}\int_{p_z}\ln\left[1+e^{-\beta\sqrt{p_z^2+M_B^2}}\right] \\ &= -\frac{8|q_fB|}{(4\pi)^2}(e^{\gamma_E}\Lambda^2)^{\epsilon}\frac{\Gamma(\frac{1}{2})}{\Gamma(\frac{3}{2}-\epsilon)}\sum_{s=\pm1}\sum_{k=0}^{\infty}\int_0^{\infty}\frac{p_z^{2-2\epsilon}dp_z}{\sqrt{p_z^2+M_B^2}}\frac{1}{e^{\beta\sqrt{p_z^2+M_B^2}}+1}. \\ &= -\frac{2}{(4\pi)^2}\left(\frac{\Lambda^2}{2|q_fB|}\right)^{\epsilon}K_0^B(\beta m_f)|q_fB|T^2,\end{aligned} \tag{42}$$

where $K_0^B(\beta m_f)$ is defined in Eq. (B18). The sum of Eqs. (40) and (42) is then Eq. (B10). The other sum integrals needed can be calculated using the same techniques. They are listed in Appendix B.

We close this section with some comments on regulators. By changing variables $p_\perp^2 = 2k|q_fB|$, summing over s, and taking the limit $B \to 0$ in Eq. (35), the first term reduces to

$$\mathcal{F}_1^{T=0} = -2\int_p \sqrt{p^2+m_f^2}, \tag{43}$$

where $p^2 = p_\perp^2 + p_z^2$. Using dimensional regularization, this becomes

$$\mathcal{F}_1^{T=0} = \frac{1}{(4\pi)^2}\left(\frac{\Lambda^2}{m_f^2}\right)^\epsilon \left[\left(\frac{1}{\epsilon}+\frac{3}{2}\right)m_f^4 + \mathcal{O}(\epsilon)\right]. \tag{44}$$

This is the same result one finds if one takes the limit $B \to 0$ in Eq. (40) and uses the large-x_f expansion of $\zeta^{(1,0)}(-1, x_f)$ given by Eq. (C5). Using a sharp three-dimensional cutoff Λ, one obtains

$$\mathcal{F}_{T=0} = \frac{1}{(4\pi)^2}\left\{-2\Lambda\sqrt{\Lambda^2+m_f^2}(2\Lambda^2+m_f^2) + 2m_f^4 \ln\left[\frac{\Lambda}{m_f}+\sqrt{1+\frac{\Lambda^2}{m_f^2}}\right]\right\}. \tag{45}$$

If the starting point is the expression for the free energy density as a four-dimensional Euclidean integral, one finds by imposing a four-dimensional cutoff Λ (Ebert and Klimenko, 1999)

$$\mathcal{F}_{T=0} = -2\int \frac{d^4p}{(2\pi)^4}\ln[p^2+m_f^2] = \frac{1}{(4\pi)^2}\left\{-\Lambda^4 \ln\left[1+\frac{m_f^2}{\Lambda^2}\right] - \Lambda^2 m_f^2 + m_f^4 \ln\left[1+\frac{\Lambda^2}{m_f^2}\right]\right\}, \tag{46}$$

where we subtracted the value of the integral at $m_f = 0$. Notice that the coefficient of the logarithmic term is independent of the regulator, while the power divergences (for $\Lambda \to \infty$) depend on the regulator. In particular, they are all set to zero in dimensional regularization while the logarithimic divergence in the cutoff scheme corresponds to a pole in ϵ in dimensional regularization.

IV. SCHWINGER'S RESULTS

In this section, we rederive Schwinger's classic results (Schwinger, 1951) for the vacuum energy of a boson and a fermion in a constant magnetic field B. In the original derivation, the results were given for an arbitrary constant electromagnetic field. Not only is the calculation useful to see the connection with the derivation in Sec. III, but the one-loop expression for the vacuum energy also takes a form such that it is straightforward to use a simple ultraviolet cutoff Λ instead of dimensional regularization and ζ-function regularization. This will be useful when we consider Nambu–Jona-Lasinio models in which the ultraviolet divergences often are regulated by a simple UV cutoff.

The starting point is the zero-temperature expression for the one-loop free energy density for a charged boson with mass m and charge q, and its antiparticle with mass m and charge $-q$. In the limit $T \to 0$, the sum over Matsubara frequencies approaches an integral over the continuous variable p_0. The free energy density reads

$$\mathcal{F}_1 = \frac{|qB|}{2\pi}\sum_{k=0}^{\infty}\int_{-\infty}^{\infty}\frac{dp_0}{2\pi}\int_{p_z}\ln[p_0^2+p_z^2+M_B^2], \tag{47}$$

where $M_B^2 = m^2 + |qB|(2k+1)$. The derivative of $\mathcal{F}_1$ with respect to m^2 is

$$\frac{\partial\mathcal{F}_1}{\partial m^2} = \frac{|qB|}{2\pi}\sum_{k=0}^{\infty}\int_{-\infty}^{\infty}\frac{dp_0}{2\pi}\int_{p_z}\frac{1}{p_0^2+p_z^2+M_B^2}. \tag{48}$$

The effective propagator in momentum space $1/(p_0^2+p_z^2+M_B^2)$ has the integral representation

$$\frac{1}{p_0^2+p_z^2+M_B^2} = \int_0^\infty e^{-s(p_0^2+p_z^2+M_B^2)}ds. \tag{49}$$

Inserting Eq. (49) into Eq. (48), we obtain

$$\frac{\partial\mathcal{F}_1}{\partial m^2} = \frac{|qB|}{2\pi}\sum_{k=0}^{\infty}\int_{-\infty}^{\infty}\frac{dp_0}{2\pi} \times \int_{p_z}\int_0^\infty e^{-s(p_0^2+p_z^2+M_B^2)}ds. \tag{50}$$

The integral over p_z is finite for $\epsilon = 0$ and after integration over p_z and p_0, Eq. (50) reduces to

$$\frac{\partial\mathcal{F}_1}{\partial m^2} = \frac{2|qB|}{(4\pi)^2}\sum_{k=0}^{\infty}\int_0^\infty \frac{e^{-sM_B^2}}{s}ds. \tag{51}$$

Likewise, the sum over Landau levels is convergent and after summation over k, Eq. (51) reduces to

$$\frac{\partial\mathcal{F}_1}{\partial m^2} = \frac{1}{(4\pi)^2}\int_0^\infty \frac{ds}{s^2}e^{-sm^2}\frac{|qB|s}{\sinh(|qB|s)}. \tag{52}$$

Finally integrating over m^2, we obtain the one-loop free energy density

$$\mathcal{F}_1 = -\frac{1}{(4\pi)^2}\int_0^\infty \frac{ds}{s^3}e^{-sm^2}\frac{|qB|s}{\sinh(|qB|s)}, \tag{53}$$

where the constant of integration has been set to zero. The result, Eq. (53), is divergent at $s = 0$. Since s has mass dimension -2, this corresponds to an ultraviolet divergence in momentum space. It is therefore convenient to organize the result by adding and subtracting divergent terms to Eq. (53), writing it as

$$\mathcal{F}_{0+1} = \frac{1}{2}B^2 + \frac{(qB)^2}{6(4\pi)^2}\int_0^\infty\frac{ds}{s}e^{-sm^2} - \frac{1}{(4\pi)^2}\int_0^\infty\frac{ds}{s^3}e^{-sm^2} - \frac{1}{(4\pi)^2}\int_0^\infty\frac{ds}{s^3}e^{-sm^2}\left[\frac{|qB|s}{\sinh(|qB|s)} - 1 + \frac{(qBs)^2}{6}\right], \tag{54}$$

where we added the tree-level term $\frac{1}{2}B^2$. The first and second integrals are divergent at $s = 0$, while the third integral is finite. The divergent integrals are regulated by introducing an ultraviolet cutoff Λ via $s = 1/\Lambda^2$ and evaluating Eq. (54), we obtain

$$\mathcal{F}_{0+1} = \frac{1}{2}B^2\left[1+\frac{q^2}{3(4\pi)^2}\left(\ln\frac{\Lambda^2}{m^2}-\gamma_E\right)\right] - \frac{1}{2(4\pi)^2}\left[\Lambda^4 - 2\Lambda^2 m^2 + m^4\left(\ln\frac{\Lambda^2}{m^2}-\gamma_E+\frac{3}{2}\right)\right] + \frac{4(qB)^2}{(4\pi)^2}\left[\zeta^{(1,0)}\left(-1,\frac{1}{2}+x\right)+\frac{1}{4}x^2-\frac{1}{2}x^2\ln x+\frac{1}{24}\ln x+\frac{1}{24}\right], \tag{55}$$

where $x = m^2/2|qB|$. In most applications, one omits the Λ^4 term as it is independent of m and B.

For fermions with mass m_f and electric charge q_f, one obtains in a similar manner the result

$$\begin{aligned}\mathcal{F}_{0+1} &= \frac{1}{2}B^2 + \frac{2(q_fB)^2}{3(4\pi)^2}\int_0^\infty\frac{ds}{s}e^{-sm_f^2} + \frac{2}{(4\pi)^2}\int_0^\infty\frac{ds}{s^3}e^{-sm_f^2} + \frac{2}{(4\pi)^2}\int_0^\infty\frac{ds}{s^3}e^{-sm_f^2}\left[|q_fB|s\coth(|q_fB|s)-1-\frac{1}{3}(q_fBs)^2\right]\\ &= \frac{1}{2}B^2\left[1+\frac{4q_f^2}{3(4\pi)^2}\left(\ln\frac{\Lambda^2}{m_f^2}-\gamma_E\right)\right] + \frac{1}{(4\pi)^2}\left[\Lambda^4-2\Lambda^2m_f^2+m_f^4\left(\ln\frac{\Lambda^2}{m_f^2}-\gamma_E+\frac{3}{2}\right)\right]\\ &\quad -\frac{8(q_fB)^2}{(4\pi)^2}\left[\zeta^{(1,0)}(-1,x_f)+\frac{1}{4}x_f^2-\frac{1}{2}x_f^2\ln x_f+\frac{1}{2}x_f\ln x_f-\frac{1}{12}\ln x_f-\frac{1}{12}\right].\end{aligned} \tag{56}$$

We end this section by noting that there is an alternative way of regularizing the divergent integrals over s. Instead of performing these integrals in one dimension, we use dimensional regularization. For example, the second integral in Eq. (54) is replaced by

$$\begin{aligned}\frac{(e^{\gamma_E}\Lambda^2)^\epsilon}{(4\pi)^2}\int_0^\infty\frac{ds}{s^{3-\epsilon}}e^{-sm^2} &= \frac{m^4}{(4\pi)^2}\left(\frac{e^{\gamma_E}\Lambda^2}{m^2}\right)^\epsilon\Gamma(-2+\epsilon)\\ &= \frac{m^4}{2(4\pi)^2}\left[\frac{1}{\epsilon}+\frac{3}{2}+\ln\left(\frac{\Lambda^2}{m^2}\right)+\mathcal{O}(\epsilon)\right].\end{aligned} \tag{57}$$

With the extra factor of $e^{\gamma_E\epsilon}$, the result (57) is identical to that obtained in the $\overline{\text{MS}}$ scheme; cf. Eq. (B7).

V. EFFECTIVE THEORIES AND MODELS

A. MIT bag model

The MIT bag model was introduced in the 1970s as a simple phenomenological model for the confinement of quarks inside hadrons (Chodos *et al.*, 1974). The quarks are confined to a spherical cavity by requiring that the quark vector current vanishes on the boundary. The quarks inside the bag are considered noninteracting which is justified by appealing to the asymptotic freedom of QCD. The idea is that the vacuum energy density of the perturbative vacuum inside the bag is larger than that of the nonperturbative vacuum outside the bag. This difference is denoted by $\mathcal{B}$, the bag constant. Equivalently, the vacuum pressure inside the bag is smaller than that outside the bag and the radius R of a hadron is (heuristically) given by the balance between this difference and the pressure generated by the quarks inside the bag. The bag constant $\mathcal{B}$ can be estimated as follows (Johnson, 1975). The pressure generated by the quarks inside a spherical cavity is, by the uncertainty relation, on the order of $1/R$. Balancing this contribution and that from the bag, which is on the order of R^3, one finds a relation between the mass and the radius of a hadron. Minimizing the total mass with respect to R gives $R\sim\mathcal{B}^{-1/4}$ and using the mass of a proton gives a bag constant on the order of $(100\text{ MeV})^4$. In the actual bag-model calculations discussed later, only the bag constant $\mathcal{B}$ is needed, while all the complications due to the boundary conditions do not enter.

Chakrabarty (1996) was the first to discuss the MIT bag model in a magnetic field in the context of compact stars and the stability of strange quark matter. More recently, the deconfinement transition was investigated using the bag model (Fraga and Palhares, 2012).

One can investigate the phase structure of QCD by calculating the pressure in the hadronic phase as well as in the deconfined phase as a function of temperature, particle masses, and magnetic field B. The phase with the larger pressure wins and the transition takes place when the pressure in the two phases is equal. Note there is no order parameter for the deconfinement transition in the bag model. This is different from the chiral models we discuss later, such as the Polyakov-loop extended Nambu–Jona-Lasinio model and the Polyakov-loop extended quark-meson model. In these models, we analyze the behavior of the Polyakov-loop variable which is an order parameter for confinement in pure-glue QCD and an approximate order parameter in QCD with dynamical quarks (Yaffe and Svetitsky, 1982a, 1982b).

The free energy density of the hadronic phase is approximated by that of an ideal gas of massive pions and reads

$$\mathcal{F}_{\text{HHG}} = \frac{1}{2}B^2 + \frac{1}{2}\sum\!\!\!\!\!\!\int_P^B \ln[P^2+m_\pi^2] + \sum\!\!\!\!\!\!\int_P^B \ln[P_0^2+p_z^2+M_B^2], \tag{58}$$

where the subscript HHG means hot hadron gas. The first term is the tree-level contribution from the constant magnetic field and the second term is from the neutral pions that do not couple to the magnetic field. The third term is the contribution from the charged pions. This expression is the same as obtained from a one-loop approximation to the free energy density in chiral perturbation theory. We discuss χPT later.

Using the expressions for the bosonic sum integrals given by Eqs. (B7) and (B8), Eq. (58) can be written as

$$\mathcal{F}_{\rm HHG}=\frac{1}{2}B^2+\frac{1}{2(4\pi)^2}\left(\frac{\Lambda^2}{|2qB|}\right)^{\epsilon}\left[\left(\frac{(qB)^2}{3}-m_\pi^4\right)\left(\frac{1}{\epsilon}+1\right)+8(qB)^2\zeta^{(1,0)}\left(-1,\frac{1}{2}+x\right)-2J_0^B(\beta m_\pi)|qB|T^2\right]-\frac{1}{4(4\pi)^2}\left(\frac{\Lambda^2}{m_\pi^2}\right)^{\epsilon}\left[m_\pi^4\left(\frac{1}{\epsilon}+\frac{3}{2}\right)+2J_0(\beta m_\pi)T^4\right], \quad (59)$$

where the thermal integrals $J_n(\beta m)$ and $J_n^B(\beta m)$ are defined in Appendix B. The first divergence is proportional to $(qB)^2$ which is removed by wave-function renormalization of the term $(1/2)B^2$ in Eq. (59). This is done by making the replacement $B^2 \to Z^2B^2$, where Z is the wave-function renormalization term. The second divergence, which is proportional to m_π^4, can be removed by adding an appropriately chosen vacuum counterterm $\Delta\mathcal{E}$ to the free energy density. The counterterms are given by

$$Z^2=1-\frac{q^2}{3(4\pi)^2\epsilon}, \qquad \Delta\mathcal{E}=\frac{3m_\pi^4}{4(4\pi)^2\epsilon}. \quad (60)$$

After renormalization, the free energy density of the hot hadronic gas is

$$\mathcal{F}_{\rm HHG}=\frac{1}{2}B^2\left[1+\frac{q^2}{3(4\pi)^2}\ln\frac{\Lambda^2}{2|qB|}\right]-\frac{3m_\pi^4}{4(4\pi)^2}\left[\ln\frac{\Lambda^2}{m_\pi^2}+\frac{3}{2}\right]+\frac{4(qB)^2}{(4\pi)^2}\left[\zeta^{(1,0)}\left(-1,\frac{1}{2}+x\right)+\frac{1}{4}x^2-\frac{1}{2}x^2\ln x+\frac{1}{24}\right]-\frac{1}{2(4\pi)^2}[J_0(\beta m_\pi)T^4+2J_0^B(\beta m_\pi)|qB|T^2]. \quad (61)$$

Note that here, and in the following, the thermal integrals $J_n(\beta m)$, $J_n^B(\beta m)$, $K_n(\beta m)$, and $K_n^B(\beta m)$ are always evaluated at $\epsilon=0$ whenever they appear in renormalized expressions for the free energy density and other physical quantities.

The free energy density in the quark-gluon plasma (QGP) phase is

$$\mathcal{F}_{\rm QGP}=\frac{1}{2}B^2+(N_c^2-1)\sum\!\!\!\!\!\!\int_P \ln(P^2)-N_c\sum_f\sum\!\!\!\!\!\!\int_{\{P\}}^{B}\ln[P_0^2+p_z^2+M_B^2]+\mathcal{B}, \quad (62)$$

where the first term is from the constant magnetic field, the second term is from the gluons, the third term is from the quarks, and the last term $\mathcal{B}$ is the bag constant. This term represents the difference in the vacuum energy between the two phases. Using the expressions for the bosonic and fermionic sum integrals Eqs. (B7) and (B10), we find

$$\mathcal{F}_{\rm QGP}=-(N_c^2-1)\frac{\pi^2T^4}{45}+\frac{1}{2}B^2+\frac{N_c}{(4\pi)^2}\left(\frac{\Lambda^2}{|2q_fB|}\right)^{\epsilon}\times\sum_f\left[\left(\frac{2(q_fB)^2}{3}+m_f^4\right)\left(\frac{1}{\epsilon}+1\right)-8(q_fB)^2\zeta^{(1,0)}(-1,x_f)-2|q_fB|m_f^2\ln x_f-2K_0^B(\beta m_f)|q_fB|T^2\right]+\mathcal{B}. \quad (63)$$

Again, the ultraviolet divergences are removed by wave-function renormalization and by adding a vacuum counterterm. This amounts to the substitutions $B^2 \to Z^2B^2$ and $\mathcal{B} \to \mathcal{B}+\Delta\mathcal{B}$, where

$$Z^2=1-N_c\sum_f\frac{4q_f^2}{3(4\pi)^2\epsilon}, \qquad \Delta\mathcal{B}=-N_c\sum_f\frac{m_f^4}{(4\pi)^2\epsilon}. \quad (64)$$

The renormalized free energy density in the quark-gluon plasma phase then reduces to

$$\mathcal{F}_{\rm QGP}=-(N_c^2-1)\frac{\pi^2T^4}{45}+\frac{1}{2}B^2\left(1+N_c\sum_f\frac{4q_f^2}{3(4\pi)^2}\ln\frac{\Lambda^2}{|2q_fB|}\right)+\frac{N_c}{(4\pi)^2}\sum_f m_f^4\left[\ln\frac{\Lambda^2}{m_f^2}+\frac{3}{2}\right]-\frac{8N_c}{(4\pi)^2}\sum_f(q_fB)^2\left[\zeta^{(1,0)}(-1,x_f)+\frac{1}{4}x_f^2-\frac{1}{2}x_f^2\ln x_f+\frac{1}{2}x_f\ln x_f-\frac{1}{12}\right]-\frac{2N_c}{(4\pi)^2}\sum_f K_0^B(\beta m_f)|q_fB|T^2+\mathcal{B}. \quad (65)$$

Fraga and Palhares (2012) took a slightly different approach to the renormalization of the MIT bag model than the one presented so far. The divergent terms $(qB)^2/\epsilon$ and $(q_fB)^2/\epsilon$ in the two phases remain after the subtraction of the vacuum energy at $T=B=0$. These divergences can be removed as done previously, but leave us with some finite terms. They argued that the finite terms proportional to $(qB)^2$ and $(q_fB)^2$ must be subtracted in an *ad hoc* fashion since the charges that generate the magnetic field are not included in the description. They therefore subtract all mass-independent terms that are proportional to $(qB)^2$ or $(q_fB)^2$, which leads to free energy densities in the two phases

$$\mathcal{F}_{\rm HHG}=\frac{4(qB)^2}{(4\pi)^2}\left[\zeta^{(1,0)}\left(-1,\frac{1}{2}+x\right)-\zeta^{(1,0)}\left(-1,\frac{1}{2}\right)+\frac{1}{4}x^2-\frac{1}{2}x^2\ln x\right]-\frac{1}{2(4\pi)^2}[J_0(\beta m_\pi)T^4+2J_0^B(\beta m_\pi)|qB|T^2], \quad (66)$$

$$\mathcal{F}_{\rm QGP}=-(N_c^2-1)\frac{\pi^2T^4}{45}-\frac{8N_c}{(4\pi)^2}\sum_f(q_fB)^2\left[\zeta^{(1,0)}(-1,x_f)-\zeta^{(1,0)}(-1,0)+\frac{1}{4}x_f^2-\frac{1}{2}x_f^2\ln x_f+\frac{1}{2}x_f\ln x_f\right]-\frac{2N_c}{(4\pi)^2}\sum_f K_0^B(\beta m_f)|q_fB|T^2+\mathcal{B}. \quad (67)$$

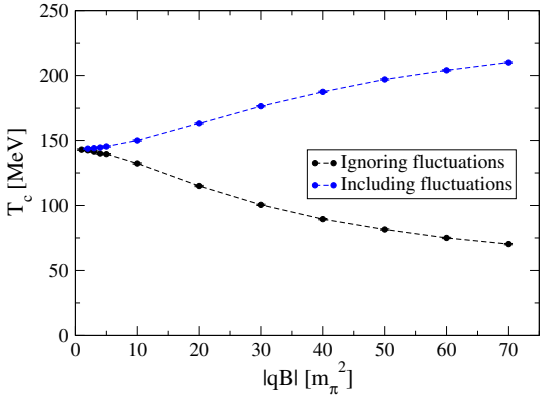

FIG. 2. Critical temperature as a function of $|qB|/m_\pi^2$ in the MIT bag model. See the main text for details.

In Fig. 2 we show the critical temperature T_c for the phase transition as a function of $|qB|/m_\pi^2$ for $N_c = 3$ and $N_f = 2$. We used $m_\pi = 140$ MeV, $m_u = m_d = 5$ MeV, as well as $\Lambda = 600$ MeV, and $\mathcal{B} = (200\ \text{MeV})^4$. The black (bottom) curve is with the $B = 0$ vacuum fluctuations and the blue (top) curve is where the $B = 0$ vacuum fluctuations have been subtracted. Clearly the figure demonstrates the importance of how one treats the vacuum fluctuations in the model. In both cases, we have an effective B-dependent bag constant, which can be easily found by absorbing all the $T = 0$ terms into $\mathcal{B}$. The value we used for the renormalization scale is that of a typical UV cutoff in the NJL model. Since there are logarithms of ratios of several scales, not all logarithms can be made small at the same time. Moreover, it is not obvious that one should choose the same scale in the two phases. Our point is to demonstrate how sensitive the results are to the inclusion of the vacuum fluctuations.

We close this section by mentioning two related calculations (Agasian and Fedorov, 2008; Orlovsky and Simonov, 2014). Instead of a bag constant, the pressure contains another constant term arising from the gluonic condensate. The energy density term in the hadrodnic phase is of the form

$$\mathcal{E}_{\text{vac}} = -\frac{b}{8(4\pi)^2}\langle G^2\rangle, \tag{68}$$

where $b = (11N_c - 2N_f)/3$ and $G^2 = (g_s G^a_{\mu\nu})^2$. At temperatures around the transition temperature, the condensate is approximately half the value at $T = 0$. Lattice calculations at zero magnetic field give the value $\langle G^2\rangle = (0.87\ \text{GeV})^4$ and a critical temperature of 177 MeV. Agasian and Fedorov (2008) showed that the critical temperature as well as the latent heat decreases as functions of the magnetic field B. The deconfinement transition is first order as defined by a nonzero latent heat between the two phases for magnetic fields smaller than $\sqrt{|qB|} \sim 600$ MeV. The transition is a crossover for magnetic fields larger than this value.

As pointed out by Orlovsky and Simonov (2014), the masses of the pions are strongly dependent on the magnetic field and should be taken into account. Similarly, the vacuum energy density (68) also depends on B (Ozaki, 2014). This calls for a more systematic study at finite magnetic field.

B. Chiral perturbation theory

Chiral perturbation theory is an effective low-energy theory for QCD in the hadronic phase (Weinberg, 1979; Gasser and Leutwyler, 1984, 1985). It is a model-independent framework in the sense that it depends only on the symmetries of QCD, the symmetry breaking pattern of QCD in the vacuum, and the relevant degrees of freedom. At sufficiently low energy or temperature, only the pseudo-Goldstone bosons are relevant degrees of freedom, although other degrees of freedom can be systematically added. In massless QCD with N_f flavors, the chiral Lagrangian has a global $\text{SU}(N_f)_L \times \text{SU}(N_f)_R$ symmetry describing $N_f^2 - 1$ massless excitations. If the quarks have equal masses, this symmetry is explicitly broken to $\text{SU}(N_f)_V$. Explicit symmetry breaking in the chiral Lagrangian can be systematically included by adding terms to the Lagrangian that respect the $\text{SU}(N_f)_V$ symmetry.

In QCD, when one couples the quarks to an electromagnetic field, the flavor symmetry is broken. One can no longer freely transform a u quark into a d quark or an s quark. For massless QCD with $N_f = 2$, the $\text{SU}(2)_L \times \text{SU}(2)_R$ symmetry is broken down to $\text{U}(1)_V \times \text{U}(1)_A$ by electromagnetic interactions. The $\text{U}(1)_V$ symmetry corresponds to the invariance under a rotation of a u quark by an angle α, $u \to e^{i\alpha}u$, and a rotation of a d quark by the opposite angle $d \to e^{-i\alpha}d$. The $\text{U}(1)_A$ symmetry corresponds to the invariance under chiral rotations $u \to e^{i\gamma_5\alpha}u$ and $d \to e^{-i\gamma_5\alpha}d$.

Chiral perturbation theory is not an expansion in some small coupling constant, but is an expansion in powers of momentum p, where a derivative in the Lagrangian counts as one power and a quark mass counts as two powers. χPT is a nonrenormalizable quantum field theory, implying that a calculation at a given order n in momentum p requires that one adds higher-order operators in order to cancel the divergences arising in this calculation. One needs more and more couplings as one goes to higher loop orders and therefore more measurements to determine them. However, this poses no problem; as long as one is content with finite precision, a nonrenormalizable field theory has predictive power and is as good as any other field theory. This is the essence of effective field theory.

In this section, we restrict ourselves to two-flavor QCD. χPT is then an effective theory for the three pions and the effective Lagrangian can be written as a power series

$$\mathcal{L}_{\text{eff}} = \mathcal{L}^{(2)} + \mathcal{L}^{(4)} + \cdots, \tag{69}$$

where the superscript indicates the order in momentum. In Euclidean space, the leading term is given by

$$\mathcal{L}^{(2)} = \tfrac{1}{4}F^2\text{Tr}[(D_\mu U)^\dagger(D_\mu U) - M^2(U + U^\dagger)], \tag{70}$$

where M and F are the tree-level values of the pion mass and pion decay constant, respectively. Moreover $U = e^{i\tau_i\pi_i/F}$ is a unitary SU(2) matrix, τ_i are the Pauli matrices, π_i are the pion fields, and D_μ is the covariant derivative defined by

$$D_\mu U = \partial_\mu U + i[Q, U]A^{\text{EM}}_\mu, \tag{71}$$

where Q is the charge matrix of the quarks, $Q = \mathrm{diag}(2/3, -1/3)e$. As explained earlier, a constant magnetic field B explicitly breaks the global chiral symmetry that transforms u and d quarks into each other, but leaves a residual $\mathrm{U}(1)_A$ symmetry. Because of this reduced symmetry, there is only one true Goldstone boson, namely, the neutral pion $\pi^0 \equiv \pi_3$. If the magnetic field is sufficiently strong, the charged pions are very heavy and expected to decouple from the low-energy dynamics. In this regime, the low-energy field theory involves a single massless particle. The spacetime symmetry is $\mathrm{SO}(1,1) \times \mathrm{SO}(2)$, which are Lorentz boosts in the x_0x_3 plane as well as rotations in the x_1x_2 plane perpendicular to B. We therefore need to separately consider the derivative operators $\partial_\perp = (\partial_1, \partial_2)$ and $\partial_\parallel = (\partial_0, \partial_3)$ and build our invariants from these. The effective Lagrangian for π^0 then reads

$$\mathcal{L}_{\mathrm{eff}} = \tfrac{1}{4}[F_\perp^{(1)}]^2(\partial_\perp U_\perp)^\dagger(\partial_\perp U_\perp) + \tfrac{1}{4}[F_\parallel^{(1)}]^2(\partial_\parallel U_\parallel)^\dagger(\partial_\parallel U_\parallel) + \cdots, \tag{72}$$

where $U_\perp = e^{i\pi^0/F_\perp}$ and $U_\parallel = e^{i\pi^0/F_\parallel}$. Note that we must allow for two different decay constants $F_\perp^{(1)}$ and $F_\parallel^{(1)}$ (Fayazbakhsh and Sadooghi, 2013; Kamikado and Kanazawa, 2014). The Lagrangian (72) is a special case (albeit with different notation) of the general case with N_u up-quark flavors and N_d down-quark flavors considered by Miransky and Shovkovy (2002). In this case the symmetry is $\mathrm{SU}(N_u)_L \times \mathrm{SU}(N_u)_R \times \mathrm{SU}(N_d)_L \times \mathrm{SU}(N_d)_R \times \mathrm{U}(1)_A$ which is broken down to the diagonal subgroup $\mathrm{SU}(N_u)_V \times \mathrm{SU}(N_d)_V$. This gives rise to $N_u^2 + N_d^2 - 1$ massless Goldstone particles. We now return to the Lagrangian $\mathcal{L}^{(2)}$ given in Eq. (70). It can be expanded in powers of the pion fields. Through fourth order, we obtain

$$\begin{aligned}\mathcal{L}^{(2)} = {} & -F^2M^2 + \frac{1}{2}(\partial_\mu\pi^0)^2 + \frac{1}{2}M^2(\pi^0)^2 \\ & + (\partial_\mu + iqA_\mu^{\mathrm{EM}})\pi^+(\partial_\mu - iqA_\mu^{\mathrm{EM}})\pi^- + M^2\pi^+\pi^- \\ & - \frac{M^2}{24F^2}[(\pi^0)^2 + 2\pi^+\pi^-]^2 + \frac{1}{6F^2}\{2\pi^0[\partial_\mu\pi^0][\partial_\mu(\pi^+\pi^-)] \\ & - 2\pi^+\pi^-(\partial_\mu\pi^0)^2 - 2[(\pi^0)^2 + 2\pi^+\pi^-](\partial_\mu\pi^+)(\partial_\mu\pi^-) \\ & + [\partial_\mu(\pi^+\pi^-)]^2\},\end{aligned} \tag{73}$$

where we defined the complex pion fields as

$$\pi_\pm = \frac{1}{\sqrt{2}}(\pi_1 \pm i\pi_2).$$

In the same manner, we can expand the Lagrangian $\mathcal{L}^{(4)}$ to second order in the pion fields

$$\begin{aligned}\mathcal{L}^{(4)} = {} & \frac{1}{4}F_{\mu\nu}^2 + \frac{2l_5}{F^2}(qF_{\mu\nu})^2\pi^+\pi^- + \frac{2il_6}{F^2}qF_{\mu\nu}[(\partial_\mu\pi^-)(\partial_\nu\pi^+) \\ & + iqA_\mu^{\mathrm{EM}}\partial_\nu(\pi^+\pi^-)] + (l_3 + l_4)\frac{M^4}{F^2}(\pi^0)^2 \\ & + 2(l_3 + l_4)\frac{M^4}{F^2}\pi^+\pi^- + l_4\frac{M^2}{F^2}(\partial_\mu\pi^0)^2 + 2l_4\frac{M^2}{F^2}(\partial_\mu \\ & + iqA_\mu^{\mathrm{EM}})\pi^+(\partial_\mu - iqA_\mu^{\mathrm{EM}})\pi^-.\end{aligned} \tag{74}$$

The Lagrangian $\mathcal{L}^{(6)}$ contains more than 50 terms for two flavors. However, in a two-loop calculation of the pressure at finite B only one term contributes, namely, $M^2(qF_{\mu\nu})^2$ (Agasian and Shushpanov, 2000; Werbos, 2008).

As mentioned previously, the parameters M and F in the Lagrangian can be interpreted as the tree-level values of the pion mass m_π and pion decay constant F_π, respectively. However, these quantities receive loop corrections and they can no longer be identified with the bare parameters of the Lagrangian $\mathcal{L}$. The loop integrals are ultraviolet divergent and the divergences are canceled by the renormalization of the low-energy constants l_i $(i = 1, 2, 3, \ldots)$ that appear in the Lagrangian. The relation between the bare low-energy constants l_i and their renormalized counterparts $\bar{l}_i$ is

$$l_i = -\frac{\gamma_i}{2(4\pi)^2}\left[\frac{1}{\epsilon} + \bar{l}_i\right], \tag{75}$$

evaluated at the scale $\Lambda = M$. The coefficients γ_i have been tabulated by Gasser and Leutwyler (1984). In the actual calculations, presented later, we need $\gamma_3 = 1/2$ and $\gamma_4 = 2$. Note that our Eq. (75) does not involve the renormalization scale Λ as in Gasser and Leutwyler (1984) since it is a part of the definition of the sum integrals. Moreover, our Eq. (73) for the truncated Lagrangian $\mathcal{L}^{(2)}$ differs from the expression found in Agasian and Shushpanov (2000) and Werbos (2008) since they use a different parametrization for the unitary matrix U, namely, the Weinberg parametrization. However, we obtain the same expressions for physical quantities independent of parametrization (Bochkarev and Kapusta, 1996). This simply reflects the fact that physical quantities are independent of the coordinate system used.

To leading order in chiral perturbation theory and second order in the pion fields, the Lagrangian describes free bosons in a magnetic field. Thus a one-loop calculation of the free energy density is the same as the one we did in the hadronic phase for the MIT bag model and the renormalized result is given by Eq. (61), except that one must add the tree-level term $-F^2M^2$ from Eq. (73), i.e., $\mathcal{F}_1^{\chi\mathrm{PT}} = -F^2M^2 + \mathcal{F}_{\mathrm{HHG}}$. The vacuum energy to one-loop order at finite B was first calculated by Schwinger (1951) and generalized to two loops by Agasian and Shushpanov (2000). The two-loop result for the free energy density at finite temperature first appeared in Andersen (2012a, 2012b).

1. Quark condensate, pion mass, and pion decay constant

The zero-temperature quark condensate at one loop in the chiral limit was first derived by Shushpanov and Smilga (1997) and later generalized to finite quark mass, i.e., finite m_π by Cohen, McGady, and Werbos (2007). They also generalized their result to constant electromagnetic fields. The two-loop result for the chiral condensate in the chiral limit was calculated by Agasian and Shushpanov (2000) and generalized to finite pion mass by Werbos (2008). Agasian and Shushpanov also calculated the finite-temperature quark condensate at one loop (Agasian and Shushpanov, 2001), which was extended to two loops by Andersen (2012a, 2012b).

Let us write the free energy density through n loops as $\mathcal{F}_n = \mathcal{F}_n^{\text{vac}} + \mathcal{F}_n^T + \mathcal{F}_n^B$, where $\mathcal{F}_n^{\text{vac}}$ is the contribution in the vacuum, i.e., for $B = T = 0$, $\mathcal{F}_n^B$ is the zero-temperature contribution due to a finite magnetic field, and $\mathcal{F}_n^T$ is the finite-temperature contribution. The chiral condensate is given by (Gerber and Leutwyler, 1989)

$$\langle \bar{q}q \rangle_B = \langle \bar{q}q \rangle_0 \left[1 - \frac{c}{F^2} \frac{\partial (\mathcal{F}_n^B + \mathcal{F}_n^T)}{\partial m_\pi^2} \right], \tag{76}$$

where $\langle \bar{q}q \rangle_0$ denotes the quark condensate at $T = B = 0$, and

$$c = -F^2 \frac{\partial m_\pi^2}{\partial m} \langle \bar{q}q \rangle_0^{-1}.$$

Using $\mathcal{F}_1^B + \mathcal{F}_1^T = \mathcal{F}_{\text{HHG}} - \mathcal{F}_{\text{HHG}}(T = B = 0)$ and the fact that $c = 1$ to leading order (Gerber and Leutwyler, 1989), one obtains the one-loop result for the quark condensate

$$\langle \bar{q}q \rangle_B = \langle \bar{q}q \rangle_0 \left[1 + \frac{1}{(4\pi)^2 F^2} \left(I_B(M) - \frac{1}{2} J_1(\beta M) T^2 - J_1^B(\beta M) |qB| \right) \right], \tag{77}$$

where the function $I_B(M)$ is defined by

$$I_B(M) = M^2 \ln \frac{M^2}{2|qB|} - M^2 - 2|qB| \zeta^{(1,0)} \left(0, \frac{1}{2} + x \right). \tag{78}$$

Here $x = M^2/2|qB|$. Taking the limit $M \to 0$ and using the first term of the small-x expansion [Eq. (C4)], one finds that the condensate at $T = 0$ grows linearly with the field in the chiral limit (Shushpanov and Smilga, 1997),

$$\langle \bar{q}q \rangle_B = \langle \bar{q}q \rangle_0 \left[1 + \frac{|qB| \ln 2}{(4\pi)^2 F^2} \right]. \tag{79}$$

Expanding Eq. (77) around $B = 0$ at $T = 0$ and using Eq. (C8) yields to second order in B (Werbos, 2008):

$$\langle \bar{q}q \rangle_B = \langle \bar{q}q \rangle_0 \left[1 + \frac{1}{6(4\pi)^2} \frac{(qB)^2}{F^2 M^2} \right]. \tag{80}$$

The interesting observation here, first made by Endrődi (2013), is that the prefactor is proportional to the one-loop β function of scalar QED, $\beta = 1/3(4\pi)^2$.

In Fig. 3, we show the one- and two-loop results for the normalized quark condensate $\langle \bar{q}q \rangle_B / \langle \bar{q}q \rangle_0$ in the chiral limit as a function of T for $|qB| = 5m_\pi^2$ and for $B = 0$ for comparison. The vacuum contribution has been included and amounts to an increase of the chiral condensate of about 5% in this case. The effects are large due to the very strong magnetic field, and for weaker fields, the difference between the two sets of curves is smaller. The curves suggest that the critical temperature for the chiral transition is increasing as a function of B, but since χPT breaks down at perhaps

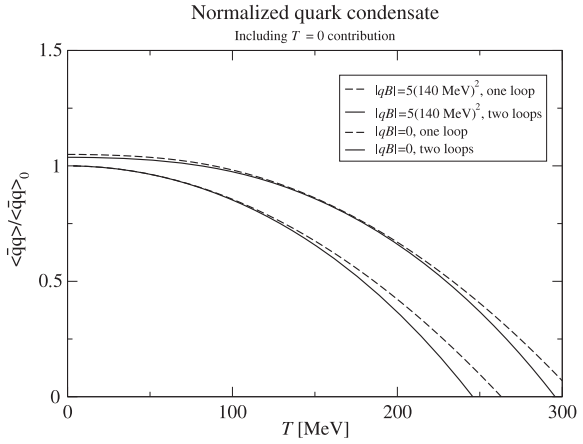

FIG. 3. Normalized quark condensate at one and two loops in the chiral limit as a function of T for $B = 0$ and $|qB| = 5m_\pi^2$. From Andersen, 2012a.

$T \sim 150$ MeV, one should be careful making quantitative statements. For temperatures where χPT can be trusted the curves suggest that perturbation theory in a magnetic field converges at least as well as for $B = 0$.

We next consider the correction to the neutral pion mass m_{π^0} due to a magnetic field. The Feynman diagrams contributing to the one-loop self-energy $\Pi(P_0, \mathbf{p})$ are shown in Fig. 4.

The inverse propagator can be written as

$$\Gamma^{(2)}(P_0, \mathbf{p}) = P^2 + M^2 + \Pi(P_0, \mathbf{p}), \tag{81}$$

where the the one-loop self-energy is given by

$$\begin{aligned} &\Pi(P_0, \mathbf{p}) \\ &= -\frac{2}{3F^2} P^2 \sum_K^B \frac{1}{K_0^2 + k_z^2 + M_B^2} \\ &\quad + \frac{1}{6F^2} M^2 \left[2 \sum_K^B \frac{1}{K_0^2 + k_z^2 + M_B^2} - 3 \sum_P \frac{1}{K^2 + M^2} \right] \\ &\quad + 2l_4 P^2 \frac{M^2}{F^2} + 2(l_3 + l_4) \frac{M^4}{F^2}, \end{aligned} \tag{82}$$

where the terms in the second line are counterterms coming from $\mathcal{L}^{(4)}$. Collecting all terms proportional to P^2, we redefine the field π^0 such that the coefficient of P^2 in Eq. (81) equals unity (Loewe and Villavicencio, 2003). This yields

$$\Gamma^{(2)}(P_0, \mathbf{p}) = P^2 + m_{\pi^0}^2, \tag{83}$$

where the physical pion mass squared $m_{\pi^0}^2$ is

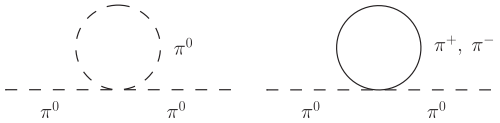

FIG. 4. One-loop graphs contributing to the self-energy of the neutral pion.

$$m_{\pi^0}^2 = M^2 + \frac{M^2}{F^2}\sum_P^B \frac{1}{P_0^2 + p_z^2 + M_B^2} - \frac{1}{2}\frac{M^2}{F^2}\sum_P \frac{1}{P^2 + M^2} + 2l_3\frac{M^4}{F^2} = M^2\left[1 - \frac{1}{(4\pi)^2F^2}\left(I_B(M) + \frac{1}{2}J_1(\beta M)T^2 - J_1^B(\beta M)|qB|\right)\right]. \quad (84)$$

This result was first obtained at zero temperature by Shushpanov and Smilga (1997) and later generalized to finite temperature by Agasian and Shushpanov (2000). We note that m_{π^0} vanishes in the chiral limit $M \to 0$, as it must since the neutral pion is a Goldstone boson. This massless excitation is associated with the breakdown of the $U(1)_A$ symmetry mentioned previously.

We next consider the pion decay constant for the neutral pion F_{π^0}. The components of the axial current $\mathcal{A}_\mu^0$ are given by

$$\mathcal{A}_\mu^0 = -F\partial_\mu\pi^0 + \frac{2}{3F}[2\pi^+\pi^-\partial_\mu\pi^0 - \pi^0\partial_\mu(\pi^+\pi^-)] - 2M^2l_4\partial_\mu\pi^0. \quad (85)$$

In order to calculate the pion decay constant, we need to evaluate the matrix element $F_{\pi^0} = \langle 0|\mathcal{A}_\mu^0|\pi^0\rangle$. In a consistent one-loop calculation, one needs to take into account wave-function renormalization of the tree-level term $-F\partial_\mu\pi^0$.[2] Calculating the matrix element, one finds

$$F_{\pi^0} = F\left[1 - \frac{1}{F^2}\sum_P^B \frac{1}{P_0^2 + p_z^2 + M_B^2} + \frac{M^2}{F^2}l_4\right]. \quad (86)$$

After renormalization, we find

$$F_{\pi^0} = F\left[1 + \frac{1}{(4\pi)^2F^2}[I_B(M) - J_1^B(\beta M)|qB|]\right]. \quad (87)$$

Using Eqs. (84) and (87), we see that

$$m_{\pi^0}^2F_{\pi^0}^2 = 2m\langle\bar{q}q\rangle_B, \quad (88)$$

which is the Oakes–Gell-Mann–Renner relation in a magnetic field. This relation was first shown by Agasian and Shushpanov (2001).

C. Nambu–Jona-Lasinio model

The NJL model was originally proposed as a theory for interacting nucleons and pions in the 1960s before the discovery of quarks (Nambu and Jona-Lasinio, 1961a, 1961b). After the discovery of quarks and the formulation of QCD as the theory of the strong interactions, the fermion fields in the Lagrangian were reinterpreted as quark fields and the NJL model as an effective low-energy model for QCD. We make a few remarks on the NJL model later, but for a detailed discussion of its properties, see Klevansky (1992) and Buballa (2005). In the NJL model, one-gluon exchange between the quarks is replaced by local four-point quark interactions. Thus there are no gauge fields in the model and the local $SU(N_c)$ gauge symmetry of QCD is replaced by a global $SU(N_c)$ symmetry. As a result, two of the most prominent features of QCD, asymptotic freedom and confinement, are lost. The latter can be seen by the fact that the polarization function for pions $\Pi_M(p^2)$ develops an imaginary part for $p^2 > 4M^2$, where M is the constituent quark mass and the pions become unstable against decay into a quark-antiquark pair (Buballa, 2005).

Another important aspect of QCD, namely, that of chiral symmetry breaking in the vacuum, is taken into account by the NJL model. The spontaneous breaking of chiral symmetry guarantees via the Goldstone theorem the appearance of massless, or light if chiral symmetry is explicitly broken, bosonic excitations in the spectrum. For $N_f = 2$, these particles are the (light) pions and the explanation of the low pion mass was a success of the NJL model. We note that in Lorentz invariant theories the number of Goldstone bosons equals the number of broken generators. When Lorentz invariance is broken, for example, at finite density, the number of massless excitations may be strictly smaller than the number of broken generators (Nielsen and Chadha, 1976; Brauner, 2010) and some of them have a quadratic dispersion relation $E \sim p^2$ instead of a linear one.

However, chiral symmetry breaking is not seen at any finite order in perturbation theory and one needs to sum an infinite number of a certain class of diagrams to obtain a nonzero chiral condensate. This is done by introducing a set of collective bosonic or auxiliary fields such that the Lagrangian becomes bilinear in the quark fields. One can then exactly integrate out the fermions in the path integral and afterward expand the resulting functional determinant in powers of the collective fields and their derivatives. This expansion is an expansion in $1/N_c$. To leading order in $1/N_c$, i.e., in the large-N_c limit, this gives rise to a gap equation for the chiral condensate. This is also referred to as the mean-field approximation, since the collective fields are replaced by their expectation values. At next-to-leading order, this expansion generates kinetic terms for the bosonic fields and so they become propagating quantum fields. At next-to-next-to-leading order, the expansion generates interaction terms among the bosons (Eguchi, 1976; Klevansky, 1992; Boomsma and Boer, 2009).

The NJL model is nonrenormalizable in the sense that loop diagrams generate divergences that cannot be canceled by local counterterms of the same type as those appearing in the original Lagrangian. One therefore needs to add new operators to cancel these divergences. The operators that are induced this way are suppressed by some power of some (large) mass scale Λ. This mass scale signals new physics that is not captured by the model, but as long as we stay well below this scale, this is not a problem. At finite precision, only a finite number of operators contribute to a given physical quantity. One way of dealing with the ultraviolet divergences in the momentum integrals is by cutting them off using a sharp three-dimensional cutoff Λ or a smooth ultraviolet cutoff. In the case of a sharp cutoff, the momentum scale Λ can be interpreted as an upper scale below which the model or theory is valid.

[2]This wave-function renormalization counterterm is the same we used to obtain Eq. (84).

A smooth cutoff is often referred to as a form factor and denoted by $F(p)$, where $p = |\mathbf{p}|$. A form factor that mimics asymptotic freedom is

$$F(p) = \frac{\Lambda^2}{\Lambda^2 + p^2}, \tag{89}$$

where Λ is a mass scale. The function $F(p)$ guarantees that loop integrals converge for large momentum p. A three-dimensional cutoff breaks Lorentz invariance in contrast to, e.g., dimensional regularization. There are other form factors that are tailored to the problem of a magnetic background and we briefly discuss them later.

The Minkowski space Lagrangian of the NJL model with $N_f = 2$ can be written as

$$\mathcal{L} = \mathcal{L}_0 + \mathcal{L}_{\bar{q}q} + \mathcal{L}_{\rm det}, \tag{90}$$

where the various terms are

$$\mathcal{L}_0 = \bar{\psi}[i\not{D} - m_0]\psi, \tag{91}$$

$$\mathcal{L}_{\bar{q}q} = G_1[(\bar{\psi}\psi)^2 + (\bar{\psi}\boldsymbol{\tau}\psi)^2 + (\bar{\psi}i\gamma_5\psi)^2 + (\bar{\psi}i\gamma_5\boldsymbol{\tau}\psi)^2], \tag{92}$$

$$\mathcal{L}_{\rm det} = G_2[(\bar{\psi}\psi)^2 - (\bar{\psi}\boldsymbol{\tau}\psi)^2 - (\bar{\psi}i\gamma_5\psi)^2 + (\bar{\psi}i\gamma_5\boldsymbol{\tau}\psi)^2], \tag{93}$$

where $\boldsymbol{\tau}$ are the Pauli spin matrices, and $\not{D} = \gamma^\mu D_\mu$. $D_\mu = \partial_\mu + iQA_\mu$ is the covariant derivative, where $Q = \mathrm{diag}(2/3, -1/3)e$ is the charge matrix. G_1 and G_2 are coupling constants and m_0 is the mass matrix, $m_0 = \mathrm{diag}(m_u, m_d)$. As is normally done in the literature, we use $m_u = m_d$. For $N_f = 2$, ψ is an isospin doublet,

$$\psi = \begin{pmatrix} u \\ d \end{pmatrix}. \tag{94}$$

The terms $\mathcal{L}_0 + \mathcal{L}_{\bar{q}q}$ are invariant under the global symmetries $\mathrm{SU}(N_c)\times\mathrm{SU}(2)_L\times\mathrm{SU}(2)_R\times\mathrm{U}(1)_B\times\mathrm{U}(1)_A$ in the chiral limit and $\mathrm{SU}(N_c)\times\mathrm{SU}(2)_V\times\mathrm{U}(1)_B$ at the physical point.[3] These are the symmetries of QCD, except that the color symmetry is global and not local. The term $\mathcal{L}_{\rm det}$ breaks the $\mathrm{U}(1)_A$ symmetry while preserving the others. This is the 't Hooft instanton-induced interaction term and mimics the breaking of the axial $\mathrm{U}(1)_A$ symmetry in the QCD vacuum ('t Hooft, 1976). In three-color QCD, this is a six-quark interaction which is necessary to explain the relatively large mass of the η' particle.

We next consider the two nonzero quark condensates $\langle\bar{u}u\rangle$ and $\langle\bar{d}d\rangle$. These can be expressed in terms of $\langle\bar{\psi}\psi\rangle$ and $\langle\bar{\psi}\tau_3\psi\rangle$ as $\frac{1}{2}(\langle\bar{\psi}\psi\rangle \pm \langle\bar{\psi}\tau_3\psi\rangle)$ and a nonzero $\langle\bar{\psi}\tau_3\psi\rangle$ implies that $\langle\bar{u}u\rangle \neq \langle\bar{d}d\rangle$. We can write $(\bar{\psi}\psi)^2 = (\bar{\psi}\psi - \langle\bar{\psi}\psi\rangle)^2 + 2\langle\bar{\psi}\psi\rangle\bar{\psi}\psi - \langle\bar{\psi}\psi\rangle^2$ and $(\bar{\psi}\tau_3\psi)^2 = (\bar{\psi}\tau_3\psi - \langle\bar{\psi}\tau_3\psi\rangle)^2 + 2\langle\bar{\psi}\tau_3\psi\rangle\bar{\psi}\tau_3\psi - \langle\bar{\psi}\tau_3\psi\rangle^2$. In the mean-field approximation, we linearize the interaction terms in the presence of the two condensates $\langle\bar{\psi}\psi\rangle$ and $\langle\bar{\psi}\tau_3\psi\rangle$, i.e., we neglect the fluctuations around the mean field. Hence, we approximate the quartic terms by

$$(\bar{\psi}\psi)^2 \approx 2\langle\bar{\psi}\psi\rangle\bar{\psi}\psi - \langle\bar{\psi}\psi\rangle^2, \tag{95}$$

$$(\bar{\psi}\tau_3\psi)^2 \approx 2\langle\bar{\psi}\tau_3\psi\rangle\bar{\psi}\tau_3\psi - \langle\bar{\psi}\tau_3\psi\rangle^2. \tag{96}$$

Substituting Eqs. (95) and (96) into Eq. (90), we obtain the Lagrangian which is bilinear in the fermion fields:

$$\mathcal{L}_{\rm bilinear} = -\frac{(M_0 - m_0)^2}{4G_0} - \frac{M_3^2}{4(1-2c)G_0} + \bar{\psi}[i\not{D} - M]\psi, \tag{97}$$

where $M = M_0 + \tau_3 M_3$ and we introduced

$$M_0 = m_0 - 2G_0\langle\bar{\psi}\psi\rangle, \tag{98}$$

$$M_3 = -2(1-2c)G_0\langle\bar{\psi}\tau_3\psi\rangle, \tag{99}$$

$$G_1 = (1-c)G_0, \tag{100}$$

$$G_2 = cG_0. \tag{101}$$

The parameter c controls the instanton interaction or the amount of explicit breaking of the $\mathrm{U}(1)_A$ symmetry. The constituent quark masses for the u and d quarks can be expressed as $M_u = M_0 + M_3$ and $M_d = M_0 - M_3$. Generally these constituent quark masses are different, and only for $G_1 = G_2$ are they identical. This corresponds to $c = 1/2$. The fact that $\langle\bar{u}u\rangle$ generally is different from $\langle\bar{d}d\rangle$ should come as no surprise as the electric charge of the u quark is different from that of the d quark.

The Lagrangian (97) is bilinear in the quark fields and we can integrate over them exactly. The resulting vacuum energy density is evaluated using dimensional regularization together with ζ-function regularization in the usual way and whose M-independent (divergent and finite) terms are omitted.[4] The remaining divergences can be isolated by adding and subtracting the vacuum energy for $B = 0$. The difference between the two vacuum energies is finite, while the subtracted vacuum energy is evaluated using a hard three-dimensional cutoff Λ. This yields the free energy density (Menezes *et al.*, 2009; Boomsma and Boer, 2010)

$$\begin{aligned}\mathcal{F}_{0+1} = {} & \frac{1}{2}B^2 + \frac{(M_0 - m_0)^2}{4G_0} + \frac{M_3^2}{4(1-2c)G_0} + \frac{2N_c}{(4\pi)^2} \\ & \times \sum_f \left[M_f^4 \ln\left(\frac{\Lambda}{M_f} + \sqrt{1 + \frac{\Lambda^2}{M_f^2}}\right) \right. \\ & \left. - M_f\Lambda(M_f^2 + 2\Lambda^2)\sqrt{1 + \frac{\Lambda^2}{M_f^2}}\right] \\ & - \frac{8N_c}{(4\pi)^2}\sum_f (q_f B)^2 \left[\zeta^{(1,0)}(-1, x_f) + \frac{1}{4}x_f^2 - \frac{1}{2}x_f^2 \ln x_f \right. \\ & \left. + \frac{1}{2}x_f \ln x_f\right] - \frac{2N_c T^2}{(4\pi)^2}\sum_f K_0^B(\beta M_f)|q_f B|, \end{aligned} \tag{102}$$

[3] This is for the case $m_u = m_d$. If $m_u \neq m_d$, the symmetry $\mathrm{SU}(2)_V$ reduces to $\mathrm{U}(1)_{I_3}$.

[4] This corresponds to ignoring wave-function renormalization of the tree-level term $(1/2)B^2$ in the free energy density.

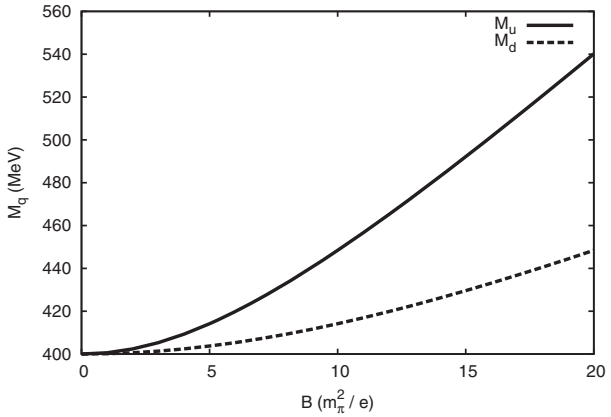

FIG. 5. Constituent quark masses M_u and M_d as functions of B measured in units of m_π^2/e for $c = 0$. From Boomsma and Boer, 2010.

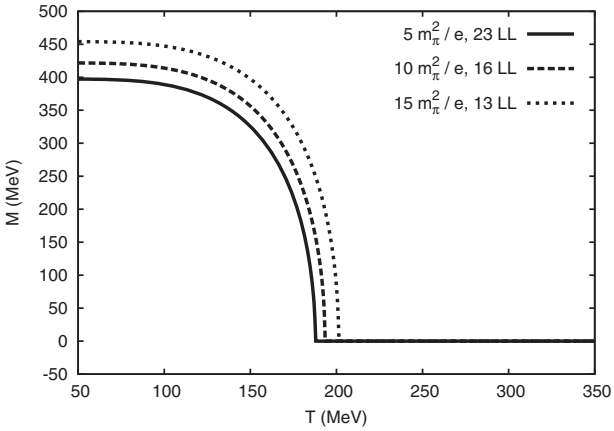

FIG. 6. Constituent quark mass M in the chiral limit as a function of T for three different values of the magnetic field and for $c = 1/2$. From Boomsma and Boer, 2010.

where $x_f = M_f^2/|2q_fB|$. A similar expression can be found in Ebert and Klimenko (1999), where a four-dimensional cutoff is used; cf. Eq. (46).

1. Quark condensates

The calculations discussed in this section were presented by Boomsma and Boer (2010). In these calculations, they used $m_0 = 6$ MeV, $\Lambda = 590$ MeV, and $G_0\Lambda^2 = 2.435$. These values lead to a pion mass of 140.2 MeV, a pion decay constant of 92.6 MeV, and a quark condensate $\langle\bar{u}u\rangle = \langle\bar{d}d\rangle = (-241.5\ \text{MeV})^3$, all in the vacuum.

The constituent quark masses M_u and M_d are obtained by solving the gap equations

$$\frac{\partial\mathcal{F}_{0+1}}{\partial M_f} = 0, \qquad f = u, d. \tag{103}$$

In Fig. 5, the constituent quark masses M_u and M_d are shown as functions of B measured in units of m_π^2/e for $c = 0$, i.e., with the $\mathrm{U}(1)_A$ symmetry intact. Notice that $M_u = M_d$ for $B = 0$, while they split for the finite magnetic field and the splitting increases as B grows. This difference is due to the different electric charges of the u and d quarks. A nonzero c will bring the masses closer together and at $c = 1/2$ they are equal.

In Fig. 6, the constituent quark mass $M_u = M_d = M$ is shown as a function of T for three different values of the magnetic field. The results are in the chiral limit and for $c = 1/2$. The number x in x LL is the number of Landau levels one must include such that the error is less than 1%. The stronger the magnetic field, the fewer Landau levels need to be included in the sum in order to obtain a certain accuracy. The reason is that the effective mass of the fermions increases with the magnetic field and that more Landau levels are effectively Boltzmann suppressed. The transition is second order with mean-field critical exponents for all values of the magnetic field (Inagaki, Kimura, and Murata, 2004; Boomsma and Boer, 2010). The order of the phase transition in various approximations is discussed further in Secs. V.D and VII.

In Fig. 7, the constituent quark mass $M_u = M_d = M$ at the physical point and for $c = 1/2$ is shown as a function of T for four different values of the magnetic field. The constituent quark mass is a strictly positive continuous function of T and hence the transition is a crossover.

2. Other condensates

So far we discussed the quark condensates $\langle\bar{u}u\rangle$ and $\langle\bar{d}d\rangle$ as functions of the magnetic field. However, due to the external magnetic field, the symmetry of the system is reduced and other nonzero condensates are possible. Ferrer *et al.* (2014) considered a one-flavor NJL model in the chiral limit in a constant external magnetic field B. A constant magnetic field breaks Lorentz invariance down to $SO(1,1) \times SO(2)$, where the latter corresponds to rotations around the axis in the direction of the magnetic field B. The standard interaction term they consider is

$$\mathcal{L}_{\text{int}}^{(1)} = \frac{G}{2}[(\bar{\psi}\psi)^2 + (\bar{\psi}i\gamma^5\psi)^2], \tag{104}$$

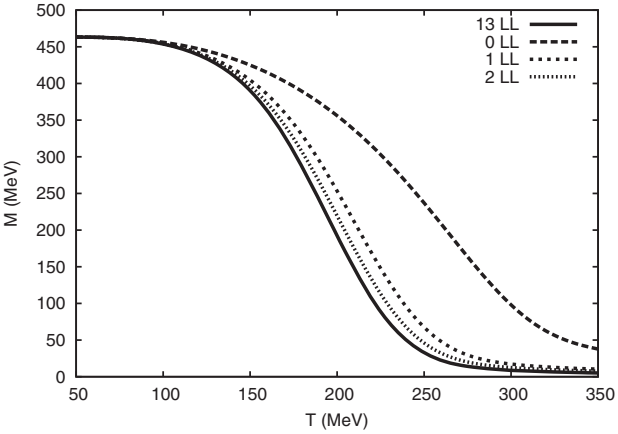

FIG. 7. Constituent quark mass M at the physical point as a function of T for four different values of the magnetic field and for $c = 1/2$. From Boomsma and Boer, 2010.

where $G = 2G_0$ is the usual coupling in the NJL model The new interaction term that respects chiral symmetry and is invariant under $SO(1,1) \times SO(2)$ is

$$\mathcal{L}_{\rm int}^{(2)} = \frac{G'}{2}[(\bar{\psi}\Sigma^3\psi)^2 + (\bar{\psi}i\gamma^5\Sigma^3\psi)^2], \tag{105}$$

where $\Sigma^3 = (i/2)[\gamma^1, \gamma^2]$ is the spin operator along the field direction and G' is a new coupling constant. The interaction terms in Eqs. (104) and (105) can be derived from one-gluon exchange in QCD using Fierz identities. The value of the coupling constant G' is unknown, but vanishes in the limit $B \to 0$. The reduced symmetry gives rise to a new nonzero condensate

$$\xi = -G'\langle\bar{\psi}i\gamma^1\gamma^2\psi\rangle, \tag{106}$$

in addition to $\sigma = -G\langle\bar{\psi}\psi\rangle$. Calculating the thermodynamic potential Ω in the mean-field approximation and using the equations of motion $\partial\Omega/\partial\sigma = 0$ and $\partial\Omega/\partial\xi = 0$, they showed that

$$\xi = \frac{G'}{G}\sigma. \tag{107}$$

Thus the spin condensate vanishes in zero magnetic field as expected and for nonzero magnetic field it is proportional to the quark condensate. Because of Eq. (107), the two condensates evaporate at the same critical temperature. The same behavior was found on the lattice (Bali *et al.*, 2012b), where ξ and σ drop to zero at around $T = 160$ MeV.

The spectrum of fermionic excitations was calculated by Ferrer *et al.* (2014) and reads

$$E_k^2 = p_z^3 + (\sigma + \xi)^2, \qquad k = 0, \tag{108}$$

$$E_k^2 = p_z^3 + \left(\sqrt{\sigma^2 + 2|q_f B|k} \pm \xi\right)^2, \qquad k \geq 1, \tag{109}$$

where $\pm$ correspond to the positive and negative spin projections, respectively. Here we notice that there is a Zeeman splitting in the spectrum for $k \geq 1$ but not so for $k = 0$. The interpretation of the term involving ξ is that it arises from an anomalous magnetic moment of the quarks and antiquarks.

The critical temperature T_c for the system changes due to the existence of the condensate ξ. If the magnetic field is sufficiently strong that all the particles are in the lowest Landau level (LLL) (at finite T this is obviously an approximation), one can calculate the critical temperature analytically. In this case, the dynamical mass of the quarks in the LLL is given by $M_\xi = \sigma + \xi$ and the critical temperature is proportional to M_ξ. A calculation by Ferrer *et al.* (2014) showed that

$$T_c = 0.58 M_\xi. \tag{110}$$

Thus the critical temperature increases linearly with M_ξ and is governed by the coupling G'.

We close this section with a brief discussion of a possible new phase in the QCD vacuum at very strong magnetic fields. In this phase, charged ρ mesons condense and as a result the vacuum behaves as a superconductor. The idea goes back to Nielsen and Olesen (1978) and Ambjørn and Olesen (1989a, 1989b) who showed that the $W^\pm$ bosons condense in a sufficiently strong magnetic field: the energy of a $W^\pm$ boson becomes purely imaginary signaling an instabilty of the electroweak vacuum and the formation of a condensate. The dispersion relation for a charged ρ meson in a magnetic field is

$$E_k^2 = m_\rho^2 + p_z^2 + |qB|(2k + 1 - 2s), \tag{111}$$

where $s = \pm 1$. For a particle in the lowest Landau level with zero longitudinal momentum p_z, the energy becomes purely imaginary when the magnetic field exceeds $B_c = m_\rho^2/q$, with $m_\rho = 775$ MeV. This suggests that the QCD vacuum is unstable against condensation of charged ρ mesons (Chernodub, 2010, 2011; Callebaut, Dudal, and Verschelde, 2013). The condensate is inhomogeneous and breaks a U(1) symmetry, however, this is not in conflict with the Vafa-Witten theorem as no massless Nambu-Goldstone bosons appear in the spectrum (Hidaka and Yamamoto, 2013; Chernodub, 2014).

D. Quark-meson model

Introducing the collective fields and integrating over the quark fields in the NJL model leads to a fermion determinant in the expression for the effective action. This functional determinant is a function of the background fields σ and $\boldsymbol{\pi}$. As explained earlier, the mean-field approximation consists of replacing the quantum fields fields σ and $\boldsymbol{\pi}$ by their expectation values and ignoring fluctuations. Expanding the fluctuation determinant around the expectation values of the fields one generates kinetic terms for the mesons as well as interaction terms. The terms that are generated are in principle all those that are consistent with the symmetries of the NJL model. These terms can be organized according to the powers of the fields and their derivatives. If one truncates the series at second order in derivatives and fourth order in the fields, we are effectively left with a quark-meson model whose coupling constants depend on the parameters of the NJL model and some one-loop fermionic integrals. We discuss this model next.

The Euclidean Lagrangian of the two-flavor quark-meson model can be written as

$$\mathcal{L} = \bar{\psi}[\gamma_\mu D_\mu + g(\sigma + i\gamma_5\boldsymbol{\tau}\cdot\boldsymbol{\pi})]\psi + \frac{1}{2}[(\partial_\mu\sigma)^2 + (\partial_\mu\boldsymbol{\pi})^2] + \frac{1}{2}m^2[\sigma^2 + \boldsymbol{\pi}^2] + \frac{\lambda}{24}[\sigma^2 + \boldsymbol{\pi}^2]^2 - h\sigma. \tag{112}$$

The Lagrangian has an $\mathrm{SU}(2)_L \times \mathrm{SU}(2)_R$ symmetry for $h = 0$, which is explicitly broken to $\mathrm{SU}(2)_V$ for nonzero h.[5] This term gives rise to nonzero pion masses after spontaneous symmetry breaking. However, once we couple the quark-meson model to an Abelian gauge field, the model is only $\mathrm{U}(1)_V \times \mathrm{U}(1)_A$ invariant for $h = 0$ and $\mathrm{U}(1)_V$ invariant for $h \neq 0$. The transformations are $\psi \to e^{i\tau_3\alpha}\psi$ and $\psi \to e^{i\gamma_5\tau_3\alpha}\psi$. Introducing the linear combinations

[5] In addition to a global $\mathrm{SU}(N_c)$ symmetry.

$$\Delta = \frac{1}{\sqrt{2}}(\pi_1 + i\pi_2) = \pi^+$$

and

$$v = \frac{1}{\sqrt{2}}(\sigma + i\gamma_5\pi_0),$$

it can be shown that the transformations are

$$\begin{aligned} &\Delta \to e^{-2i\alpha}\Delta, \qquad && v \to v && \text{(vector)},\\ &\Delta \to \Delta, && v \to e^{-2i\gamma_5\alpha}v && \text{(axial)}. \end{aligned} \tag{113}$$

This implies that we have two invariants $|v|^2 = \sigma^2 + \pi_0^2$ and $|\Delta|^2 = \pi^+\pi^-$ instead of a single invariant $\sigma^2 + \boldsymbol{\pi}^2$. We therefore have two mass parameters m_1^2 and m_2^2 instead of a single mass parameter m^2, and three coupling constants λ_1, λ_2, and λ_3 instead of a single coupling λ. Finally, the Yukawa interaction term splits into the two terms $g_1\bar{\psi}(\sigma + i\gamma_5\tau_3\pi_3)\psi$ and $g_2\bar{\psi}i\gamma_5(\tau_1\pi_1 + \tau_2\pi_2)\psi$. These couplings are in principle functions of the magnetic field B but we do not know their B dependence, only that their values are identical for $B = 0$. As is commonly done in the literature, we therefore set all the couplings and masses equal and equal to their values in the vacuum.

Denoting the expectation value of v by $(1/\sqrt{2})\phi$, the tree-level potential is

$$\mathcal{F}_0 = \frac{1}{2}B^2 + \frac{1}{2}m^2\phi^2 + \frac{\lambda}{24}\phi^4 - h\phi. \tag{114}$$

The tree-level masses of the sigma, the pions, and the quark are (before coupling to B)

$$m_\sigma^2 = m^2 + \frac{\lambda}{2}\phi^2, \tag{115}$$

$$m_\pi^2 = m^2 + \frac{\lambda}{6}\phi^2, \tag{116}$$

$$m_q = g\phi. \tag{117}$$

The pion mass satisfies $h = m_\pi^2\phi$ at the minimum of the tree-level potential and therefore vanishes for $h = 0$ in agreement with the Goldstone theorem. The one-loop potential then becomes

$$\begin{aligned} \mathcal{F}_{0+1} = {}& \frac{1}{2}B^2 + \frac{1}{2}m^2\phi^2 + \frac{\lambda}{24}\phi^4 - h\phi - \frac{1}{4(4\pi)^2}\left(\frac{\Lambda^2}{m_\sigma^2}\right)^\epsilon\left[\left(\frac{1}{\epsilon}+\frac{3}{2}\right)m_\sigma^4 + 2J_0(\beta m_\sigma)T^4\right]\\ & - \frac{1}{4(4\pi)^2}\left(\frac{\Lambda^2}{m_{\pi^0}^2}\right)^\epsilon\left[\left(\frac{1}{\epsilon}+\frac{3}{2}\right)m_{\pi^0}^4 + 2J_0(\beta m_{\pi^0})T^4\right] + \frac{1}{2(4\pi)^2}\left(\frac{\Lambda^2}{|2qB|}\right)^\epsilon\left[\left(\frac{(qB)^2}{3} - m_{\pi^0}^4\right)\left(\frac{1}{\epsilon}+1\right)\right.\\ & \left. + 8(qB)^2\zeta^{(1,0)}\left(-1,\frac{1}{2}+x\right) - 2J_0^B(\beta m_{\pi^0})|qB|T^2\right] + \frac{N_c}{(4\pi)^2}\sum_f\left(\frac{\Lambda^2}{2|q_fB|}\right)^\epsilon\left[\left(\frac{2(q_fB)^2}{3} + m_q^4\right)\left(\frac{1}{\epsilon}+1\right)\right.\\ & \left. - 8(q_fB)^2\zeta^{(1,0)}(-1,x_f) - 2|q_fB|m_q^2\ln x_f - 2K_0^B(\beta m_q)|q_fB|T^2 + \mathcal{O}(\epsilon)\right]. \end{aligned} \tag{118}$$

The B-dependent divergence is removed by making the replacement $B^2 \to Z^2B^2$, where

$$Z^2 = \left[1 - \frac{q^2}{3(4\pi)^2\epsilon} - N_c\sum_f\frac{4q_f^2}{3(4\pi)^2\epsilon}\right]. \tag{119}$$

The other divergences are removed by making the replacement $m^2 \to m^2 + \Delta m^2$, $\lambda \to \lambda + \Delta\lambda$, and adding a vacuum energy counterterm $\Delta\mathcal{E}$, where

$$\begin{aligned} &\Delta m^2 = \frac{\lambda m^2}{(4\pi)^2\epsilon}, \qquad && \Delta\lambda = \frac{2\lambda^2 - 24N_cN_fg^4}{(4\pi)^2\epsilon},\\ &\Delta\mathcal{E} = \frac{m^4}{(4\pi)^2\epsilon}. \end{aligned} \tag{120}$$

The renormalized one-loop effective potential becomes

$$\begin{aligned} \mathcal{F}_{0+1} = {}& \frac{1}{2}B^2\left[1 + \frac{q^2}{3(4\pi)^2}\ln\frac{\Lambda^2}{|2qB|} + N_c\sum_f\frac{4q_f^2}{3(4\pi)^2}\ln\frac{\Lambda^2}{|2q_fB|}\right] + \frac{1}{2}m^2\phi^2 + \frac{\lambda}{24}\phi^4 - h\phi - \frac{m_\sigma^4}{4(4\pi)^2}\left[\ln\frac{\Lambda^2}{m_\sigma^2} + \frac{3}{2}\right]\\ & - \frac{3m_{\pi^0}^4}{4(4\pi)^2}\left[\ln\frac{\Lambda^2}{m_{\pi^0}^2} + \frac{3}{2}\right] + \frac{N_cm_q^4}{(4\pi)^2}\sum_f\left[\ln\frac{\Lambda^2}{m_q^2} + \frac{3}{2}\right] + \frac{4(qB)^2}{(4\pi)^2}\left[\zeta^{(1,0)}\left(-1,\frac{1}{2}+x\right) + \frac{1}{4}x^2 - \frac{1}{2}x^2\ln x + \frac{1}{24}\right]\\ & - \frac{8N_c}{(4\pi)^2}\sum_f(q_fB)^2\left[\zeta^{(1,0)}(-1,x_f) + \frac{1}{4}x_f^2 - \frac{1}{2}x_f^2\ln x_f + \frac{1}{2}x_f\ln x_f - \frac{1}{12}\right]\\ & - \frac{1}{2(4\pi)^2}[J_0(\beta m_\sigma)T^4 + J_0(\beta m_{\pi^0})T^4 + 2J_0^B(\beta m_{\pi^0})|qB|T^2] - \frac{2N_cT^2}{(4\pi)^2}\sum_f K_0^B(\beta m_q)|q_fB|. \end{aligned} \tag{121}$$

A common approximation in the QM model is to neglect the quantum and thermal fluctuations of the mesons (Scavenius *et al.*, 2001; Fraga and Mizher, 2008). We make this approximation in the remainder of this section and discuss the inclusion of mesonic fluctuations in Sec. VII on the functional renormalization group,

$$\begin{aligned}\mathcal{F}_{0+1} &= \frac{1}{2}B^2\left[1+N_c\sum_f \frac{4q_f^2}{3(4\pi)^2}\ln\frac{\Lambda^2}{|2q_fB|}\right]+\frac{1}{2}m^2\phi^2\\ &+\frac{\lambda}{24}\phi^4-h\phi+\frac{N_cm_q^4}{(4\pi)^2}\sum_f\left[\ln\frac{\Lambda^2}{m_q^2}+\frac{3}{2}\right]\\ &-\frac{8N_c}{(4\pi)^2}\sum_f(q_fB)^2\left[\zeta^{(1,0)}(-1,x_f)+\frac{1}{4}x_f^2\right.\\ &\left.-\frac{1}{2}x_f^2\ln x_f+\frac{1}{2}x_f\ln x_f-\frac{1}{12}\right]\\ &-\frac{2N_cT^2}{(4\pi)^2}\sum_f K_0^B(\beta m_q)|q_fB|. \end{aligned} \tag{122}$$

In the literature, the parameters are often fixed at tree level. The parameters m^2, λ, and h in the Lagrangian (112) can be expressed in terms of the sigma mass, the pion mass, and the pion decay constant as[6]

$$m^2=-\tfrac{1}{2}(m_\sigma^2-3m_\pi^2), \tag{123}$$

$$\lambda=\frac{3(m_\sigma^2-m_\pi^2)}{f_\pi^2}, \tag{124}$$

$$h=f_\pi m_\pi^2. \tag{125}$$

Having determined the parameters as described earlier, the tree-level potential has its minimum at the correct value $\phi=f_\pi=93$ MeV, while the minimum of the one-loop potential depends on the renormalization scale. We can choose Λ such that the minimum of the one-loop effective potential (122) in the vacuum, i.e., $T=B=0$, still is at $\phi=f_\pi=93$ MeV for the same set of parameters. This is done by requiring

$$\left.\frac{d\mathcal{F}_{0+1}}{d\phi}\right|_{\phi=f_\pi}=0. \tag{126}$$

A straightforward calculation yields

$$\frac{N_cg^4f_\pi^2}{(2\pi)^2}\left[\ln\frac{\Lambda^2}{g^2f_\pi^2}+1\right]=0. \tag{127}$$

Using $f_\pi=93$ MeV and $g=3.2258$ (see below), this yields $\Lambda=181.96$ MeV. Even if we use this value for the renormalization scale such that $\mathcal{F}_{0+1}$ has its minimum at $\phi=f_\pi$, it is strictly speaking not correct to use the parameters Eqs. (123)–(125) in the one-loop effective potential. The reason is that the sigma and pion masses receive radiative corrections, which must be taken into account in the equations that relate the physical masses and the parameters of the theory. In other words, Eqs. (123)–(125) receive corrections. The sigma mass is often defined by the curvature or the second derivative of the effective potential. At tree level, this is given by Eq. (115), but the expression for m_σ changes if we take the one-loop correction to the effective potential into account. To illustrate the dramatic difference, we calculated the second derivative of the effective potential at tree level and at one loop. Using parameters such that the sigma mass at tree level is 750 MeV and the pion mass is 140 MeV, the curvature of the one-loop effective potential with $\Lambda=182$ MeV corresponds to a sigma mass of 530 MeV. Even if one takes radiative corrections into account and determines the parameters at the one-loop level, this procedure is not entirely correct. Determining the sigma mass by the curvature of the effective potential corresponds to including its self-energy evaluated at zero external momentum $p^2=0$. However, the physical mass of the sigma is given by the pole of the propagator, which involves the self-energy evaluated self-consistently at $p^2=-m_\sigma^2$. The difference between the self-energy evaluated at these two points gives rise to a finite shift of the sigma mass that is normally not taken into account. A similar remark applies to the pion mass at the physical point.

We present next numerical results based on the effective potential (122). At the physical point, we use a pion mass of $m_\pi=140$ MeV, a sigma mass of $m_\sigma=800$ MeV, a constituent quark mass of $m_q=300$ MeV, and a pion decay constant of $f_\pi=93$ MeV. This yields the parameters $m^2=-290\,600$ MeV^2, $\lambda=215.19$, and $g=3.2258$. In the chiral limit, we instead use $m_\pi=0$, which yields $m^2=-320\,000$ MeV^2, $\lambda=222$, and $g=3.2258$. We use these parameter values to generate the results presented in Figs. 8–11.

In Fig. 8, we show the renormalized effective potential at $T=0$ normalized to f_π^4 as a function of ϕ for different values

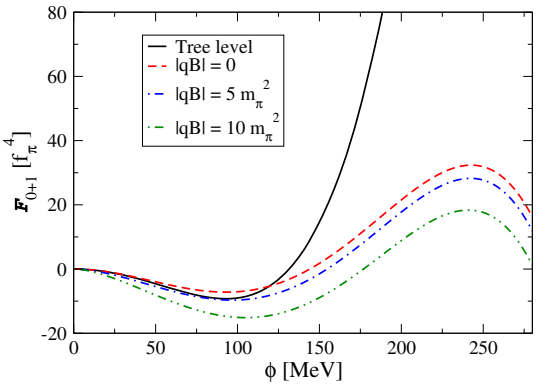

FIG. 8. Normalized effective potential $\mathcal{F}_{0+1}/f_\pi^4$ in the chiral limit for $T=0$. Tree level (solid curve), one loop with $|qB|=0$ (dashed curve), one loop with $|qB|=5m_\pi^2$ (dash-dotted curve), and one loop with $|qB|=10m_\pi^2$ (double dot-dashed curve).

[6]The parameter g is determined by the value of the constituent quark mass $m_q=gf_\pi$.

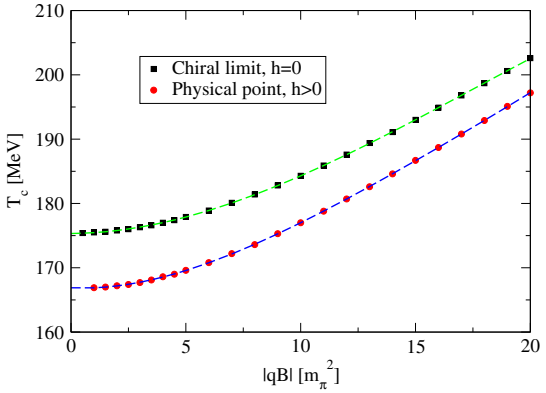

FIG. 9. The transition temperature for the chiral transition as a function of $|qB|/m_\pi^2$. Black squares are the chiral limit and red circles are the physical point.

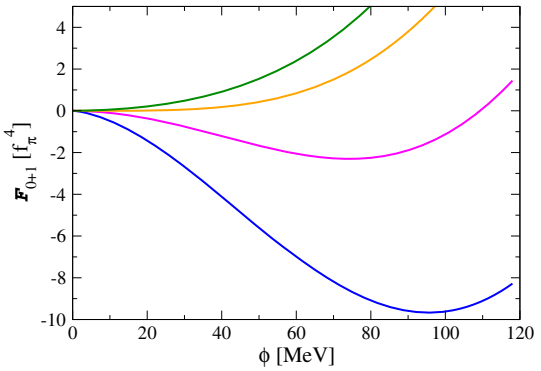

FIG. 10. The effective potential in the chiral limit normalized by f_π^4 for four different temperatures and $|qB| = 5m_\pi^2$, where we have included the vacuum fluctuations (bottom curve, blue: $T = 0$, next-to-bottom curve, pink: $T = 140$ MeV, next-to-top curve, orange: $T = T_c = 177.9$ MeV, and top curve, green: $T = 185$ MeV).

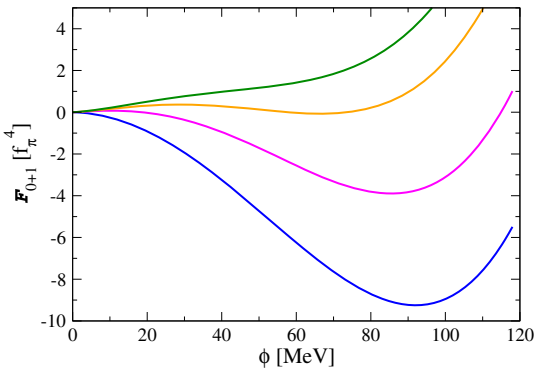

FIG. 11. The effective potential in the chiral limit normalized by f_π^4 for four different temperatures and $|qB| = 5m_\pi^2$, where we omitted the vacuum fluctuations (bottom curve, blue: $T = 0$, next-to-bottom curve, pink: $T = 120$ MeV, next-to-top curve, orange: $T = T_c = 158.0$ MeV, and top curve, green: $T = 176$ MeV).

of the magnetic field. The minimum is moving to the right as the magnetic field increases and so the model exhibits magnetic catalysis as expected. Moreover, the effective potential is unstable for large values of the field ϕ. This instability is present already for $B = 0$ and is due to a term $\sim m_q^4 \ln(\Lambda^2/m_q^2)$, which dominates the effective potential at large ϕ and becomes negative[7] for $m_q = g\phi > \Lambda$. The one-loop bosonic term is also of the form $m^4 \ln(\Lambda^2/m^2)$ with the opposite sign and may stabilize the effective potential if the prefactor is suffiently large. However, perturbative calculations typically break down for large value of the field. In fact, a renormalization group improvement is necessary to make large values of ϕ accessible by removing large logarithms. These issues are discussed in detail by Sher (1989), Ford *et al.* (1993), and Einhorn and Jones (2007).

In Fig. 9, we show the transition temperature for the QM model as a function of $|qB|/m_\pi^2$ in the chiral limit (black squares) and at the physical point (red circles). Both are growing functions of the magnetic field, which shows that the QM model exhibits magnetic catalysis. Vacuum fluctuations are included.

In Fig. 10, we show the normalized effective potential in the chiral limit for four different temperatures, $|qB| = 5m_\pi^2$, and with vacuum fluctuations. The curves show that the phase transition is of second order.

In Fig. 11, we show the normalized effective potential in the chiral limit for four different temperatures $|qB| = 5m_\pi^2$, where we omitted the vacuum fluctuations. The curves show that the phase transition is of first order. Moreover, we notice that including the vacuum fluctuations gives a significantly higher critical temperature T_c.

We have now seen numerically that the phase transition is first order if the fermionic vacuum fluctuations are neglected and second order if they are included. It turns out that the role of vacuum fluctuations in the quark-meson model is the same also in the absence of a magnetic field. This case was carefully analyzed by Skokov *et al.* (2010) in the case of the chiral transition in the QM model with $B = 0$. Recently, the analysis was generalized to a finite B field by Ruggieri, Tachibana, and Greco (2013).

One wants an analytic understanding of this result. The basic idea is to construct a Ginzburg-Landau effective potential of the form

$$V_{\mathrm{GL}} = \tfrac{1}{2}\alpha_2 m_q^2 + \tfrac{1}{4}\alpha_4 m_q^4, \tag{128}$$

where $m_q = g\phi$, and α_2 and α_4 are parameters that depend on the temperature T, the parameters of the Lagrangian, and the magnetic field B. A temperature T_c^* is defined by a vanishing coefficient α_2, i.e., $\alpha_2(T_c^*) = 0$. If $\alpha_4(T_c^*) > 0$, then the transition is second order and the critical temperature is $T_c = T_c^*$. If $\alpha_4(T_c^*) < 0$, the effective potential has two degenerate minima for T slightly larger than T_c^*. The transition is first order and the critical temperature is $T_c > T_c^*$.

In Figs. 12–14, the parameters used correspond to $f_\pi = 92.4$ MeV, $m_q = 335$ MeV, $m_\pi = 0$, and $m_\sigma = 700$ MeV. We first consider the renormalized case, i.e., the

[7]This is the leading term in the large-x expansion (C5).

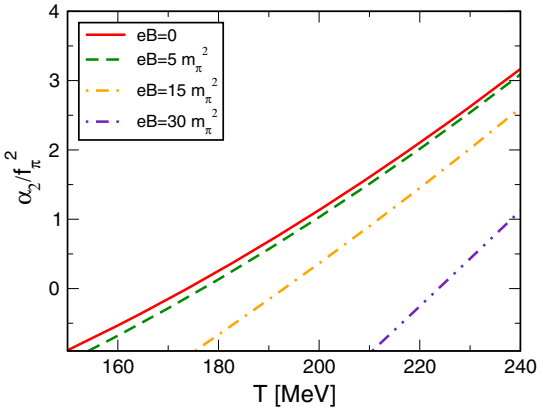

FIG. 12. Coefficient α_2 normalized to f_π^2 as a function of temperature T for different values of the magnetic field. From Ruggieri, Tachibana, and Greco, 2013.

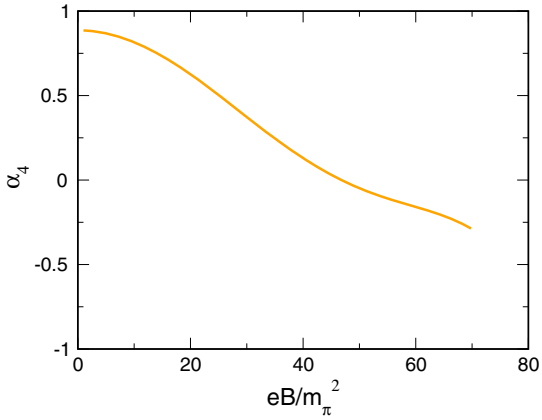

FIG. 14. Coefficient α_4 as a function of magnetic field B at T_c^*. From Ruggieri, Tachibana, and Greco, 2013.

case where one adds counterterms for the mass and coupling and imposes some appropriate renormalization conditions. In Fig. 12, the normalized coefficient α_2/f_π^2 is shown as a function of T for different values of the magnetic field B. We see that α_2 is an increasing function of T and T_c^* is an increasing function of $|qB|$.

In Fig. 13, the dimensionless coefficient α_4 is shown as a function of T for different values of the magnetic field B. The coefficient is positive for all values of T implying that the transition is second order.

We next consider the unrenormalized case, i.e., the case where one regularizes the divergences by a sharp ultraviolet cutoff Λ. In Fig. 14, the coefficient α_4 is shown as a function of B evaluated at T_c^* for $\Lambda = 550$ MeV. The coefficient is negative for $|qB| > |qB_c| \approx 47\ m_\pi^2$ and so the transition is first order for large magnetic fields. The position of B_c depends on Λ and, for $\Lambda \to \infty$, one recovers the results in the renormalized case. On the other hand, if the cutoff Λ is below a critical value Λ_c, the transition is first order for all values of B. The sensitivity to the value of the sharp cutoff suggests that one should be careful and, in particular, not choose a cutoff below the scale set by the largest mass of the particles in the theory.

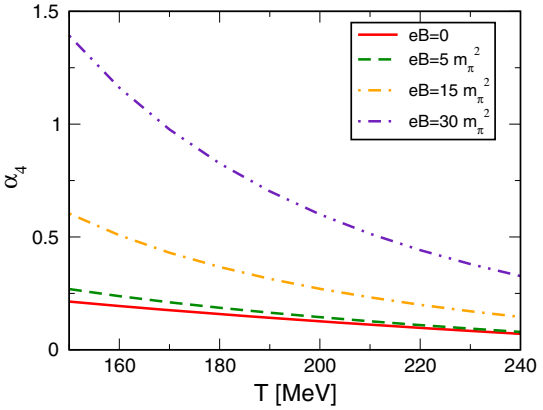

FIG. 13. Coefficient α_4 as a function of temperature T for different values of the magnetic field. From Ruggieri, Tachibana, and Greco, 2013.

E. Hadron resonance gas model

In this section, we briefly discuss the hadron resonance gas (HRG) model in a magnetic background. This model was studied in detail by Endrődi (2013). It can be used to access the low-temperature phase of QCD, even at nonzero chemical potential. The partition function is given by a sum of partition functions of noninteracting hadrons and resonances. This approach gives a surprisingly good description of the thermodynamics of QCD in the confined phase up to temperatures just below the transition region (Karsch, Redlich, and Tawfik, 2003; Borsanyi *et al.*, 2010; Huovinen and Petreczky, 2010).

We can schematically write the free energy density as

$$\mathcal{F} = \sum_h d_h \mathcal{F}_h(B, T, m_h, q_h, s_h, g_h), \tag{129}$$

where d_h, m_h, q_h, s_h, and g_h are the multiplicity, mass, electric charge, spin, and gyromagnetic ratio of hadron h, respectively. For simplicity, the gyromagnetic ratio in Endrődi (2013) was set to $g_h = 2q_h/e$. The hadrons taken into account in the sum are $\pi^\pm, \pi^0, \ldots, \sum^0$.

Since the free energy density is a sum of the free energy densities of noninteracting mesons and baryons, Eq. (129) is given by a sum of the one-loop terms Eqs. (B8) and (B10). Renormalization can be performed using minimal subtraction as discussed previously. However, they used Schwinger's renormalization scheme which involves an extra logarithmic term. For example, the wave-function counterterm for a boson is[8]

[8]There is an extra factor of $\ln(4\pi/e^{\gamma_E})$ since the $\overline{\text{MS}}$ scheme is used.

$$Z^2 = \left[1 - \frac{q^2}{3(4\pi)^2\epsilon} + \frac{q^2}{3(4\pi)^2}\ln\frac{m^2}{\Lambda^2}\right]. \tag{130}$$

Defining the renormalized magnetic field B_r via $B_r^2 = B^2 Z^2$ and subtracting the free energy density at $B = 0$, the one-loop free energy density for a boson is

$$\mathcal{F}_{0+1} = \frac{1}{2}B_r^2 + \frac{4(qB)^2}{(4\pi)^2}\left[\zeta^{(1,0)}\left(-1, \frac{1}{2} + x\right) + \frac{1}{4}x^2 - \frac{1}{2}x^2\ln x + \frac{1}{24}\ln x + \frac{1}{24}\right], \tag{131}$$

where the Hurwitz ζ function $\zeta(s, q)$ is defined in Eq. (38) and $x = m^2/|2qB|$. This is turn implies that the renormalized free energy density approaches zero in the limit $m_h \to \infty$ instead of growing logarithmically. However, the prescription cannot be used in the massless limit due to infrared divergences coming from this extra term. Furthermore, the order-B^2 term is given by the first term in Eq. (131) as the term in the bracket vanishes in the limit of small B.

Figures 15 and 16 show the individual contributions to the HRG pressure as a function of the temperature T for zero magnetic field and for $|qB| = 0.2$ GeV^2, respectively. We first note that the contribution from the neutral particles is independent of B as the gyromagnetic ratio was set to zero.

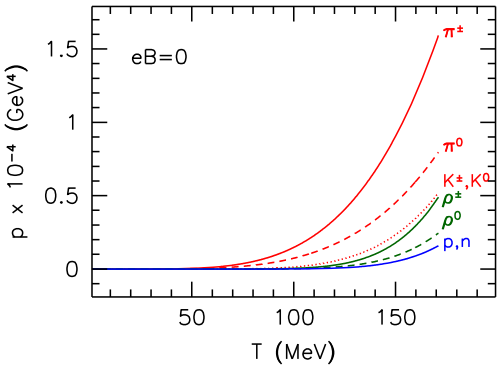

FIG. 15. Individual contributions to the HRG pressure as a function of the temperature T for $B = 0$. From Endrődi, 2013.

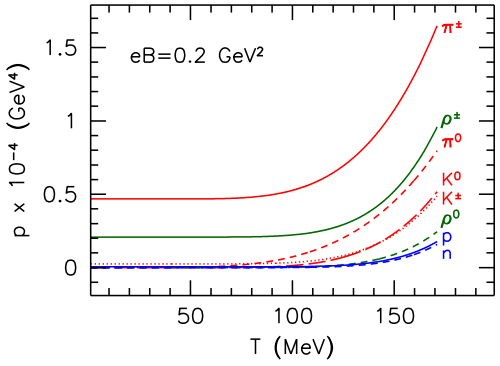

FIG. 16. Individual contributions to the HRG pressure as a function of the temperature T for $|qB| = 0.2$ GeV^2. From Endrődi, 2013.

The relative contribution of the charged particles is changing with B. The reason is that the effective mass is essentially $m_{\text{eff}} = \sqrt{m_h^2 + |q_h B|(1 - 2s)}$, and this increases for $m_{\pi^\pm}$ ($s = 0$) and decreases for $\rho^\pm$ ($s = 1$) and so the Boltzmann weight changes with B. This is clearly seen in Figs. 15 and 16.

Moreover, the pressure is an increasing function of the magnetic field for fixed temperature T. This implies that the magnetization is positive and hence that the hadronic phase is paramagnetic. The speed of sound c_s (not shown) displays a peak, which moves to lower temperatures as the magnetic fields grows. The peak is for T in the 40–70 MeV range for $|qB|$ up to 0.3 GeV^2.

VI. POLYAKOV-LOOP EXTENDED MODELS

As mentioned earlier, the NJL model is not confining. Likewise, the QM model is an effective theory that consists of deconfined quarks as well as mesons as effective degrees of freedom (Bowman and Kapusta, 2009). This is probably a good description at temperatures around the transition temperature, but for very low temperatures it is certainly not. At low temperatures, the thermodynanmics is dominated by the light pions. While these models incorporate chiral symmetry breaking, they are not confining. This is a serious shortcoming as an effective low-energy description of QCD. Next we see that we can mimic, in a statistical sense, the effects of confinement by coupling the chiral models to an SU(3) background gauge field A_μ (Fukushima, 2004). One can express this background gauge field in terms of the complex-valued Polyakov-loop variable Φ and so the effective potential becomes a function of the expectation value of the chiral condensate as well as the expectation value of the Polykov loop operator. Finally, one adds the contribution to the free energy density from the gluons via a phenomenological Polyakov-loop potential $U(\Phi, \bar{\Phi})$.

A. Coupling to the Polyakov loop

In the pure gauge theory, the Polyakov loop Φ is an order parameter for deconfinement (Yaffe and Svetitsky, 1982a, 1982b). For QCD with dynamical quarks, it is an approximate order parameter. It is defined as the trace of the thermal Wilson line L, which is given by

$$L(\mathbf{x}) = \mathcal{P}\exp\left[i\int_0^\beta d\tau A_0(\mathbf{x}, \tau)\right], \tag{132}$$

where $A_0 = A_0^a T_a$ and $\mathcal{P}$ denotes path ordering. Here A_μ^a are the SU(N_c) gauge fields and T_a the generators. For SU$(3)_c$, we have $T_a = (1/2)\lambda_a$, where λ_a are the Gell-Mann matrices. The Polyakov-loop operator l and its complex conjugate are then given by

$$l = \frac{1}{N_c}\,\mathrm{Tr}L, \tag{133}$$

$$l^\dagger = \frac{1}{N_c}\,\mathrm{Tr}L^\dagger. \tag{134}$$

The expectation values of l and $l^\dagger$ are denoted by Φ and $\bar{\Phi}$, respectively. The expectation value of the Polykov loop transforms nontrivially under the center group Z_{N_c} of the gauge group $\mathrm{SU}(N_c)$, $\Phi \to e^{2\pi i n/N_c}\Phi$, where $n = 0, 1, 2, \ldots, N_c - 1$. The behavior of Φ in the pure gauge theory is

$$\Phi \sim 0, \qquad \text{confinement at low } T, \tag{135}$$

$$\Phi \sim 1, \qquad \text{deconfinement at high } T, \tag{136}$$

and so the center symmetry Z_{N_c} is broken in the high-temperature phase.

A constant non-Abelian background is now introduced via the covariant derivative which takes the form

$$D_\mu = \partial_\mu - iq_f A_\mu^{\mathrm{EM}} - iA_\mu, \tag{137}$$

where $A_\mu^{\mathrm{EM}} = (0, 0, -Bx, 0)$ and $A_\mu = \delta_{\mu 0} A_0$. In the Polyakov gauge, we can write the background gauge field A_0 as

$$A_0 = t_3 A_0^{(3)} + t_8 A_0^{(8)}. \tag{138}$$

For constant gauge fields, the thermal Wilson line can be written as

$$L = \begin{pmatrix} e^{i(\phi_1+\phi_2)} & 0 & 0 \\ 0 & e^{i(-\phi_1+\phi_2)} & 0 \\ 0 & 0 & e^{-2i\phi_2} \end{pmatrix}, \tag{139}$$

where $\phi_1 = (1/2)\beta A_0^{(3)}$ and $\phi_2 = (1/2\sqrt{3})\beta A_0^{(8)}$. In the perturbative vacuum $\phi_1 = \phi_2 = 0$ and in the confining vacuum $\phi_1 = \phi_2 = \pi/3$. Using $\phi_1 = \phi_2$, the Polyakov loop reduces to

$$\Phi = \tfrac{1}{3}[1 + 2\cos(2\phi_1)]. \tag{140}$$

The zeroth component of the gauge field acts as a chemical potential in the covariant derivative (137). With this observation and the definition (132), we can immediately make the following replacement for a fermion in the background field:

$$\ln[1 + e^{-\beta E_q}] \to \frac{1}{2N_c}\,\mathrm{Tr}\ln[1 + Le^{-\beta E_q}] + \frac{1}{2N_c}\,\mathrm{Tr}\ln[1 + L^\dagger e^{-\beta E_q}], \tag{141}$$

where the trace on the right-hand side is in color space and E_q is the energy of the fermionic excitations. Performing the trace of the first term in Eq. (141) using Eq. (139), one obtains

$$\frac{1}{N_c}\mathrm{Tr}\ln[1 + Le^{-\beta E_q}] = \frac{1}{3}\ln[1 + 3(\Phi + \bar{\Phi}e^{-\beta E_q})e^{-\beta E_q} + e^{-3\beta E_q}], \tag{142}$$

and where the second term in Eq. (141) can be obtained by Hermitean conjugation. The temperature-dependent part of the one-loop fermionic contribution to the free energy density can then be written as

$$\mathcal{F}_1^T = -T\sum_f \frac{|q_f B|}{2\pi} \times \sum_{s=\pm 1}\sum_{k=0}^{\infty}\int_{p_z} \{\ln[1 + 3(\Phi + \bar{\Phi}e^{-\beta E_q})e^{-\beta E_q} + e^{-3\beta E_q}] + \ln[1 + 3(\bar{\Phi} + \Phi e^{-\beta E_q})e^{-\beta E_q} + e^{-3\beta E_q}]\}. \tag{143}$$

It reduces to the second term in Eq. (35) in the limit $\Phi, \bar{\Phi} \to 1$, with an extra factor of $N_c = 3$, as it should. We note in passing that the vacuum part of the one-loop fermionic free energy density is unchanged and therefore the PNJL model reduces to the NJL model at $T = 0$.

Taking the trace in color space, the Fermi-Dirac distribution is generalized to

$$n_F(\beta E) = \frac{1 + 2\bar{\Phi}e^{\beta E_q} + \Phi e^{2\beta E_q}}{1 + 3\bar{\Phi}e^{\beta E_q} + 3\Phi e^{2\beta E_q} + e^{3\beta E_q}}. \tag{144}$$

It is instructive to look at the behavior of Eq. (144) at very low and very high temperatures. At low temperatures, we have $\Phi \approx 0$ and therefore the Fermi-Dirac distribution reduces to

$$n_F(\beta E_q) \approx \frac{1}{e^{3\beta E_q} + 1}, \tag{145}$$

which is the distribution function of a fermion with energy $3E_q$. Thus the contribution from the fermions to the effective potential is suppressed at low temperature as compared to the corresponding chiral model without the Polyakov loop. This is referred to as statistical confinement. In the same manner, we see that Eq. (144) at high temperature behaves as

$$n_F(\beta E_q) \approx \frac{1}{e^{\beta E_q} + 1}, \tag{146}$$

where we have $\Phi \approx 1$. This is a distribution function of a fermion with energy E_q, i.e., that of deconfined quarks. A word of caution here is appropriate. The same behavior as Eq. (145) is found in two-color QCD with quarks in the adjoint representation (Zhang, Brauner, and Rischke, 2010) and so the number x in $x\beta E_q$ does not necessarily give the correct number of quarks to form a color singlet.

We have now coupled the Polyakov-loop variable to the matter sector of theory. However, we must also include the contribution to the free energy density from the gauge sector and this is done by adding a phenomenological Polyakov-loop potential $U(\Phi, \bar{\Phi})$. This potential is required to reproduce the pressure for pure-glue QCD as calculated on the lattice for the temperatures around the transition temperature.

A number of forms for the Polyakov-loop potential have been proposed and investigated at the mean-field level for the PNJL model (Lourenco *et al.*, 2011) and the PQM model with $\mu_B = 0$ (Schaefer, Wagner, and Wambach, 2010). In the following we review three different Polyakov-loop potentials. Since the Polyakov-loop variable is the order parameter for the Z_3 center symmetry of pure-glue QCD,

a Ginzburg-Landau–type potential should incorporate this. A polynomial expansion then leads to (Ratti, Thaler, and Weise, 2006)

$$\frac{U_{\rm poly}}{T^4} = -\frac{1}{2}b_2(T)\Phi\bar{\Phi} - \frac{1}{6}b_3(\Phi^3+\bar{\Phi}^3) + \frac{1}{4}b_4(\Phi\bar{\Phi})^2, \quad (147)$$

where the coefficients are

$$b_2(T) = 6.75 - 1.95\left(\frac{T_0}{T}\right) + 2.625\left(\frac{T_0}{T}\right)^2 - 7.44\left(\frac{T_0}{T}\right)^3, \quad (148)$$

$$b_3 = 0.75, \quad (149)$$

$$b_4 = 7.5. \quad (150)$$

The parameter T_0 is the transition temperature for pure-glue QCD lattice calculations, $T_0 = 270$ MeV (Karsch, Laermann, and Peikert, 2001). Ratti *et al.* (2007) and Roessner, Ratti, and Weise (2007) proposed another form of the Polyakov-loop potential based on the SU(3) Haar measure:

$$\frac{U_{\rm log}}{T^4} = -\frac{1}{2}a(T)\Phi\bar{\Phi} + b(T)\ln[1 - 6\bar{\Phi}\Phi + 4(\Phi^3+\bar{\Phi}^3) - 3(\bar{\Phi}\Phi)^2], \quad (151)$$

where the coefficients are

$$a(T) = 3.51 - 2.47\left(\frac{T_0}{T}\right) + 15.2\left(\frac{T_0}{T}\right)^2, \quad (152)$$

$$b(T) = -1.75\left(\frac{T_0}{T}\right)^3. \quad (153)$$

We note that the logarithmic term ensures that the magnitudes of Φ and $\bar{\Phi}$ are constrained to be in the region between -1 and 1, i.e., the possible attainable values for the normalized trace of an element of SU(3). The coefficient $a(T)$ approaches $16(\pi^2/90) \approx 3.51$ as $T \to \infty$ such that the potential Eq. (151) reproduces the Stefan-Boltzmann limit. Finally, Fukushima (2008) proposed the following Polyakov-loop potential:

$$\frac{U_{\rm Fuku}}{T^4} = -\frac{b}{T^3}\{54e^{-aT_0/T}\Phi\bar{\Phi} + \ln[1 - 6\Phi\bar{\Phi} + 4(\Phi^3+\bar{\Phi}^3) - 3(\Phi\bar{\Phi})^2]\}, \quad (154)$$

where the constants are $a = 664/270$ and $b = (196.2\ \text{MeV})^3$. This potential differs from the logarithmic potential (151) only by the coefficient of the first term. Finally, note that the effective potential including the glue potential is symmetric under $\Phi \leftrightarrow \bar{\Phi}$ for $\mu_B = 0$. Hence $\Phi = \bar{\Phi}$.

A problem with all the proposed Polyakov-loop potentials is that they are independent of the number of flavors and the baryon chemical potential. However, we know that, for example, the transition temperature for the deconfinement transition is a function of N_f. In other words, one ought to incorporate the backreaction from the fermions to the gluonic sector. Schaefer, Pawlowski, and Wambach (2007) used perturbative arguments to estimate the effects of the number of flavors and the baryon chemical potential on the deconfinement transition temperature T_0. The functional form of T_0 (Herbst, Pawlowski, and Schaefer, 2011) for $\mu_B = 0$ is

$$T_0 = T_\tau e^{-1/\alpha_0 b(N_f)}, \quad (155)$$

where

$$b(N_f) = \frac{1}{6\pi}(11N_c - 2N_f), \quad (156)$$

and the parameters are $T_\tau = 1.77$ GeV and $\alpha_0 = 0.304$. This yields a deconfinement transition temperature of 240 and 208 MeV for $N_f = 1$ and $N_f = 2$, respectively. Another way of including the backreaction from the fermions was implemented by Haas *et al.* (2013) and Herbst *et al.* (2014). They calculated the glue potential as a function of a background gauge field with and without dynamical fermions using the functional renormalization group. They compared the two potentials and found a mapping between them and this mapping is used to modify the Polyakov-loop potential discussed previously.

The phase stucture of the Polyakov-loop extended model is then found by simultaneously solving the gap equations

$$\frac{\partial\mathcal{F}}{\partial M_0} = 0, \qquad \frac{\partial\mathcal{F}}{\partial\Phi} = 0 \qquad \text{(PNJL)}, \quad (157)$$

$$\frac{\partial\mathcal{F}}{\partial\phi} = 0, \qquad \frac{\partial\mathcal{F}}{\partial\Phi} = 0 \qquad \text{(PQM)}, \quad (158)$$

where $\mathcal{F}$ is the sum of the free energy density from the fermions and the Polyakov-loop potential U.

Gatto and Ruggieri (2010) considered the PNJL model using the logarithmic potential Eq. (151). They used $G_1 = G_2$ and added an eight-quark interaction term of the form

$$\delta\mathcal{L} = G_8[(\bar{\psi}\psi)^2 + (\bar{\psi}i\gamma_5\boldsymbol{\tau}\psi)^2]^2, \quad (159)$$

where G_8 is a coupling constant. In this case, the constituent quark mass reads $M_0 = m_0 - 2G_0\langle\bar{\psi}\psi\rangle - 4G_8\langle\bar{\psi}\psi\rangle^3$. They also used a form factor of the form

$$F(p) = \frac{\Lambda^{2N}}{\Lambda^{2N} + (p_z^2 + 2|q_f B|k)^N}, \quad (160)$$

choosing the values $N = 5$ and $N = 7$.

Figure 17 shows the phase diagram in the B-T plane for the chiral (dot-dashed) as well as the deconfinement transition (dashed) for $N = 5$. The critical temperatures T_χ and T_P have been normalized to the common pseudocritical temperature $T_0 = 175$ MeV at $B = 0$. We note that the transition temperature T_χ is increasing more with the magnetic field than T_P is. The shaded area corresponds to a phase where the quarks are deconfined but where chiral symmetry is still broken.

The PNJL model was extended by several using a nonlocal NJL vertex (Sasaki, Friman, and Redlich, 2007; Hell *et al.*, 2009; Kondo, 2010). Kondo (2010) derived from QCD a

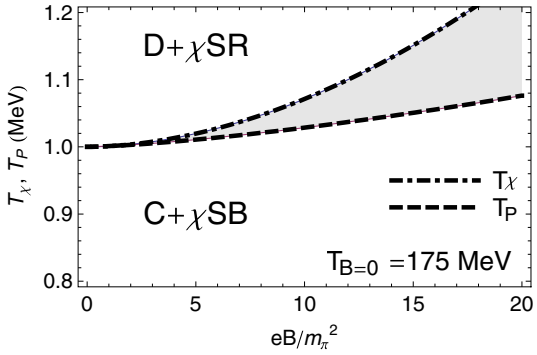

FIG. 17. Phase diagram in the B-T plane. From Gatto and Ruggieri, 2010.

nonlocal vertex that depends explicitly on T as well as the phase of the Polyakov loop. Such a model is called the entangled Polyakov-loop model (EPNJL), which was used by Gatto and Ruggieri (2011) at finite B to study the chiral and deconfinement transitions. In contrast to the PNJL model, there is basically no splitting of the two transitions in the EPNJL model.

Another mean-field analysis was carried out by Mizher, Chernodub, and Fraga (2010) using the PQM model focusing on the physical point. Renormalization is carried out by subtracting the divergent fluctuation determinant for $B = 0$. They made several interesting observations. If the fermionic vacuum fluctuations are neglected,[9] the transition temperature for the deconfinement transition coincides with that of the chiral transition, and they are both first order, except for very small values of the magnetic field, where they are crossovers. Moreover, the transition temperatures are decreasing with increasing B. If the vacuum fluctuations are included, the transition temperatures are increasing with B and the resulting phase diagram is qualitatively the same as in Fig. 17. The chiral transition is now a crossover.

B. Two-color PNJL model

So far we have been discussing QCD with three colors. In this section, we consider two-color QCD. Two-color QCD is interesting for a number of reasons. In contrast to three-color QCD, one can perform lattice simulations at finite baryon chemical potential μ_B. This is a consequence of the special properties of the gauge group $\mathrm{SU}(2)_c$ which leads to a real-valued Dirac determinant even for $\mu_B \neq 0$. Hence, the sign problem is absent in this case and one can use importance sampling techniques as usual. Moreover, the order of the deconfinement transition for pure-glue QCD is different in $\mathrm{SU}(2)_c$ and $\mathrm{SU}(3)_c$. For $N_c = 2$ it is second order, while for $N_c = 3$ it is first order. In two-color QCD, the critical exponents are expected to be those of the two-state Potts model, which follows from universality arguments.

In this section, we discuss two-color QCD in a strong magnetic field. While there is a number of model calculations in two-color QCD at finite temperature and baryon chemical potential, there is only a single calculation at finite B (Cruz and Andersen, 2013).

In the Polyakov gauge, the background non-Abelian gauge field is diagonal in color space,

$$A_0 = \tfrac{1}{2}\sigma_z\theta, \tag{161}$$

where θ is real. The thermal Wilson line can then be written as

$$L = \begin{pmatrix} e^{i\phi} & 0 \\ 0 & e^{-i\phi} \end{pmatrix}, \tag{162}$$

where $\phi = (1/2)\beta\theta$. The Polyakov-loop variable becomes

$$\Phi = \cos(\phi). \tag{163}$$

In analogy with Eq. (144), the Fermi-Dirac distribution function becomes

$$n_F(\beta E_q) = \frac{1 + \Phi e^{\beta E_q}}{1 + 2\Phi e^{\beta E_q} + e^{2\beta E_q}}. \tag{164}$$

At low temperature, $\Phi \approx 0$ and so Eq. (164) describes excitations with energy $2E_q$, i.e., that of a bound state.[10] Again this is referred to as statistical confinement. At high temperature, $\Phi \approx 1$ and Eq. (164) describes excitations with energy E_q, i.e., deconfined quarks.

The Polyakov-loop potential in the gauge sector used is (Brauner, Fukushima, and Hidaka, 2009)

$$\Omega_{\mathrm{gauge}} = -bT[24\Phi^2 e^{-\beta a} + \ln(1 - \Phi^2)], \tag{165}$$

where a and b are constants. This form is motivated by the lattice strong coupling expansion (Fukushima, 2008). In the gauge theory without dynamical quarks, one can find an explicit expression for the Polyakov-loop variable

$$\Phi = \sqrt{1 - \frac{1}{24}e^{\beta a}}$$

as a function of T and so $a = T_c \ln 24$. Moreover, Φ goes to zero in a continuous manner and the theory exhibits a second-order transition.

A few remarks about the parameters in two-color QCD are in order. For $N_c = 2$, there are no experimental results to guide us in the determination of the parameters. A common way of determining them is to use N_c scaling arguments (Brauner, Fukushima, and Hidaka, 2009). The pion decay constant scales as $\sqrt{N_c}$ and the chiral condensate as N_c. With a cutoff of $\Lambda = 657$ MeV, this yields $G = 7.23$ GeV^{-2} at the physical point (Brauner, Fukushima, and Hidaka, 2009).

In Fig. 18, we show the Polyakov loop as a function of T/m_π found by minimizing the Polyakov-loop potential (165) (dotted line). We also show the normalized quark condensate

[9]Note that there are still some B-dependent vacuum terms that have not been removed by this renormalization procedure.

[10]For $N_c = 2$, two (anti)quarks can form a color singlet that belongs to the same multiplet as the usual three quark-antiquark bound states. These states are the "baryons" of two-color QCD.

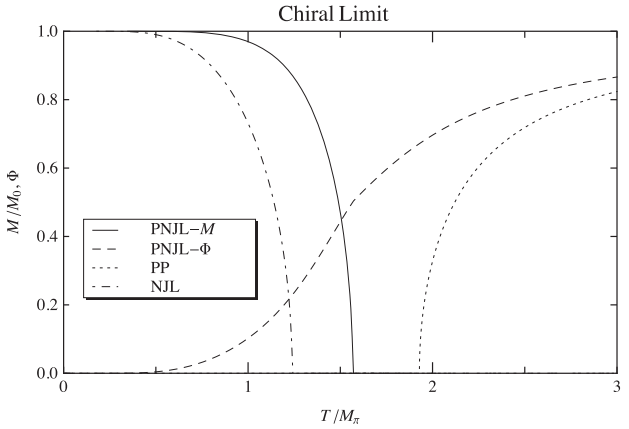

FIG. 18. Normalized constituent quark mass and Polyakov loop in the chiral limit as a function of T/m_π. From Cruz and Andersen, 2013.

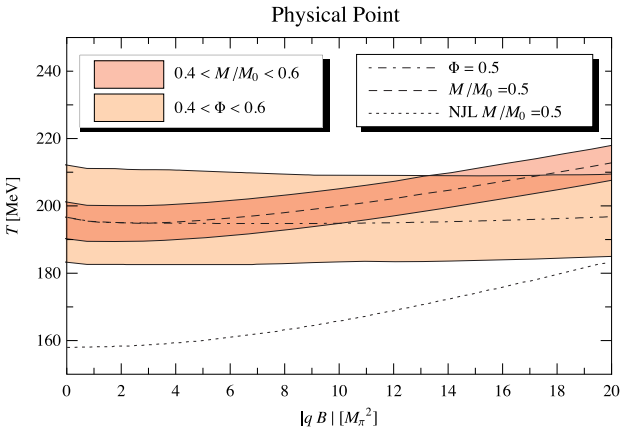

FIG. 19. Transition temperatures for the deconfinement and the chiral transition in the PNJL model as a function of $|qB|/m_\pi^2$ in two-color QCD. From Cruz and Andersen, 2013.

obtained in the NJL model (dash-dotted line). The dashed and solid lines show the Polyakov loop and normalized quark condensate as functions of T/m_π in the PNJL model. From the figure, we see that the coupling between the two variables forces the curve for the normalized quark condensate to the right and the curve for the Polyakov to the left so that the two transitions have a common transition temperature.

In Fig. 19, we show the transition temperatures for the chiral and deconfinement transitions as functions of $|qB|/m_\pi^2$. The bands show the values of the order parameters $0.4 < M/M_0 < 0.6$ and $0.4 < \Phi < 0.6$, where M_0 is the chiral condensate at $T = 0$. For comparison we also show the chiral transition for the NJL model. There seems to be a minimum in T_c for the two transitions; see the discussion in Sec. IX.B. The transitions coincide for $B = 0$ (cf. Fig. 18), but split at finite B. Note the similarity with the curves in Fig. 17 and that the deconfinement temperature is almost independent of temperature.

VII. FUNCTIONAL RENORMALIZATION GROUP

The functional renormalization group (Wetterich, 1993) is a powerful nonperturbative method that has gained popularity since its formulation more than two decades ago. It is one way of implementing the renormalization group ideas of Wilson from the early 1970s. The average effective action, which is denoted by $\Gamma_k[\phi]$, is a function of a set of fields collectively denoted by ϕ. The subscript indicates that the effective action is a function of a momentum scale k.

This sliding scale k acts as an infrared cutoff, such that all momenta q between k and the ultraviolet cutoff of the theory Λ have been integrated out. At $k = \Lambda$, no momenta have been integrated out and the effective action equals the bare action $\Gamma_\Lambda[\phi] = S[\phi]$. Thus the value $S[\phi]$ is the boundary condition for the effective action. Moreover, when $k = 0$, all the quantum and thermal fluctuations have been integrated out and $\Gamma_0[\phi]$ is equal to the full quantum effective action. The average effective action satisfies a functional integrodifferential equation, whose right-hand side depends on the particle content. For the quark-meson model, a diagrammatic representation of the flow equation is shown in Fig. 20 and it reads

$$\partial_k\Gamma_k[\phi] = \tfrac{1}{2}\mathrm{Tr}\{\partial_k R_k^B(p)[\Gamma_k^{(2,0)}[\phi] + R_k^B(p)]^{-1}\} - \{\partial_k R_k^F(p)[\Gamma_k^{(0,2)}[\phi] + R_k^F(p)]^{-1}\}, \quad (166)$$

where $\Gamma_k^{(m,n)}[\phi]$ denotes the mth functional derivative with respect to the bosonic fields and the nth functional derivative with respect to the bosonic fields of the average effective action. Moreover, the trace is over momentum space, field indices, and for fermions over Dirac indices. The so-called regulator functions $R_k^B(p)$ and $R_k^F(p)$ are added to implement the renormalization group ideas mentioned previously. These functions are large for $p < k$ and small for $p > k$ if $0 < k < \Lambda$. The regulator functions also satisfy $R_\Lambda^B(p) = R_\Lambda^F(p) = \infty$. These properties guarantee that the modes with $p < k$ are heavy and decouple and only the modes p between the sliding scale k and the ultraviolet cutoff Λ are light and integrated out. We return to the choice of regulator functions later.

A. Local-potential approximation

Of course one cannot solve the flow equation exactly, then one would have solved the theory exactly, and so one needs to make approximations. A framework for systematic approximations is the derivative expansion. The leading-order approximation in the derivative expansion is called the local-potential approximation (LPA) (Morris, 1994) since the full quantum effective action is approximated by the Euclidean action (here for $B = 0$)

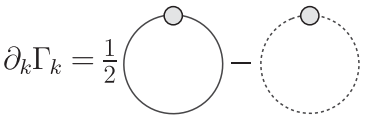

FIG. 20. Diagrammatic representation of the exact flow equation for the effective action $\Gamma_k[\phi]$ for the quark-meson model. The lines denote the exact field-dependent propagators for bosons (solid) and fermions (dashed), while the circles denote the insertion of the regulator functions $R_k^B(p)$ or $R_k^F(p)$.

$$\Gamma_k[\phi] = \int_0^\beta d\tau \int d^3x \left\{ \bar{\psi}\partial\!\!\!/\psi + g\bar{\psi}(\sigma + i\gamma_5 \tau \cdot \pi)\psi + \frac{1}{2}(\partial_\mu \sigma)^2 + \frac{1}{2}(\partial_\mu \boldsymbol{\pi})^2 + U_k - h\sigma \right\}, \tag{167}$$

where U_k is a k-dependent local potential that depends on the $O(4)$ invariant $\sigma^2 + \pi^2$. The term $\Gamma_k^{(2,0)}[\phi]$ in Eq. (166) is

$$\Gamma_k^{(2,0)}[\phi] = \begin{pmatrix} p^2 + R_k^B(p) + U_k' + 2\rho U_k'' & 0 & 0 & 0 \\ 0 & p^2 + R_k^B(p) + U_k' & 0 & 0 \\ 0 & 0 & \cdots & 0 \\ 0 & 0 & 0 & \cdots \end{pmatrix}, \tag{168}$$

where the $\cdots$ indicates $p^2 + R_k^B(p) + U_k'$. Moreover $U_k' = \partial U_k/\partial\rho$ and $U_k'' = \partial^2 U_k/\partial\rho^2$ with $\rho = (1/2)\phi^2 = (1/2)(\sigma^2 + \pi^2)$. We notice that the matrix Eq. (168) has the form of an inverse bosonic tree-level propagator where we make the substitution $V \to U_k + R_k^B(p)$, where $V = (1/2)m^2\phi^2 + (\lambda/24)\phi^4$. Similarly, the second term in Eq. (166) has the form of an inverse fermion tree-level propagator with a quark mass $m_q = g\phi$.

We used a modification of the regulators (Litim, 2001; Stokic, Friman, and Redlich, 2010)

$$R_k^B(p) = (k^2 - \mathbf{p}^2)\theta(k^2 - \mathbf{p}^2), \tag{169}$$

$$R_k^F(p) = \left(\sqrt{\frac{P_0^2 + k^2}{P_0^2 + \mathbf{p}^2}} - 1 \right) p\!\!\!/\,\theta(k^2 - \mathbf{p}^2). \tag{170}$$

The integral over three-momenta p is now easy to carry out due to the step functions. It is also straightforward to carry out the sum over Matsubara frequencies and the integrodifferential flow equation reduces to a partial differential equation (Stokic, Friman, and Redlich, 2010)

$$\partial_k U_k = \frac{4k^4}{3(4\pi)^2} \left\{ \frac{3}{\omega_{1,k}}[1 + 2n_B(\omega_{1,k})] + \frac{1}{\omega_{2,k}}[1 + 2n_B(\omega_{2,k})] - 4N_c N_f \left[\frac{1}{\omega_{q,k}}(1 - 2n_F(\omega_{q,k})) \right] \right\}, \tag{171}$$

where $\omega_{1,k} = \sqrt{k^2 + U'}$, $\omega_{2,k} = \sqrt{k^2 + U' + 2\rho U''}$, and $\omega_{q,k} = \sqrt{k^2 + 2g^2\rho}$.

The flow equation can be generalized to a constant magnetic background: we modify the regulators by making the replacements $\mathbf{p}^2 \to p_z^2 + |qB|(2n + 1)$ and $\mathbf{p}^2 \to p_z^2 + |q_f B|(2n + 1 - s)$ above. (Note that here and in the remainder of this section we denote the Landau levels by n so there is no confusion with the sliding scale k.) After integrating over p_z and summing over Matsubara frequencies P_0, the flow equation can be written as (Skokov, 2012)

$$\begin{aligned} \partial_k U_k = {} & \frac{4k^4}{3(4\pi)^2} \left\{ \frac{1}{\omega_{1,k}}[1 + 2n_B(\omega_{1,k})] + \frac{1}{\omega_{2,k}}[1 + 2n_B(\omega_{2,k})] \right\} \\ & + \frac{8|qB|}{(4\pi)^2} \sum_{n=0}^{\infty} \frac{k}{\omega_{1,k}} \sqrt{k^2 - p_\perp^2(q,n,0)}\,\theta(k^2 - p_\perp^2(q,n,0)) \\ & \times [1 + 2n_B(\omega_{1,k})] \\ & - \frac{8N_c}{(4\pi)^2} \sum_{s,f,n=0}^{\infty} \frac{|q_f B|k}{\omega_{q,k}} \sqrt{k^2 - p_\perp^2(q_f,n,s)} \\ & \times \theta(k^2 - p_\perp^2(q_f,n,s))[1 - 2n_F(\omega_{q_f,k})], \end{aligned} \tag{172}$$

where $p_\perp^2(q,n,s) = |qB|(2n + 1 - s)$.

In a constant magnetic background, U_k depends on the two invariants $|v|$ and $|\Delta|$, where $v = (1/\sqrt{2})(\sigma + i\gamma_5\pi^0)$ and $\Delta = (1/\sqrt{2})(\pi_1 + i\pi_2)$. Thus the potential depends on two $O(2)$ invariants in accordance with the discussion in Sec. V.D. We are not including a pion condensate and therefore the local potential is evaluated at $|\Delta| = 0$. However, the flow equation still depends on the two partial derivatives $\partial U_k/\partial|v|$ and $\partial U_k/\partial|\Delta|$. In the mean-field approximation, these partial derivatives are identical, but beyond they generally are not. In order to make the flow equation numerically tractable, Andersen, Naylor, and Tranberg (2014) made the approximation that they are equal.

The flow equation (172) reduces to the flow equation (171) in the limit $B \to 0$: One defines the variable $p_\perp^2 = 2|qB|n$, makes the substitution $p_\perp dp_\perp = |qB|dn$, replaces the sum by an integral over $p_\perp$, and finally performs the integral.

Sometimes, one defines a so-called extended mean-field equation by omitting the bosonic terms on the right-hand side of the flow equation. Then the terms that depend on the derivatives of U_k on the right-hand side drop out and one can formally integrate the flow equation to obtain the effective potential (Kamikado *et al.*, 2013). For $T = 0$, this can be done analytically even for nonzero magnetic field B.

The k-dependent minimum $f_{\pi,k}$ satisfies

$$\left.\frac{\partial U_k}{\partial\phi}\right|_{\phi = f_{\pi,k}} = h, \tag{173}$$

i.e., by minimizing the modified effective potential $\tilde{U}_k = U_k - h\phi$. The k-dependent masses $m_{\pi,k}^2$ and $m_{\sigma,k}^2$ can be

expressed in terms of the second derivatives of the k-dependent effective potential at the k-dependent minimum $f_{\pi,k}$ as follows:

$$m_{\pi,k}^2 = \left.\frac{\partial U_k}{\partial \rho}\right|_{\phi=f_{\pi,k}}, \tag{174}$$

$$m_{\sigma,k}^2 = m_\pi^2 + \rho \left.\frac{\partial^2 U_k}{\partial \rho^2}\right|_{\phi=f_{\pi,k}}. \tag{175}$$

Combining Eqs. (173) and (174), we find $f_{\pi,k} m_{\pi,k}^2 = h$. For $k = h = 0$, this is Goldstone's theorem.

The boundary condition for the effective potential at $k = \Lambda$ has the $O(4)$-invariant form

$$U_\Lambda = \frac{1}{2} m_\Lambda^2 \phi^2 + \frac{\lambda_\Lambda}{24} \phi^4. \tag{176}$$

The bare parameters m_Λ^2 and λ_Λ are tuned such that one obtains the correct pion mass and pion decay constant in the vacuum at $k = 0$. In the calculation we use an ultraviolet cutoff $\Lambda = 800$ MeV, although the results are not too sensitive to the exact value. We ignore the running of the Yukawa coupling and set $g = g_k = 3.2258$ for all values of k. This gives a constituent quark mass of $m_q = g\phi_0 = g f_\pi = 300\,\mathrm{MeV}$. Further details of the numerical implementation can be found in Andersen and Tranberg (2012) and Andersen, Naylor, and Tranberg (2014).

Once we have determined the parameters m_Λ^2 and λ_Λ, we can solve the flow equation (172) for each value of B and T. From these calculations, one can extract the critical temperature for the chiral transition. In Fig. 21, we show the critical temperature as a function of the magnetic field B at the physical point. The dashed curve is the quark-meson model and solid curve is the Polyakov-loop extended quark-meson model. In agreement with various mean-field results, the critical temperature is an increasing function of B.

It is interesting to note that the coupling to the Polyakov-loop variable Φ lowers T_c. This is an interesting observation, in particular, since the Polyakov loop has no influence on magnetic catalysis at zero temperature. This effect can be understood by calculating the free energy density in a given background ϕ_1 and comparing it with the free energy density in the deconfining background $\phi_1 = 0$ (Bruckmann, Endrődi, and Kovacs, 2013).[11] The difference between these two free energy densities is

$$\Delta\mathcal{F} = \frac{|q_f B|}{\pi^2} \int_0^\infty \frac{ds}{s^2} e^{-m^2 s} \coth(|q_f B| s) \times \left[\theta_3\left(\phi_1 + \frac{1}{2}\pi, e^{-1/4sT^2}\right) - \theta_3\left(\frac{1}{2}\pi, e^{-1/4sT^2}\right)\right], \tag{177}$$

where the elliptic theta function $\theta_3(u, q)$ is defined by

[11]Recall $\Phi = (1/3)[1 + 2\cos(2\phi_1)] = 1$ for $\phi_1 = 0$.

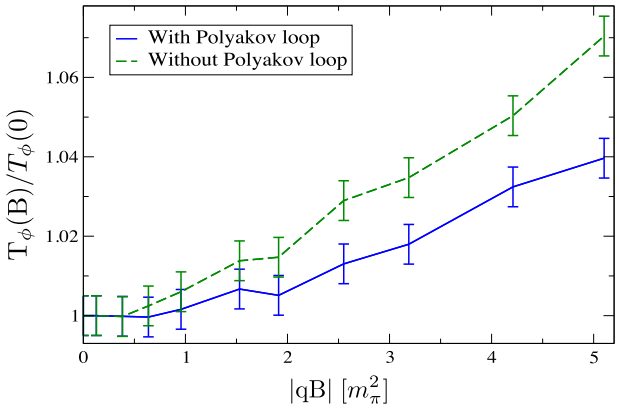

FIG. 21. Normalized critical temperature $T_\phi(B)/T_\phi(0)$ for the chiral transition as a function of the magnetic field B with and without the inclusion of the Polyakov loop.

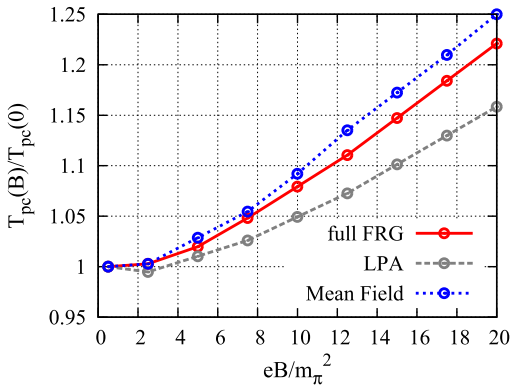

FIG. 22. The transition temperature for the chiral transition as a function of $|qB|/m_\pi^2$ for three different approximations normalized to the transition temperature at $B = 0$. From Kamikado and Kanazawa, 2014.

$$\theta_3(u, q) = 1 + 2\sum_{n=1}^{\infty} q^{n^2} \cos(2nu). \tag{178}$$

The function $|q_f B| \coth(|q_f B| s)$ increases with s for all values of s. Thus a magnetic field favors deconfined Polyakov loops and therefore tends to lower the transition temperature. We also note that this effect decreases with larger quark masses m.

We are not aware of any mean-field calculations that directly compare the chiral transition temperature with and without the Polyakov loop.[12] However, based on this argument as well as the renormalization group calculations, we expect to see the same behavior in the mean-field approximation.

B. Beyond the local-potential approximation

The results we have been discussing so far are obtained using the local-potential approximation. Recently, Kamikado

[12]There are of course many mean-field calculations with and without the Polyakov loop, but a comparison between them requires that physical observables in the vacuum are the same.

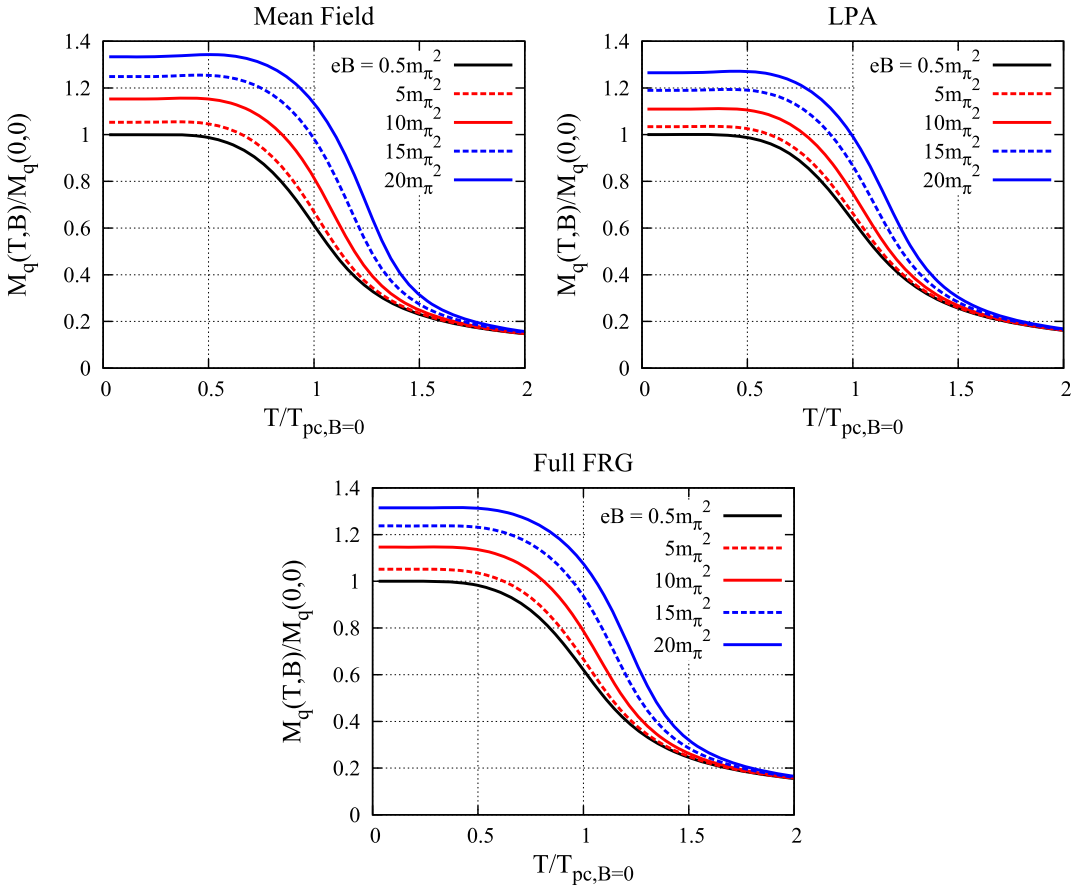

FIG. 23. Normalized constituent quark mass as a function of the normalized temperature for the three different approximations and different values $|qB|$. From Kamikado and Kanazawa, 2014.

and Kanazawa (2014) go beyond the LPA by including the wave-function renormalization terms $Z_\perp$ and $Z_\parallel$. In order to avoid the complication of having two invariants $|v|$ and $|\Delta|$ on which the effective potential U_k depends, they consider the case $N_f = 1$. In this case, the symmetry is $\mathrm{U}(1)_V \times \mathrm{U}(1)_A$ in the chiral limit or $\mathrm{U}(1)_V$ at the physical point. Either way, the quark condensate gives rise to a single (pseudo)Goldstone boson. One expects the charged pions to decouple for sufficiently large magnetic fields since they become heavy and therefore the $N_f = 2$ model essentially reduces to the model they considered; cf. the discussion after Eq. (71). Moreover, their calculations were done at the physical point.

One of the interesting aspects of their work is the systematic study of the various approximations. For example, they studied the transition temperature in the mean-field approximation, the LPA, and beyond the LPA. The transition temperature is determined by the peak of dM_q/dT, where M_q is the constituent quark mass. The result is shown in Fig. 22, where the colored lines show the normalized transition temperature in the three approximations. The inclusion of the mesonic fluctuations lowers the transition temperature compared to the mean-field approximation, while the inclusion of wave-function renormalization effects increases the slope somewhat. It would be of interest to see the effects of including the Polyakov loop as well.

The constituent quark mass as a function of B normalized to the constituent quark mass for $B = 0$ as a function of the temperature normalized to the transition temperature $T_{\mathrm{pc},B=0}$ for $B = 0$ for the three different approximations is shown in Fig. 23. For all temperatures, we see that the constituent quark mass is an increasing function of the magnetic field; thus the system shows magnetic catalysis. This is the reason for the increase of the transition temperature as a function of B displayed in Fig. 22.[13] We note that magnetic catalysis is less pronounced in the LPA as compared to the mean-field approximation and this can probably be attributed to the mesonic fluctuations that tend to counteract symmetry breaking (Andersen and Tranberg, 2012). The inclusion of the wave-function renormalizaton terms increases magnetic catalysis as a function of B such that the transition temperature lies between the mean-field and the LPA curves. Again, it would be of interest to see the effects of adding the Polyakov-loop variable.

We next consider the wave-function renormalization terms $Z_k^\parallel$ and $Z_k^\perp$. The regulator functions chosen are the anisotropic functions

$$R_k^B(p) = (k^2 - p_z^2)Z_k^\parallel \theta(k^2 - p_z^2), \tag{179}$$

$$R_k^F(p) = -\not{p}_z\left(\frac{k}{|p_z|} - 1\right)\theta(k^2 - p_z^2), \tag{180}$$

[13]The small dip in the LPA curve is probably due to numerical error (Kamikado and Kanazawa, 2015a).

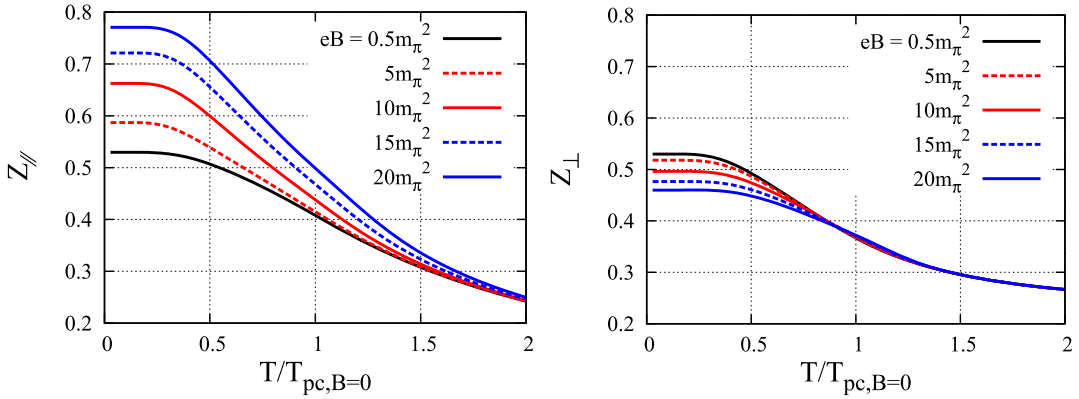

FIG. 24. Wave-function renormalization terms $Z^{\parallel}_{k=0}$ and $Z^{\perp}_{k=0}$ as functions of the normalized temperature for various magnetic fields. From Kamikado and Kanazawa, 2014.

where $\not{p}_z = \gamma_3 p_z$. Note that the regulators do not suppress $p_\perp^2$ and that they break rotational invariance even for $B = 0$. However, they give rise to a simple scale-dependent fermion propagator and so it is useful for practical calculations. The boundary condition for the wave-function renormalization terms at $k = \Lambda$ and $B = 0$ is $Z^{\parallel}_{k=\Lambda} = Z^{\perp}_{k=\Lambda} = 1$. Because of the $O(4)$ symmetry at $B = 0$, we have $Z^{\parallel}_{k=0} = Z^{\perp}_{k=0}$. However, due to the breaking of rotational invariance, they instead fine-tuned $Z^{\parallel}_{k=\Lambda}$ and $Z^{\perp}_{k=\Lambda}$ such that $Z^{\parallel}_{k=0} = Z^{\perp}_{k=0}$ at $T = 3$ MeV and $|qB| = 0.5m_\pi^2$. This gives the values $Z^{\parallel}_{k=\Lambda} = 0.002$ and $Z^{\perp}_{k=\Lambda} = 0.236$.

The wave-function renormalization terms $Z^{\parallel}$ and $Z^{\perp}$ as functions of the normalized temperature for various strengths of the magnetic field are shown in Fig. 24. We first notice that while $Z^{\parallel}_{k=0}$ increases with the magnetic field, $Z^{\perp}_{k=0}$ decreases. This can probably be attributed to the fact that the flow equation of the former has an explicit B dependence, while the flow equation of the latter does not. Second, all curves meet for sufficiently large temperatures and that the curves for $Z_\perp$ have done so already before the transition temperature.

VIII. MAGNETIC CATALYSIS

In this section, we discuss magnetic catalysis at $T = 0$. Magnetic catalysis is the effect of either of the following:

(1) The magnitude of a condensate is enhanced by the presence of an external magnetic field B if the condensate is already present for zero magnetic field.
(2) An external magnetic field induces symmetry breaking and the appearance of a condensate when the symmetry is intact for $B = 0$.

Case (2) is also referred to as dynamical symmetry breaking by a magnetic field. In the context of low-energy effective theories of QCD, the condensate is the nonzero expectation value of the sigma field or the quark condensate. The early works on magnetic catalysis dated back to the late 1980s and early 1990s and focused on the NJL model in $2 + 1$ dimensions (Klimenko, 1991, 1992a, 1992b; Gusynin, Miransky, and Shovkovy, 1994, 1995a) and in $3 + 1$ dimensions (Klevansky and Lemmer, 1989; Gusynin, Miransky, and Shovkovy, 1995b; Ebert and Klimenko, 1999; Klimenko and Zhukovsky, 2008), and QED (Gusynin, Miransky, and Shovkovy, 1995c, 1997, 1999). Other applications are in QCD (Miransky and Shovkovy, 2002; Ozaki, 2014) and the Walecka model in nuclear physics (Haber, Preis, and Schmitt, 2014). Magnetic catalysis is now considered a generic feature of matter in an external magnetic field (Shovkovy, 2013).

Inspecting the dispersion relation for fermions in a magnetic field $E_k = \sqrt{m_f^2 + p_z^2 + |q_f B|(2k + 1 - s)}$ we see that it resembles the dispersion relation of a massive particle in one spatial dimension with an effective mass $M^2_{\text{eff}} = m_f^2 + |q_f B|(2k + 1 - s)$. Only for fermions with spin $1/2$ ($s = 1$) in the lowest Landau level ($k = 0$) is this effective mass independent of the magnetic field. This property distinguishes spin-$1/2$ fermions from bosons; cf. the spectrum, Eq. (20). When the fermionic mass scale is much smaller than the magnetic mass scale $m_f^2 \ll |q_f B|$, the higher Landau levels decouple from the low-energy dynamics and the long-distance behavior is determined by the lowest Landau level. Since the particles in the lowest Landau level essentially are confined to move along the magnetic field, i.e., the z axis, the system becomes effectively one dimensional and the system exhibits dimensional reduction $D = 3 + 1 \to 1 + 1$. The $(1 + 1)$-dimensional character of the lowest Landau level at low momentum can also be inferred from the form of the fermion propagator given by Eq. (18). Isolating the $k = 0$ contribution, we find

$$\tilde{S}_0(p^0, p^3, \mathbf{p}_\perp) = i \exp\left(-\frac{p_\perp^2}{|q_f B|}\right) \frac{\gamma^0 p^0 - \gamma^3 p^3 + m_f}{p_\parallel^2 - m_f^2} \times [1 + i s_\perp \gamma^1 \gamma^2], \tag{181}$$

where we used $L^a_{-1}(x) = 0$. Note that dimensional reduction does not take place for bosons as the ground-state energy is not vanishingly small compared to the energy of the first excited state $k = 0$ and 1 in Eq. (20).

At this point, a few remarks on dimensional reduction and spontaneous symmetry breaking are in order. We have seen that a magnetic field enhances (spontaneous) symmetry breaking as well as reduces the system to being essentially $1 + 1$ dimensional. However, we know from the Coleman theorem that there is no spontaneous symmetry breaking of a

continuous symmetry in $1+1$ dimension and therefore no massless Nambu-Goldstone boson can exist (Coleman, 1973).[14] The point here is that $\langle\bar{\psi}\psi\rangle$ is neutral with respect to the magnetic field and that the Goldstone boson π^0 is a neutral excitation with respect to the magnetic field (Gusynin, Miransky, and Shovkovy, 1996). The motion of the center of mass of π^0 is not restricted to being along the magnetic field as it is an electrically neutral particle.

Let us discuss the NJL model first. For simplicity, we consider the chiral limit $m_0 = 0$ and the case $N_c = N_f = 1$. If we denote the constituent quark mass by M, the mean-field contribution to the free energy density is given by $M^2/2G$; cf. the first two terms in Eq. (102) with $M_0 = M_3 = M$ for $c = 0$. Using a four-dimensional ultraviolet cutoff Λ, the one-loop contribution to the effective potential for $B = T = 0$ is given by Eq. (46). In the limit $M \ll \Lambda$, we find

$$\mathcal{F} = \frac{M^2}{2G} + \frac{1}{(4\pi)^2}\left[-2\Lambda^2 M^2 + \frac{1}{2}M^4 + M^4 \ln\frac{\Lambda^2}{M^2}\right]. \quad (182)$$

The minimum is found by solving the gap equation, which reads

$$M\left[\frac{4\pi^2}{G} - \Lambda^2 + M^2 \ln\frac{\Lambda^2}{M^2}\right] = 0. \quad (183)$$

$M = 0$ is always a solution. However, a nontrivial solution exists for $G > G_c = 4\pi^2/\Lambda^2$. Hence, for couplings larger than the critical value G_c, quantum fluctuations induce symmetry breaking in the model. The possible solutions to the gap equation in a constant magnetic field were first considered by Klevansky and Lemmer (1989). For finite magnetic field, the gap equation is

$$\frac{4\pi^2}{G} - \Lambda^2 + M^2 \ln\left(\frac{\Lambda^2}{M^2}\right) - |2q_f B|\left[\zeta^{(1,0)}(0, x_f) + x_f - \frac{1}{2}(2x_f - 1)\ln x_f\right] = 0, \quad (184)$$

where $x_f = M^2/2|q_f B|$ as before. For nonzero magnetic field B and any G, this equation has only a nonzero solution for M. Consequently, for $G < G_c$, a nonzero magnetic field induces symmetry breaking when the symmetry is intact for $B = 0$. This effect was first observed in the context of the NJL model in $2+1$ dimensions by Klimenko (1991, 1992a, 1992b). For $G < G_c$, the solution to Eq. (184) is (Gusynin, Miransky, and Shovkovy, 1995b)

$$M^2 = \frac{|q_f B|}{\pi}\exp\left[-\frac{1}{|q_f B|}\left(\frac{4\pi^2}{G} - \Lambda^2\right)\right]. \quad (185)$$

[14]This applies to massless excitations that are linear in the momentum p for small p. Magnons are massless excitations in ferromagnets that are quadratic in the momentum p for small p and exist in $1+1$ dimension. Linear Goldstone modes exist in $2+1$ dimensions at $T = 0$. See, e.g., Watanabe and Murayama (2014) for a detailed discussion.

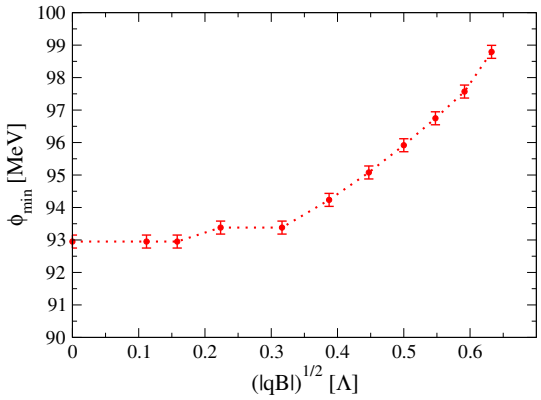

FIG. 25. Magnetic catalysis in the quark-meson model at the physical point and at $T = 0$. The vacuum expectation value of the field ϕ as a function of the magnetic field scaled by the ultraviolet cutoff Λ.

The gap (185) connects to the trivial solution in the limit $|q_f B| \to 0$ as it should. Moreover, Eq. (185) has an essential singularity at $G = 0$, which shows its nonperturbative nature: i.e., it is obtained by summing Feynman graphs from all orders of perturbation theory. Any finite-order perturbative calculation yields a vanishing gap.[15] In the lowest Landau level approximation, the solution to the gap equation (184) is $M^2 = \Lambda^2 \exp[-4\pi^2/G|q_f B|]$, where Λ is the cutoff. This has the same form as Eq. (185) if we identify the cutoff Λ with $\sqrt{|q_f B|}$. Thus dynamical symmetry breaking is essentially a $(1+1)$-dimensional phenomenon. Furthermore, it is interesting to note the dependence on G in Eq. (185) is the same dependence as the solution to the gap equation in the BCS theory for superconductivity (albeit at zero magnetic field) (Gusynin, Miransky, and Shovkovy, 1996; Shovkovy, 2013). Because of the Fermi surface, the dynamics is also $1+1$ dimensional.

We next turn to the QM model. As shown in Fig. 8, the minimum ϕ of the one-loop effective potential at zero temperature is an increasing function of B. Thus the model exhibits magnetic catalysis. If $m^2 > 0$, there is no spontaneous symmetry at zero magnetic field, but at nonzero B, the gap is $\phi^2 \sim |qB|\exp[-m^2/|qB|]$; cf. Eq. (185).

Let us next discuss the functional renormalization group. In Fig. 25, we show the minimum of the effective potential $U_{k=0}(\phi)$ at $T = 0$ as a function of $(|qB|)^{1/2}/\Lambda$ in the quark-meson model using the functional renormalization group. We see that the minimum is an increasing function of the magnetic field, so the model shows magnetic catalysis.

There have been a number of lattice calculations of the chiral condensate at $T = 0$ as a function of the magnetic field both in the quenched approximation (Buividovich *et al.*, 2010a, 2010b; Braguta *et al.*, 2012) and with dynamical quarks (D'Elia and Negro, 2011; Endrődi, 2013).

[15]Recall that the N_c expansion is nonperturbative in the sense that each order corresponds to a sum of Feynman diagrams from all orders of perturbation theory. The large N_c is the sum of all daisy and superdaisy graphs.

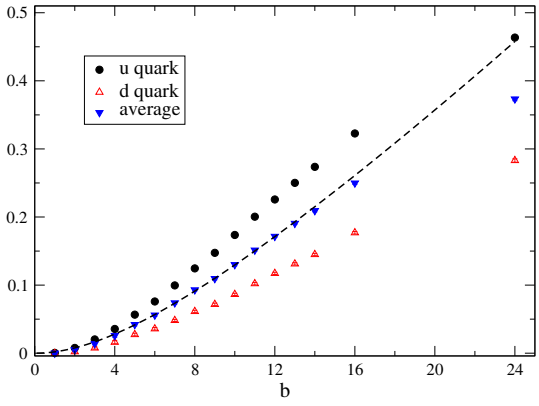

FIG. 26. Relative increment of the $\langle \bar{u}u \rangle$ (black circles) and $\langle \bar{d}d \rangle$ (red up triangles) condensates as well as their average (blue down triangles) as a function of b, where $|qB| \sim b(180\ \mathrm{MeV})^2$. From D'Elia and Negro, 2011.

In Fig. 26, the results for the relative increment of the condensates $\langle \bar{u}u \rangle$ and $\langle \bar{d}d \rangle$ as well as their average are shown as functions of the magnetic field (D'Elia and Negro, 2011). We notice that the $\bar{u}u$ condensate is larger than the $\bar{d}d$ in agreement with model calculations; cf. Fig. 5.

Bali *et al.* (2012d) defined the dimensionless quantity

$$\Sigma_f(B,T) = \frac{2m_f}{m_\pi^2 F^2}[\bar{\psi}_f\psi_f(B,T) - \bar{\psi}_f\psi_f(0,0)] + 1. \quad (186)$$

In Fig. 27, the change of the condensate $(1/2)(\langle \Delta\Sigma_u \rangle + \langle \Delta\Sigma_d \rangle)$ is shown as a function of $|qB|$ at $T = 0$ and at the physical point (Bali *et al.*, 2012d) [$\Delta\Sigma_f = \Sigma_f(B,T) - \Sigma_f(0,T)$]. The lattice results are continuum extrapolated. The model calculations are from one-loop chiral perturbation theory (Cohen, McGady, and Werbos, 2007; Andersen, 2012a, 2012b) as well as the Polyakov-loop extended NJL model (Gatto and Ruggieri, 2011). Note that at $T = 0$ the PNJL model reduces to the NJL model. Clearly, the result of the χPT calculations are in quantitative agreement with lattice simulations for magnetic fields up to

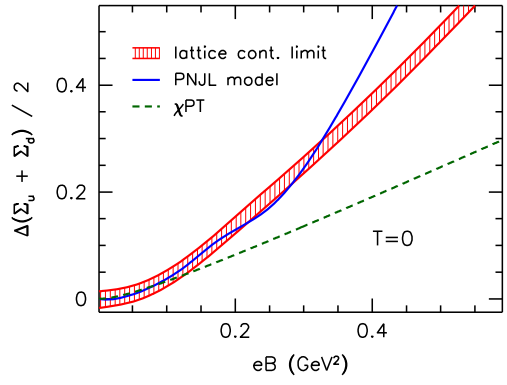

FIG. 27. Comparison of the continuum limit of the change of the condensate with that of chiral perturbation theory (Cohen, McGady, and Werbos, 2007; Andersen, 2012a, 2012b) and the (P)NJL model (Gatto and Ruggieri, 2011). From Bali *et al.*, 2012d.

$|qB| \approx 0.15\ \mathrm{GeV}^2$. For the (P)NJL model, the agreement with lattice extends up to $|qB| \approx 0.30\ \mathrm{GeV}^2$.

The behavior of the quark condensate as a function of B can also be understood in terms of the Banks-Casher relation (Banks and Casher, 1980). The quark condensate $\langle \bar{\psi}\psi \rangle$ is proportional to the spectral density $\rho(\lambda)$ of the Dirac operator around zero. The Dirac operator depends on the magnetic field, and therefore the spectral density depends on B. A constant magnetic field enhances the spectral density around zero and as a result it enhances the quark condensate; see also the discussion in Sec. IX. This behavior of the spectral density is already found in the quenched approximation (Buividovich *et al.*, 2010a, 2010b; Braguta *et al.*, 2012) in which there is no backreaction from the quarks to the non-Abelian gauge fields. In model calculations, the quark condensate is given by the expectation value of the operator $\mathrm{Tr}[\not{D}(B) + m]^{-1}$, which is enhanced by the magnetic field. This enhancement is due to an increase of the spectral density, which is a consequence of the degeneracy being proportional to the magnetic flux; cf. the discussion after Eq. (11).

Recently, Mueller, Bonnet, and Fischer (2014) investigated dynamical quark mass generation and spin polarization in a strong magnetic field B using the DS equations. They do this in both the quenched and unquenched approximations at $T = \mu_B = 0$. The starting point is the Dyson-Schwinger equation for the fermion propagator $S(x,y)$ in coordinate space

$$S^{-1}(x,y) = S_0^{-1}(x,y) + \Sigma(x,y), \quad (187)$$

where $S_0(x,y)$ is the free fermion propagator and $\Sigma(x,y)$ is the fermion self-energy

$$\Sigma(x,y) = ig^2 C_F \gamma^\mu S(x,y)\Gamma^\nu(y)D_{\mu\nu}(x,y), \quad (188)$$

where

$$C_F = \frac{N_c^2 - 1}{2N_c},$$

$\Gamma^\nu(y)$ is the dressed fermion vertex and $D_{\mu\nu}(x,y)$ is the quenched gluon propagator. The quenched gluon propagator in momentum space can be written as $D_{\mu\nu}(k^2) = D(k^2)P_{\mu\nu}$, where the projection operator is $P_{\mu\nu} = \delta_{\mu\nu} - k_\mu k_\nu/k^2$. The fermion propagator in the Ritus representation (Ritus, 1978) is

$$S(x,y) = \sum_{k=0}^{\infty} \int \frac{d^2p_\parallel}{(2\pi)^4} \int_{-\infty}^{\infty} dp_2 E_p(x) \times \frac{1}{i\gamma\cdot p_\parallel A_\parallel(p) + i\gamma\cdot p_\perp A_\perp(p) + B(p)} \bar{E}_p(y), \quad (189)$$

where $A_\parallel(p)$, $A_\perp(p)$, and $B(p)$ are the so-called dressing functions. By taking the trace in the Dyson-Schwinger equation, one finds a set of coupled equations for these functions.

The gluon propagator function $D(k^2)$ is written in terms of the dressing function $Z(k^2)$ via $D(k^2) = Z(k^2)/k^2$. The

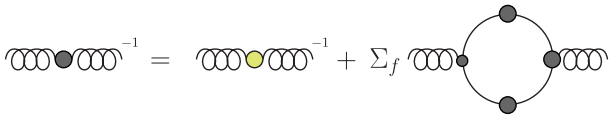

FIG. 28. Dyson-Schwinger equation for the inverse gluon propagator.

function $D(k^2)$ has been calculated to high precision both on the lattice (Leinweiber, 1999, 2000) and by solving the Dyson-Schwinger equations (Fischer, Maas, and Pawlowski, 2009; Huber and von Smekal, 2013). The quenched gluon propagator is used as input to the Dyson-Schwinger equation together with the dressed vertex $\Gamma^{\mu}(p)$. The latter is, however, poorly known, and Mueller, Bonnet, and Fischer (2014) made a simple *Ansatz* for it.

In the unquenched approximation, the gluon propagator is improved by taking into account the quark loop in the Dyson-Schwinger equation. This is shown diagrammatically in Fig. 28 and the Dyson-Schwinger equation in momentum space can then be written as

$$D_{\mu\nu}^{-1}(k) = (D_{\mu\nu}^{-1})_0(k) + \Pi_{\mu\nu}^{\mathrm{g}}(k) + \Pi_{\mu\nu}^{\mathrm{q}}(k) \approx D_{\mu\nu}^{-1,\mathrm{eff}}(k) + \Pi_{\mu\nu}^{\mathrm{q}}(k), \tag{190}$$

where $D_{\mu\nu}^{-1,\mathrm{eff}}(k)$ is an effective inverse propagator corresponding to the first diagram on the right-hand side in Fig. 28. The self-energy $\Pi_{\mu\nu}^{\mathrm{q}}(k)$ corresponds to the quark loop in Fig. 28. The big blobs represent dressed propagators and dressed vertices. Since the term $D_{\mu\nu}^{-1,\mathrm{eff}}(k)$ is isotropic, it is the quark loop that generates the anisotropies in the dressed gluon propagator.

Figure 29 displays the regularized[16] $\langle \bar{u}u \rangle$ (solid black line) and $\langle \bar{d}d \rangle$ quark condensates (solid red line) in the unquenched approximation as a function of the magnetic field. For comparison, the $\langle \bar{u}u \rangle$ condensate (dashed black line) in the quenched approximation has been shown as well. One observes that the condensates are different. This simply reflects the isospin breaking due to the different electric charges of the u and d quarks. The most interesting result is that the quenched condensate is larger than the unquenched condensate. Taking the backreaction of the quarks on the gluonic sector leads to reduced magnetic catalysis. Whether this leads to inverse magnetic catalysis around T_c is an open question, but it is certainly of interest to investigate it.

A similar approach was used by Watson and Reinhardt (2014), in which the Dyson-Schwinger equation was studied in the rainbow approximation. In this approximation, the dressed quark-gluon vertex is replaced with the bare (tree-level) vertex, while the quark propagator and its inverse are dressed. The gluon dressing function has a phenomenological form that has been used to study dynamical chiral symmetry breaking. They pay particular attention to the weak-field limit and so this is complementary to Mueller, Bonnet, and Fischer (2014). In order to connect to the case $B = 0$, a

[16]The condensate of a heavy quark has been subtracted to obtain a finite result (Mueller, Bonnet, and Fischer, 2014).

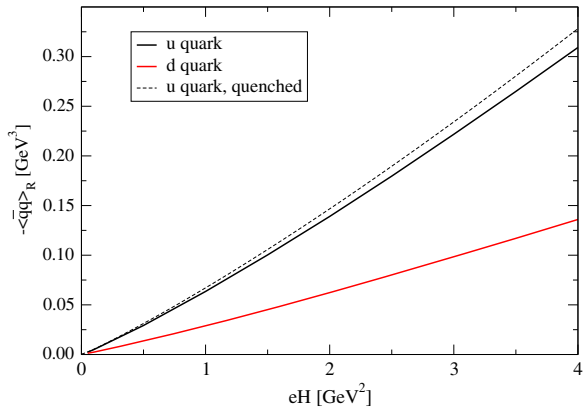

FIG. 29. Regularized $\langle \bar{u}u \rangle$ (black) and $\langle \bar{d}d \rangle$ quark condensates (red) together with the $\langle \bar{u}u \rangle$ condensate in the quenched approximation (dashed). From Mueller, Bonnet, and Fischer, 2014.

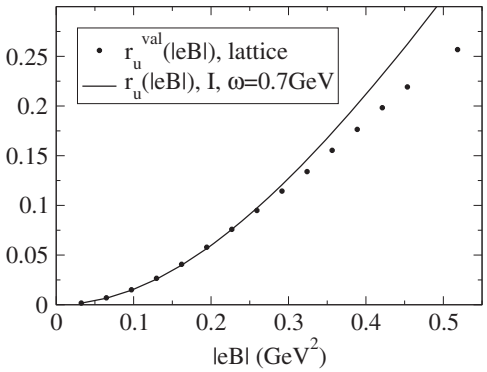

FIG. 30. Comparison of the up-quark relative increment with the lattice results of D'Elia and Negro (2011). ω is a parameter of the gluon dressing function. From Watson and Reinhardt, 2014.

nonperturbative approximation to the quark propagator is constructed, which involves a summation over the Landau levels. If one does not sum over Landau levels, the mass gap vanishes in the limit $B \to 0$, which is incorrect (see Fig. 29). In Fig. 30, the relative increment [see also Eq. (195)] is shown using the Dyson-Schwinger approach as well as lattice results from D'Elia and Negro (2011). The agreement is very good up to field strengths of $|qB| = 0.3$ GeV^2. One must be cautious, however, as the DS equations are solved in the chiral limit, while the lattice results are for quark masses that correspond to $m_\pi \approx 200$ MeV.

IX. LATTICE SIMULATIONS AND INVERSE MAGNETIC CATALYSIS

As discussed in the Introduction, QCD at zero baryon chemical potential μ_B in an Abelian background field A_μ^{EM} is free of the sign problem and so QCD can in principle be straightforwardly simulated on the lattice using standard Monte Carlo algorithms. This statement is independent of the color gauge group, which opens up the possibility for doing lattice simulations for different theories. In this section, we discuss lattice simulations and inverse magnetic catalysis for both $N_c = 2$ and 3.

A. SU(3)$_c$

In the physical case $N_c = 3$ and with $N_f = 2$, the first lattice simulations at finite magnetic field were carried out by D'Elia, Mukherjee, and Sanfilippo (2010). They used different values of the bare quark masses corresponding to a pion mass in the 200–480 MeV range. The magnetic field strengths were up to $|qB| \sim 0.75$ GeV^2 and the calculations were carried out with a lattice spacing of 0.3 fm and the results were not continuum extrapolated. They found no evidence for a splitting between the chiral and deconfinement transitions in contrast to the PNJL and PQM model calculations. They also found that the critical temperature increases very slowly with the magnetic field as can be seen in Fig. 31. The results seem to be in agreement with model calculations presented in Secs. V and VII.

Bali *et al.* (2012c, 2012d) carried out lattice simulation using the physical pion mass of $m_\pi = 140$ MeV. Their results are shown in Fig. 32. Their results have been continuum extrapolated and show, perhaps somewhat surprisingly, that the transition temperature is decreasing with the magnetic field B. The results suggest that the critical temperature is a complicated function of the magnetic field and the quark masses.

Endrődi (2015) carried out lattice simulations up to magnetic fields of $|qB| = 325$ GeV^2. In addition, the limit $B \to \infty$ was simulated directly, by considering the effective theory relevant for this limit. This theory is an anisotropic pure gauge theory (Miransky and Shovkovy, 2002). There is strong evidence that this theory has a first-order transition implying that the QCD phase diagram has a critical point and the location of it was estimated based on lattice data. The resulting phase diagram is shown in Fig. 33. Note, in particular, that the numerical simulations suggest that T_c decreases with B for all values of B.

Recently Bali *et al.* (2012c, 2012d) and Bruckmann, Endrődi, and Kovacs (2013) analyzed in detail lattice results and thereby explained the discrepancy for T_c as a function of B between the model calculations such as (P)NJL and (P)QM models and their results.

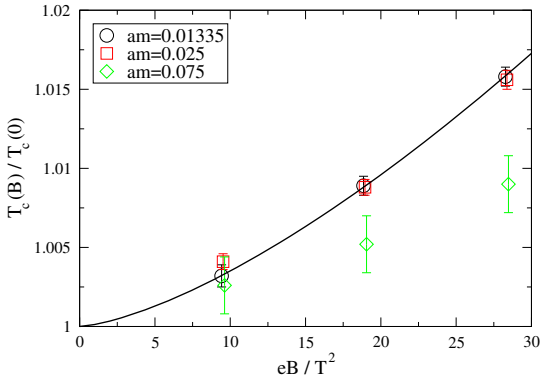

FIG. 31. Transition temperature normalized to T_c at $B = 0$ for the deconfinement and the chiral transition as a function of $|qB|/T^2$. Here $T = 1/N_t a$, where N_t is the number of lattice points and a is the lattice spacing. From D'Elia, Mukherjee, and Sanfilippo, 2010.

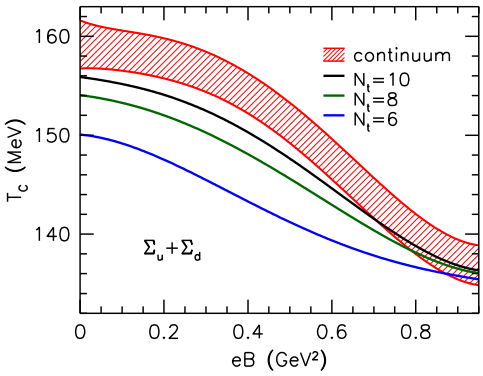

FIG. 32. Transition temperature for the deconfinement as a function of $|qB|$ for different lattice spacings (solid curves) and the continuum-extrapolated result (band). From Bali *et al.*, 2012a.

The chiral condensate can be written as

$$\langle\bar{\psi}\psi\rangle = \frac{1}{\mathcal{Z}(B)}\int d\mathcal{U}e^{-S_g}\det[\not{D}(B)+m]\mathrm{Tr}[\not{D}(B)+m]^{-1}, \tag{191}$$

where the partition function $\mathcal{Z}(B)$ is

$$\mathcal{Z}(B) = \int d\mathcal{U}e^{-S_g}\det[\not{D}(B)+m], \tag{192}$$

and S_g is the pure-glue action. The magnetic field enters via the operator $\mathrm{Tr}[\not{D}(B)+m]^{-1}$ as well as the fermion functional determinant $\det(\not{D}(B)+m)$. We can think of $\mathcal{P}(m,U,B) \equiv [1/\mathcal{Z}(B)]e^{-S_g}\det(\not{D}(B)+m)$, where U denotes the gauge-field configuration that corresponds to e^{-S_g} as a measure. In order to study the contributions to magnetic catalysis coming separately from the change in the operator and in the measure, one defines the two condensates

$$\langle\bar{\psi}\psi\rangle^{\mathrm{val}} = \frac{1}{\mathcal{Z}(0)}\int d\mathcal{U}e^{-S_g}\det[\not{D}(0)+m]\mathrm{Tr}[\not{D}(B)+m]^{-1}, \tag{193}$$

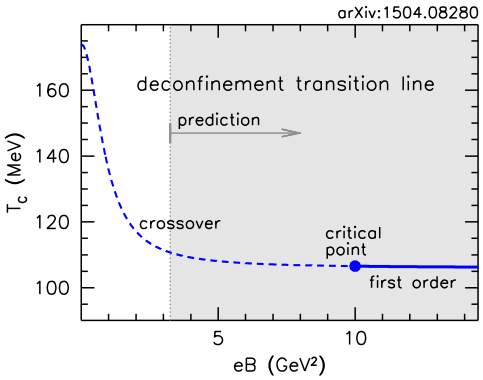

FIG. 33. Phase diagram in the B-T plane. From Endrődi, 2015.

$$\langle\bar{\psi}\psi\rangle^{\text{sea}} = \frac{1}{\mathcal{Z}(B)}\int d\mathcal{U}e^{-S_g}\det[\not{D}(B)+m]\mathrm{Tr}[\not{D}(0)+m]^{-1}. \tag{194}$$

These are the so-called valence and sea condensates. The valence condensate is the average of the trace of the propagator in a constant magnetic background, but where the sampling of the non-Abelian gauge configurations is done at $B=0$. The sea contribution is the average of the same operator in zero magnetic field, but where the sampling is done at nonzero B. The sea effect is absent in the quenched approximation. More generally, a sea observable is an observable that does not depend explicitly on the magnetic field. The Polyakov loop is another example of a sea observable. We note that the sea condensate equals a condensate of a neutral quark in a two-flavor theory with one electrically charged and one neutral quark since the magnetic field does not appear in the operator, but in the determinant.

A useful quantity is the relative increment $r(B)$ of the quark condensate as a function of B, which is defined by

$$r(B) = \frac{\langle\bar{\psi}\psi\rangle(B)}{\langle\bar{\psi}\psi\rangle(0)} - 1. \tag{195}$$

The relative increments $r^{\text{val/sea}}(B)$ are defined in a similar manner. D'Elia and Negro (2011) calculated the three quantities $r(B)$, $r^{\text{val}}(B)$, and $r^{\text{sea}}(B)$ at zero temperature. The result is shown in Fig. 34. The valence contribution $r^{\text{val}}(B)$ (up triangles, red data points) and the sea contribution $r^{\text{sea}}(B)$ (down triangles, blue data points) are both positive. The sum of the two (open circles) and $r(B)$ (full circles) are shown as well. We notice that the open circles are very close to the full circles, except for very large values of B, which suggests that the relative increment can be written as a sum of the valence and sea contributions. The same behaviors of $r^{\text{val}}(B)$ and $r^{\text{sea}}(B)$ are found in the simulations by Bruckmann, Endrődi, and Kovacs (2013) for physical quark masses at $T=0$.

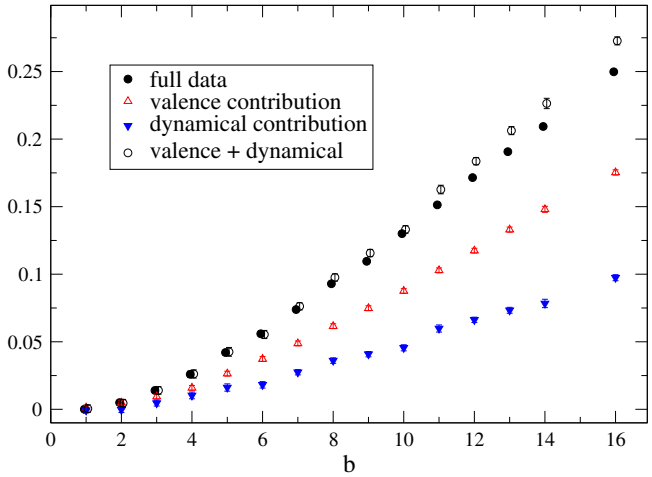

FIG. 34. Relative increments $r(B)$, $r^{\text{val}}(B)$, and $r^{\text{sea}}(B)$ at zero temperature See the main text for details. From D'Elia and Negro, 2011.

As mentioned earlier, it is possible to understand the behavior of the valence condensate by employing the Banks-Casher relation (Banks and Casher, 1980). In the chiral limit, the chiral condensate is proportional to the spectral density $\rho(\lambda)$ of the Dirac operator around zero. In Fig. 35, Bruckmann, Endrődi, and Kovacs (2013) showed the spectral density for three values of the magnetic field B. The ensembles of non-Abelian gauge-field backgrounds are generated at zero magnetic field and at $T=142$ MeV. It is evident from Fig. 35 that the spectral density and therefore the valence condensate increases with the strength of the magnetic field. This behavior is independent of the temperature.

At temperatures around the transition temperature, the valence condensate is still positive while the sea condensate is negative. Hence there is a competition between the two, leading to a net inverse catalysis. The sea contribution can be viewed as a backreaction of the fermions on the gauge fields and this effect is not present in the model calculations as there are no dynamical gauge fields. The behavior of the sea contribution was also carefully analyzed by Bruckmann, Endrődi, and Kovacs (2013). Introducing $-\Delta S_f(B) = \log\det[\not{D}(B)+m] - \log\det[\not{D}(0)+m]$, one can rewrite the full condensate as

$$\langle\bar{\psi}\psi\rangle = \frac{\langle e^{-\Delta S_f(B)}\mathrm{Tr}[\not{D}(B)+m]^{-1}\rangle_0}{\langle e^{-\Delta S_f(B)}\rangle_0}, \tag{196}$$

where the subscript 0 indicates that the expectation values are at $B=0$. We note that Eq. (196) reduces to the valence condensate if we replace the exponential factor $e^{-\Delta S_f(B)}$ by unity.

In Fig. 36, Bruckmann, Endrődi, and Kovacs (2013) showed a scatter plot of the condensate as a function of the change in the action $\Delta S_f(B)$ due to the magnetic field for a magnetic field strength of $|qB| \approx 0.5$ GeV^2 and T around the transition temperature. Each point represents a gauge configuration and they were generated at $B=0$, and therefore a simple averaging of $\mathrm{Tr}[\not{D}(B)+m]^{-1}$ without weighting each configuration in the ensemble with the Boltzmann factor $e^{-\Delta S_f(B)}$ gives the valence condensate. In order to calculate the full quark condensate, one

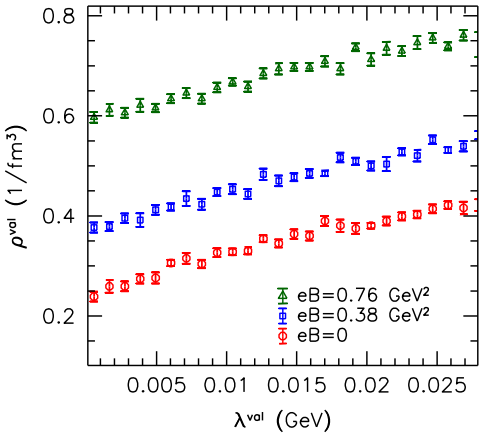

FIG. 35. Spectral density of the Dirac operator for three different values of the magnetic field B. From Bruckmann, Endrődi, and Kovacs, 2013.

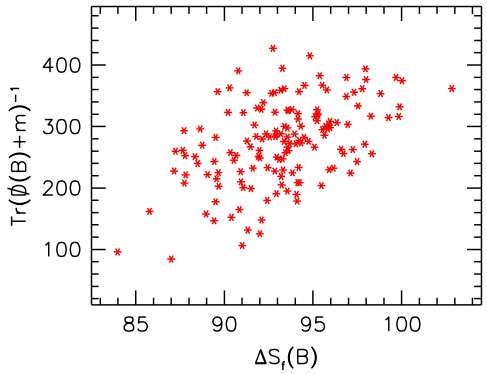

FIG. 36. Scatter plot of the down-quark condensate as a function of $\Delta S_f(B)$. The magnetic field strength is $|qB| \approx 0.5$ GeV^2 and $T \sim T_c$. From Bruckmann, Endrődi, and Kovacs, 2013.

must average $\mathrm{Tr}[\not{D}(B) + m]^{-1}$ over the gauge configurations including the weight factor $e^{-\Delta S_f(B)}$. Generally, larger values of the condensate correspond to larger values of $\Delta S_f(B)$ and, as a result, the weight of the associated gauge configuration is suppressed. This suppression is particularly effective around T_c and in fact overwhelms the valence effect and therefore leads to inverse magnetic catalysis in the transition region. This suppression is not present for larger quark masses; cf. Fig. 34. One therefore might expect the sea effect to be even more pronounced in the chiral limit. We finally add that the recent simulations of Bornyakov *et al.* (2014) with large quark masses that correspond to a pion mass of approximately 500 MeV show a different behavior. Using chiral fermions instead of staggered fermions, they found clear evidence for inverse magnetic catalysis also for large pion masses. The analysis was based on the behavior of the chiral condensate, the expectation value of the Polyakov loop, as well as the spectral density as functions of B for two different values of the temperature. The results seem to indicate that the chiral properties are an important ingredient in inverse magnetic catalysis.

B. SU(2)$_c$

Recently, Ilgenfritz *et al.* (2012, 2014) carried out lattice simulations with dynamical fermions. We focus on their second paper, which is an extension of the first to smaller quark masses. They used $N_f = 4$ and equal electric charge as well as quark masses that correspond to a pion mass m_π of approximately 175 MeV. The transition temperature for $B = 0$ is in this case $T_c \approx m_\pi$.

Figure 37 shows the mass dependence of the bare chiral condensate for three different values of the magnetic field, $B = 0$ (gray), $|qB| = 0.67$ GeV^2 (blue), and $|qB| = 1.69$ GeV^2 (red) and two different temperatures: 147 MeV (left) and 195 MeV (right). Inspecting the left panel, the data points suggest that the system is in the chirally broken phase for all three values of the magnetic field. In contrast, the data points on the right panel indicate that the chiral condensate is zero (extrapolating to the chiral limit) for $B = 0$ and $|qB| = 0.67$ GeV^2, while the chiral condensate is nonzero for $|qB| = 1.69$ GeV^2. This behavior suggests that the critical temperature grows with B for very strong magnetic fields.

Further insight can be gained from Fig. 38, where they show the expectation values of the Polyakov loop (left panel) and the chiral condensate (right panel) at $T = 195$ MeV as functions of $|qB|$ up to $|qB| = 1.69$ GeV^2. The left panel shows a rise of the Polyakov loop for magnetic fields up to approximately $|qB| = 0.7$ GeV^2. This suggests that one goes deeper into the deconfinement region and that the system exhibits inverse magnetic catalysis at low values of the magnetic field. For values of the magnetic field larger than $|qB| = 0.7$ GeV^2, there is a significant drop of the expectation value of the Polyakov loop. This indicates that we are going back into the confinement region and that the system exhibits magnetic catalysis for large values of the magnetic field.

The results suggest that the critical temperature decreases for weak magnetic fields and increases for strong magnetic fields. A conjectured phase diagram based on these observations is shown in Fig. 39. A direct comparison with the only existing model calculation (Cruz and Andersen, 2013) is not straightforward since $N_f = 2$ with $q_u = 2/3$ and $q_d = -1/3$ were used. Nevertheless, note the similarity with Fig. 19, where a small minimum can be seen. However, to firmly conclude, a thorough analysis involving separating the valence and sea effects along the lines of Bruckmann, Endrődi, and Kovacs (2013) would be of interest.

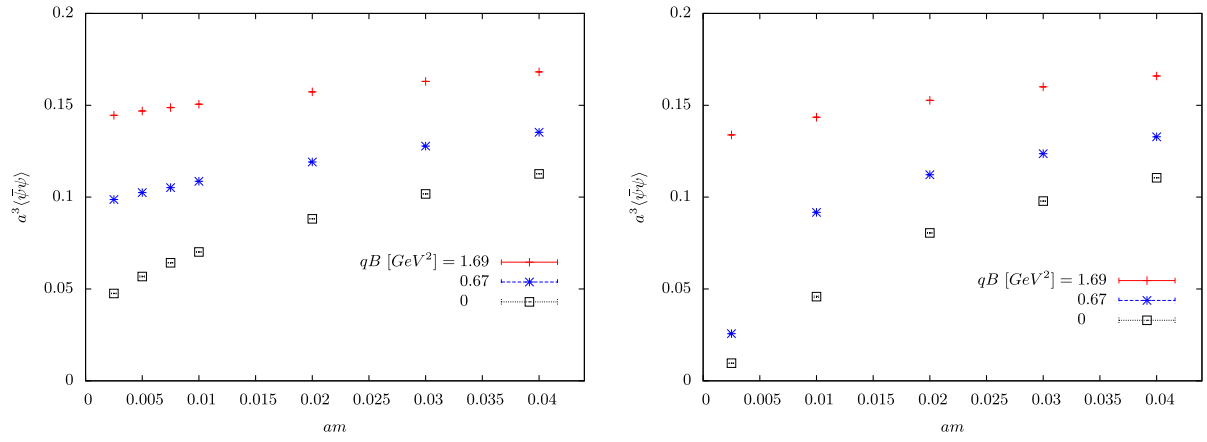

FIG. 37. Mass dependence of the bare chiral condensate for three different values of the magnetic field and two different temperatures: 147 MeV (left) and 195 MeV (right). From Ilgenfritz *et al.*, 2014.

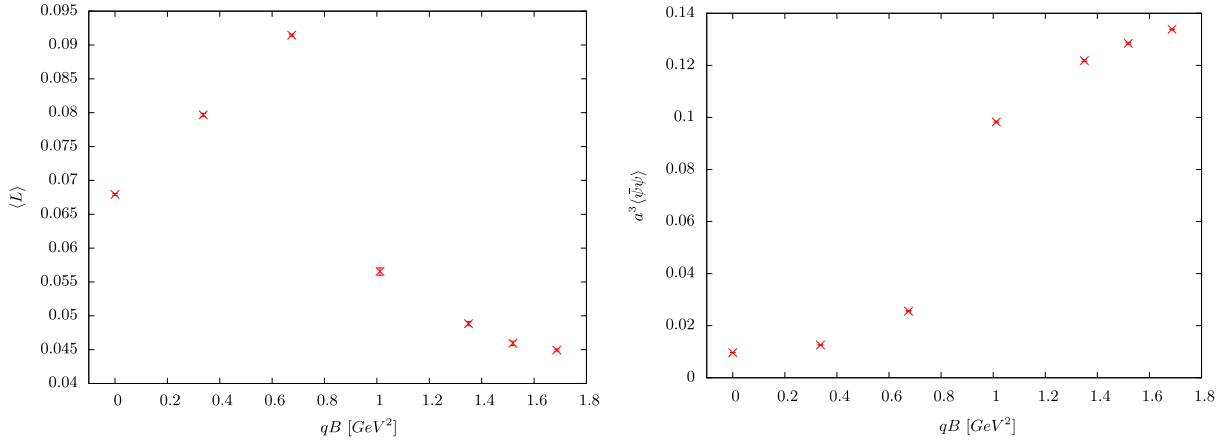

FIG. 38. Expectation values of the Polyakov loop (left) and the chiral condensate (right) vs $|qB|$ at $T = 195$ MeV. From Ilgenfritz *et al.*, 2014.

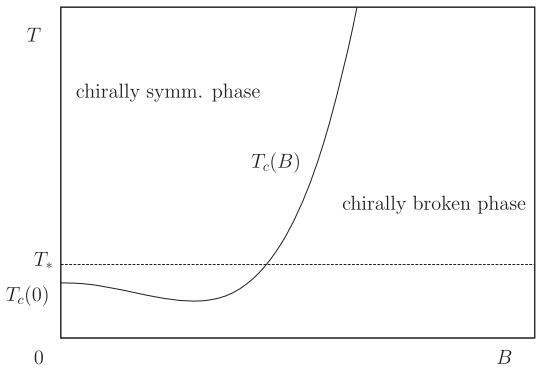

FIG. 39. Conjectured phase diagram in the B-T plane. The horizontal line is $T^* = 195$ MeV. From Ilgenfritz *et al.*, 2014.

X. MODEL CALCULATIONS REVISITED

After it was realized that most model calculations were in disagreement with the lattice calculations, there has been significant effort to modify them such that they reproduce the correct behavior of T_c as a function of B, or to propose a mechanism for inverse magnetic catalysis around T_c (Fukushima and Pawlowski, 2012; Chao, Chu, and Huang, 2013; Fraga, Noronha, and Palhares, 2013; Fukushima and Hidaka, 2013; Kojo and Su, 2013; Ayala *et al.*, 2014; Braun, Mian, and Rechenberger, 2014; Farias *et al.*, 2014; Fayazbakhsh and Sadooghi, 2014; Ferreira, Costa, Lourenco *et al.*, 2014; Ferreira, Costa, Menezes *et al.*, 2014; Ferreira, Costa, and Providência, 2014; Fraga, Mintz, and Schaffner-Bielich, 2014; Tawfik and Magdy, 2014; Yu, Liu, and Huang, 2014; Ayala, Loewe, and Zamora, 2015; Ferrer, de la Incera, and Wen, 2015; Mueller and Pawlowski, 2015; Yu, Van Doorsselaere, and Huang, 2015). A large number of papers have been focusing on B-dependent coupling constants or B-dependent parameters in the model and we discuss some of them next.

A. B-dependent transition temperature T_0

The parameter T_0 that enters the Polyakov-loop potential depends on the number of flavors N_f (and on the chemical potential at finite density). At finite B, one expects T_0 to depend on the magnetic field B as well as N_f, which can be taken into account by using a B-dependent function $b = b(N_f, B)$ in analogy with Eq. (155). The first attempt to incorporate a B-dependent transition temperature $T_0(qB)$ was made by Ferreira, Costa, Menezes *et al.* (2014) using the entangled PNJL model. They made the *Ansatz*

$$T_0(qB) = T_0(qB = 0) + \zeta(qB)^2 + \xi(qB)^4, \quad (197)$$

and fitted the parameters ζ and ξ to reproduce the transition temperature extracted from the strange quark number susceptibility data (Bali *et al.*, 2012c). This approach gives a crossover for $|qB| < 0.25$ GeV^2 and a first-order transition for $|qB| > 0.25$ GeV^2, when $T_0(qB = 0) = 186$ MeV, which corresponds to the critical temperature for $2 + 1$ massless flavors. The range of crossover transitions increases significantly by using $T_0(qB = 0) = 270$ MeV, which corresponds to the transition temperature for pure glue, i.e., by omitting the backreaction from the fermions at $B = 0$.

Recently Fraga, Mintz, and Schaffner-Bielich (2014) analyzed the possibility of inverse magnetic catalysis by allowing the parameter T_0 to be a a function of B in the PQM model. They calculated the transition temperature T_c for the chiral transition as a function of the parameter T_0 in the mean-field approximation. The result is plotted in Fig. 40. Any parametrization of $T_0(B)$ gives rise to a continuous curve that starts at some point on the black curve corresponding to $B = 0$ and crosses the other curves as B is varied. T_c as a function of B can be a decreasing function only if $T_0(B)$ decreases sufficiently fast. This can be the case for low values of the magnetic field, if the point $T_0(B = 0)$ is sufficiently far to the right on the black curve. However, since the curves become flatter as one moves to the left in the figure, it is clear that this behavior cannot be sustained. In other words, even if the critical temperature initially is decreasing with B, eventually it will have a minimum and start increasing again for larger values of B. Specific parametrizations $b(n_f, B) = b(N_f) - 60(qB)^2/m_\tau^4$ and $b(n_f, B) = b_0 - 60\sqrt{|qB|}/m_\tau$

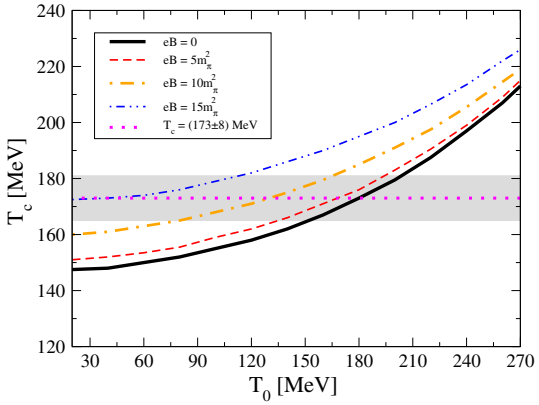

FIG. 40. Transition temperature T_c for the chiral transition as a function of T_0 for different values of the magnetic field. From Fraga, Mintz, and Schaffner-Bielich, 2014.

were given by Fraga, Mintz, and Schaffner-Bielich (2014) to illustrate this point. The result is shown in Fig. 41.

Andersen, Naylor, and Tranberg (2015) recently performed the same type of calculations using the functional renormalization group. The inclusion of mesonic fluctuations does not change the results and conclusions as anticipated by Fraga, Mintz, and Schaffner-Bielich (2014).

B. *B*-dependent coupling constant

Farias *et al.* (2014) investigated the possibility of obtaining inverse magnetic catalysis in the NJL model by using an effective coupling constant that is a function of the magnetic field B and the temperature T. Motivated by the running of the QCD coupling, they proposed a B-dependent coupling $G(B)$ given by

$$G(B) = \frac{G_0}{1 + \alpha \ln\left(1 + \beta \frac{|qB|}{\Lambda_{\mathrm{QCD}}^2}\right)}, \tag{198}$$

where $G_0 = 5.022\ \mathrm{GeV}^{-2}$ is the value of the coupling at $B = 0$. Here α and β are free parameters that are determined such that one obtains a reasonable description of the average $(1/2)(\Sigma_u + \Sigma_d)$ calculated on the lattice at $T = 0$ (Bali *et al.*, 2012d), where the dimensionless quantity Σ_f is defined in Eq. (186). We notice that $G(B) \to 0$ as $B \to \infty$, a behavior that is inspired by the running of α_s at very large magnetic fields $|qB| \gg \Lambda_{\mathrm{QCD}}^2$ (Miransky and Shovkovy, 2002): $1/\alpha_s \sim \ln(|qB|/\Lambda_{\mathrm{QCD}}^2)$. At finite temperature they propose a coupling $G(B,T)$ given by

$$G(B,T) = G(B)\left(1 - \gamma \frac{|qB|}{\Lambda_{\mathrm{QCD}}^2}\frac{T}{\Lambda_{\mathrm{QCD}}}\right). \tag{199}$$

Here γ is another parameter that is fitted to reproduce lattice data (Bali *et al.*, 2012d) for $(1/2)(\Sigma_u + \Sigma_d)$ at the highest temperatures available.

In Fig. 42, the average $(1/2)(\Sigma_u + \Sigma_d)$ is shown as a function of temperature T for different values of the magnetic field. The data points are from the lattice simulations of Bali *et al.* (2012d).

The *Ansätze* for the coupling, Eqs. (198) and (199), then give a reasonable description of the lattice data. At $T = 0$, increasing magnetic field implies larger average $(1/2)(\Sigma_u + \Sigma_d)$. However, for $T \approx 140$ MeV, the curves cross each another and the order of the curves is reversed beyond this temperature. This shows inverse magnetic catalysis around the transition temperature. The curves in Fig. 42 become steeper around the transition temperature as the magnetic field increases, suggesting that transition becomes first order for sufficiently large values of B. Strong evidence for this behavior was found by Endrődi (2015) using lattice simulations.

The thermal susceptibility is defined by

$$\chi = -m_\pi \frac{\partial \sigma}{\partial T}, \tag{200}$$

where

$$\sigma = \frac{(\langle \bar{u}u \rangle + \langle \bar{d}d \rangle)(B,T)}{(\langle \bar{u}u \rangle + \langle \bar{d}d \rangle)(B,0)}, \tag{201}$$

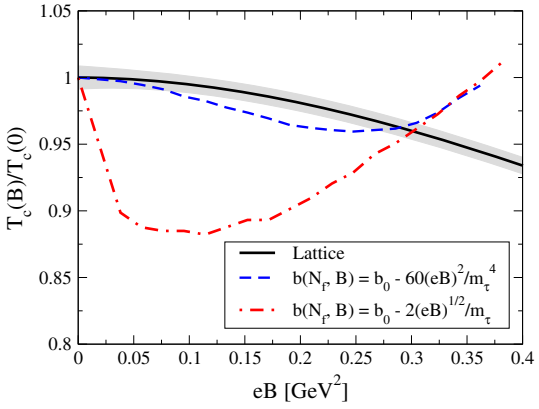

FIG. 41. Normalized transition temperature T_c for the chiral transition as a function of $|qB|$. The gray band is the lattice results from Bali *et al.* (2012d), From Fraga, Mintz, and Schaffner-Bielich, 2014.

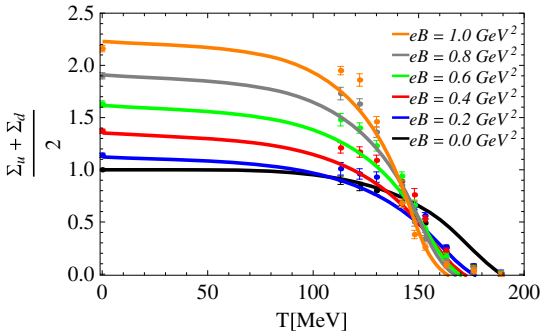

FIG. 42. The average $(1/2)(\Sigma_u + \Sigma_d)$ as a function of temperature T for different values of the magnetic field. The data points are the lattice results from Bali *et al.* (2012d). From Farias *et al.*, 2014.

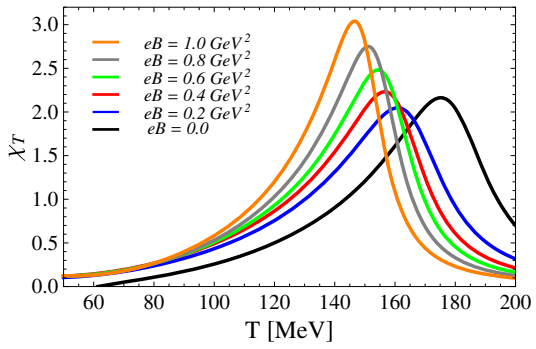

FIG. 43. Thermal susceptibility χ as a function of the temperature T for different values of the magnetic field. From Farias *et al.*, 2014.

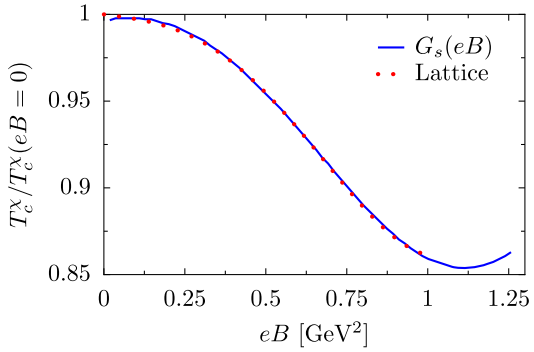

FIG. 45. Normalized pseudocritical temperature $T_c^\chi/T_c^\chi(B=0)$ as a function of $|qB|$ in the NJL model with a B and T-dependent coupling. From Ferreira, Costa, Lourenco *et al.*, 2014.

and is shown in Fig. 43 as a function of T for different values of B. The peaks move to the left as a function of the magnetic field. The peak of the thermal susceptibility χ defines a pseudocritical temperature $T_{\rm pc}$ and in Fig. 44 the pseudocritical temperature is shown as a function of $|qB|$.

A similar approach was used by Ferreira, Costa, Lourenco *et al.* (2014), where an effective coupling $G_s(|qB|/\Lambda^2_{\rm QCD})$ was determined such that the NJL model reproduces the normalized transition temperature determined on the lattice. In the fit, the lattice data points are for magnetic fields in the range $0 < |qB| < 1$ GeV^2. This way of determining the effective coupling leads to a temperature-dependent average $(1/2)(\Sigma_u + \Sigma_d)$ that qualitatively looks like the plot in Fig. 42. The resulting normalized transition temperature $T_c^\chi/T_c^\chi(B=0)$ together with lattice data points is shown in Fig. 45.

The B-dependent coupling $G_s(|qB|/\Lambda^2_{\rm QCD})$ was subsequently used as input to a PNJL calculation of the critical temperature for the chiral as well as the deconfinement transition. In the calculations, they used the value $T_0 = 210$ MeV for the parameter in the Polyakov-loop potential. The result is displayed in Fig. 46, where it is seen that a gap of approximately 30 MeV between the two transitions persists for all values of $|qB|$, with T_c for the chiral transition being higher. The interesting feature here is not the gap as such since this can probably be tuned by using a different value of T_0; rather it is the similar behavior of the two curves.

Recently Ferrer, de la Incera, and Wen (2015) studied the possibility of inverse magnetic catalysis using the NJL model in the lowest-Landau-level approximation. The starting point is the gap M at zero temperature, which is given by

$$M = \frac{2G\Lambda}{G+G'}\exp\left[-\frac{2\pi^2}{(G+G')N_c|q_fB|}\right], \qquad (202)$$

where G' is the coupling in Eq. (105). In this approximation, the phase transition is of second order and the critical temperature is given by

$$T_c = 1.16\sqrt{|q_fB|}\exp\left[-\frac{2\pi^2}{(G+G')N_c|q_fB|}\right]. \qquad (203)$$

In the absence of a magnetic field, the coupling constant G is related to the strong coupling constant α_s via the one-gluon exchange as $G = 4\pi\alpha_s/\Lambda^2$. In a magnetic field, the strong coupling splits into $\alpha_s^\parallel$ and $\alpha_s^\perp$, and only the former depends on B. Since $|q_fB|$ effectively acts as a cutoff in the LLL approximation, the effective coupling becomes $G+G' = 4\pi\alpha_s^\parallel/|q_fB|$ and so the critical temperature goes like

$$T_c = 1.16\sqrt{|q_fB|}\exp\left[-\frac{\pi}{2N_c\alpha_s^\parallel}\right]. \qquad (204)$$

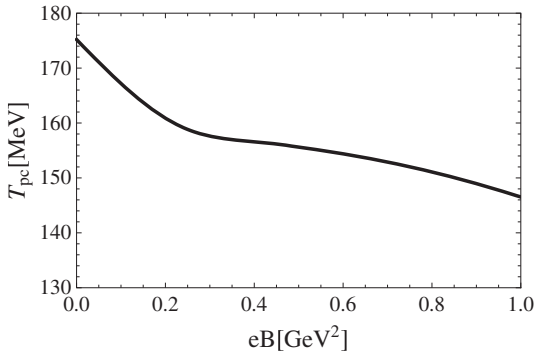

FIG. 44. Pseudocritical temperature $T_{\rm pc}$ temperature as a function of the magnetic field B in the NJL model with the B and T-dependent coupling (199). From Farias *et al.*, 2014.

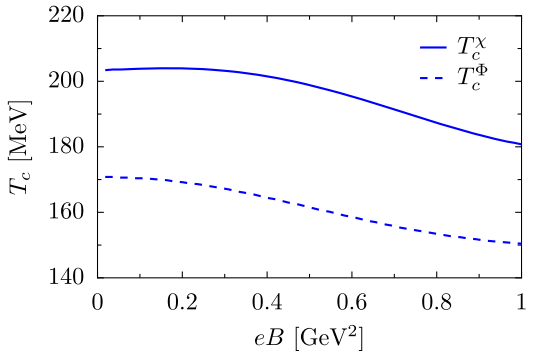

FIG. 46. Pseudocritical temperatures for the chiral (solid line) and deconfinement (dashed line) transitions as functions of $|qB|$ in the PNJL model. From Ferreira, Costa, Lourenco *et al.*, 2014.

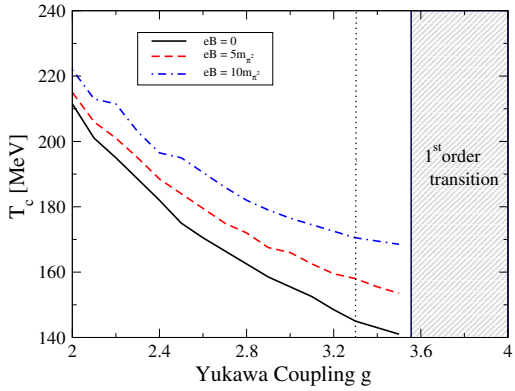

FIG. 47. T_c as a function of the Yukawa coupling g for various values of B. $B = 0$: black solid line, $|qB| = 5m_\pi^2$: red dashed line, and $|qB| = 10m_\pi^2$: blue dash-dotted line. From Fraga, Mintz, and Schaffner-Bielich, 2014.

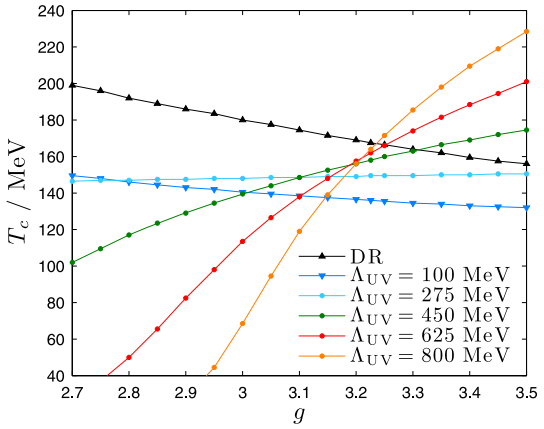

FIG. 48. Critical temperature as a function of the Yukawa coupling g for various values of the sharp cutoff as well as a renormalization scale of $\Lambda = 100$ MeV. From Andersen, Naylor, and Tranberg, 2015.

Since $\alpha_s^{\parallel}$ is a decreasing function of the magnetic field (Ferrer, de la Incera, and Wen, 2015), it is clear that T_c decreases with B.

There have been attempts at obtaining inverse magnetic catalysis by varying the Yukawa coupling g in the QM model (Fraga, Mintz, and Schaffner-Bielich, 2014). This is possible if g is an increasing function of B; see Fig. 47. However, any curve $g(B)$ must start at $g(0) = 3.22$ (indicated by the vertical dotted line) and successively cross the dashed (red) and solid (black) curves. One therefore soon enters the shaded region which indicates a first-order transition in the QM model. The existence of a critical point suggested by lattice simulations at very high B fields (Endrődi, 2015) then requires that $g(B)$ grows rapidly with B.

Motivated by the recent work on inverse magnetic catalysis at finite temperature, Andersen, Naylor, and Tranberg (2015) studied the quark-meson model using both dimensional regularization and a sharp cutoff Λ_{UV}. The critical temperature for the chiral transition was calculated as a function of the Yukawa coupling using different values of a sharp cutoff. The results are shown in Fig. 48. The results using dimensional regularization and a renormalization scale of $\Lambda = 100$ MeV and a low value for the sharp cutoff are in qualitative agreement with the results of Fraga, Mintz, and Schaffner-Bielich (2014), namely, a decreasing transition temperature as a function of g.[17] At larger values of the sharp cutoff, i.e., for more reasonable cutoffs, the transition temperature is an increasing function of the Yukawa coupling. This suggests that magnetic catalysis is much more delicate than using a B-dependent coupling constant; cf. the discussion of the sea and valence effects in Sec. IX.

Recent papers (Braun, Mian, and Rechenberger, 2014; Mueller and Pawlowski, 2015) studied the problem using the Dyson-Schwinger equation and fixed-point analysis of the effective four-quark coupling G at finite temperature and magnetic field. Here the effects of the strong coupling are incorporated in the quark gap equation and the renormalization group equation for G. The results show inverse magnetic catalysis for values of the magnetic field up to approximately $|qB| \sim 1$ GeV^2. For larger values of the magnetic field, magnetic catalysis is observed. The reason for this nonmonotonous behavior is screening effects of the gauge sector (Mueller and Pawlowski, 2015).

XI. CONCLUSIONS AND OUTLOOK

In this review, we discussed a number of low-energy models and theories that are used to describe QCD in a magnetic background at zero and finite temperature.

One aspect we think is missing in the literature is systematic studies of various approximations. As discussed, parameter fixing is important and nontrivial. There are many papers in which a certain model and a specific set of parameters are employed. However, it would be useful to compare various approximations and levels of sophistication using the same values for physical quantities. For example, it would be useful to calculate the critical temperature or the magnetization in the NJL model and its Polyakov-loop extended version and compare the two. One of the few papers where a systematic study was carried out is by Kamikado and Kanazawa (2014), where the critical temperature is calculated in the mean-field approximation, in the LPA, and beyond the LPA.

It is instructive to compare the results of the (P)NJL model and the (P)QM model at the mean-field level. In this case, only fermionic fluctuations are taken into account. If one takes into account the vacuum fluctuations of the (P)QM model, the results are similar. For example, the nature of the transition is the same and the phase diagrams closely resemble each other. This is not surprising as one is essentially evaluating the same fermionic functional determinant. However, we have seen that if the vacuum contribution is omitted in the (P)QM model, the crossover at finite pion mass turns into a first-order transition. In the same manner, the second-order transition in the chiral limit becomes first order. In the (P)NJL model it makes no sense to subtract the vacuum fluctuations as they are responsible for spontaneous symmetry breaking in the vacuum. In

[17]The result in dimensional regularization is insensitive to the precise value of Λ.

the (P)QM model, spontaneous symmetry breaking is present already at tree level provided by the quartic Higgs potential.

Regarding the calculations using the functional renormalization group, there are several directions for further improvement. For the physically most interesting cases $N_f = 2$ and 3 [see Kamikado and Kanazawa (2015b) for a recent application with $N_f = 2 + 1$], one should solve the flow equation for the effective potential as a function of the two invariants $|v|$ and $|\Delta|$, including wave-function renormalization terms in the calculations. One might consider another regulator function that ensures $Z^{\parallel}_{k=0} = Z^{\perp}_{k=0}$ in the vacuum. Finally, including new condensates that are invariant under rotations about the z axis is of interest. However, this requires the inclusion of new interaction terms in the Lagrangian of the quark-meson model and the problem is that one does not know the value of their couplings.

The most important issue that we discussed is the disagreement between model and lattice calculations regarding the behavior of the transition temperature as a function of the magnetic field. On the lattice, two contributions to the quark condensate have been identified, namely, the valence and sea contributions. While the former increases as a function of B for all temperatures, the behavior of the latter is more complicated. At zero temperature the sea contribution is also increasing with the magnetic field and together with the valence contribution, they give rise to magnetic catalysis. Around the transition temperature, however, it decreases as a function of B for physical quark masses. The sea contribution overwhelms the valence contribution such that there is a net suppression of the condensate, which leads to inverse magnetic catalysis and a decrease of the transition temperature as a function of B. The mechanism behind this effect is that the magnetic field in the quark determinant changes the relative weight of the gauge configurations and that gauge configurations with larger values of the condensate are suppressed by the quark determinant (Bruckmann, Endrődi, and Kovacs, 2013). Moreover, using staggered fermions, the backreaction of the quark determinant on the glue sector is very delicate; small quark masses lead to inverse catalysis while large quark masses lead to magnetic catalysis. Calculations employing the (P)NJL model or the (P)QM show a different behavior; the transition temperature increases with the strength of the magnetic field. In hindsight, this disagreement should perhaps not be surprising as there is no sea effect in the (P)NJL and (P)QM models. However, it is interesting to note that the coupling to the Polyakov loop in the QM model gives less magnetic catalysis around the transition temperature than without; cf. Fig. 21. Regarding the attempts to modify models to accommodate inverse magnetic catalysis, most of them simply use a B-dependent coupling, but do not couple the Polyakov-loop variable to the quark determinant. The idea of using a B-dependent parameter T_0 in the Polyakov-loop potential was implemented by Fraga, Mintz, and Schaffner-Bielich (2014); however, it was shown not to lead to inverse magnetic catalysis.

In conclusion, although the level of complexity and sophistication in model calculations of the QCD transition in a magnetic background are steadily improving, it remains a challenge to properly incorporate the phenomenon of inverse magnetic catalysis.

ACKNOWLEDGMENTS

We thank G. Bali, D. Boer, T. Brauner, F. Bruckmann, M. Chernodub, P. Costa, V. de la Incera, G. Endrődi, E. S. Fraga, V. P. Gusynin, T. Kalaydzhyan K. Kamikado, T. Kanazawa, K. G. Klimenko, S. Ozaki, M. B. Pinto, A. Schmitt, R. Stiele, M. Strickland, L. von Smekal, and P. Watson for useful discussions. We also thank the authors who have granted us permission to use their figures in this review.

APPENDIX A: NOTATION AND CONVENTIONS

We use the Minkowski metric $g_{\mu\nu} = \mathrm{diag}(1, -1, -1, -1)$ and natural units such that $k_B = \hbar = c = 1$.

We use the Dirac and chiral representations of the γ matrices. In Minkowski space they are given by

$$\gamma^0 = \begin{pmatrix} \mathbb{1} & 0 \\ 0 & -\mathbb{1} \end{pmatrix}, \qquad \boldsymbol{\gamma} = \begin{pmatrix} 0 & \boldsymbol{\sigma} \\ -\boldsymbol{\sigma} & 0 \end{pmatrix}, \tag{A1}$$

$$\gamma^0 = \begin{pmatrix} 0 & \mathbb{1} \\ \mathbb{1} & 0 \end{pmatrix}, \qquad \boldsymbol{\gamma} = \begin{pmatrix} 0 & \boldsymbol{\sigma} \\ -\boldsymbol{\sigma} & 0 \end{pmatrix}, \tag{A2}$$

where $\boldsymbol{\sigma}$ are the Pauli spin matrices. The γ matrices satisfy

$$\{\gamma^\mu, \gamma^\nu\} = 2g^{\mu\nu}\mathbb{1}, \qquad \mathrm{Tr}[\gamma^\mu\gamma^\nu] = 4g^{\mu\nu}. \tag{A3}$$

The Euclidean γ matrices are related to the γ matrices in Minkowski space by $\gamma_j = i\gamma^j$ and $\gamma_0 = \gamma^0$. They satisfy

$$\{\gamma_\mu, \gamma_\nu\} = 2\delta_{\mu\nu}\mathbb{1}, \qquad \mathrm{Tr}[\gamma_\mu\gamma_\nu] = 4\delta_{\mu\nu}. \tag{A4}$$

APPENDIX B: SUM INTEGRALS

The bosonic and fermionic sum integrals are defined by

$$\sum\!\!\!\!\!\!\int_P = T \sum_{P_0 = 2\pi n T} \int_p, \tag{B1}$$

$$\sum\!\!\!\!\!\!\int_{\{P\}} = T \sum_{P_0 = (2n+1)\pi T} \int_p, \tag{B2}$$

where the integral is in $d = 3 - 2\epsilon$ dimensions,

$$\int_p = \left(\frac{e^{\gamma_E}\Lambda^2}{4\pi}\right)^\epsilon \int \frac{d^d p}{(2\pi)^d}. \tag{B3}$$

The prefactor $(e^{\gamma_E}\Lambda^2/4\pi)^\epsilon$ is chosen such that Λ is associated with the renormalization scale in the modified minimal subtraction scheme $\overline{\mathrm{MS}}$. Here γ_E is the Euler-Mascheroni constant. In the case of particles with electric charge q moving in a constant magnetic field, the sum -integral is a sum over Matsubara frequencies P_0, a sum of Landau levels k, and an integral over momenta in $d - 2 = 1 - 2\epsilon$ dimensions. For

fermions, we also sum over spin s. We define for bosons and fermions, respectively,

$$\sum\!\!\!\!\!\!\int_P^B = \frac{|qB|}{2\pi} T \sum_{k=0}^{\infty} \sum_{P_0=2\pi n T} \int_{p_z}, \tag{B4}$$

$$\sum\!\!\!\!\!\!\int_{\{P\}}^B = \frac{|q_f B|}{2\pi} T \sum_{s=\pm 1} \sum_{k=0}^{\infty} \sum_{P_0=(2n+1)\pi T} \int_{p_z}, \tag{B5}$$

where the integral is in $d-2 = 1-2\epsilon$ dimensions,

$$\int_{p_z} = \left(\frac{e^{\gamma_E}\Lambda^2}{4\pi}\right)^{\epsilon} \int \frac{d^{d-2}p}{(2\pi)^{d-2}}. \tag{B6}$$

Equations (B4) and (B5) reduce to Eqs. (B1) and (B2) in the limit $B \to 0$.

The specific sum integrals we need are

$$\sum\!\!\!\!\!\!\int_P \ln[P_0^2 + p^2 + m^2] = -\frac{1}{2(4\pi)^2}\left(\frac{\Lambda^2}{m^2}\right)^{\epsilon}\left[\left(\frac{1}{\epsilon}+\frac{3}{2}\right)m^4 + 2J_0(\beta m)T^4 + \mathcal{O}(\epsilon)\right], \tag{B7}$$

$$\sum\!\!\!\!\!\!\int_P^B \ln[P_0^2 + p_z^2 + M_B^2] = \frac{1}{2(4\pi)^2}\left(\frac{\Lambda^2}{|2qB|}\right)^{\epsilon}\left[\left(\frac{(qB)^2}{3} - m^4\right)\left(\frac{1}{\epsilon}+1\right) + 8(qB)^2\zeta^{(1,0)}\left(-1,\frac{1}{2}+x\right) - 2J_0^B(\beta m)|qB|T^2 + \mathcal{O}(\epsilon)\right], \tag{B8}$$

$$\sum\!\!\!\!\!\!\int_{\{P\}} \ln[P_0^2 + p^2 + m_f^2] = -\frac{1}{2(4\pi)^2}\left(\frac{\Lambda^2}{m_f^2}\right)^{\epsilon}\left[\left(\frac{1}{\epsilon}+\frac{3}{2}\right)m_f^4 - 2K_0(\beta m_f)T^4 + \mathcal{O}(\epsilon)\right], \tag{B9}$$

$$\sum\!\!\!\!\!\!\int_{\{P\}}^B \ln[P_0^2 + p_z^2 + M_B^2] = -\frac{1}{(4\pi)^2}\left(\frac{\Lambda^2}{|2q_fB|}\right)^{\epsilon}\left[\left(\frac{2(q_fB)^2}{3} + m_f^4\right)\left(\frac{1}{\epsilon}+1\right) - 8(q_fB)^2\zeta^{(1,0)}(-1,x_f) - 2|q_fB|m_f^2\ln x_f - 2K_0^B(\beta m_f)|q_fB|T^2 + \mathcal{O}(\epsilon)\right], \tag{B10}$$

$$\sum\!\!\!\!\!\!\int_P \frac{1}{(P_0^2 + p^2 + m^2)} = -\frac{1}{(4\pi)^2}\left(\frac{\Lambda^2}{m^2}\right)^{\epsilon}\left[\left(\frac{1}{\epsilon}+1\right)m^2 - J_1(\beta m)T^2 + \mathcal{O}(\epsilon)\right], \tag{B11}$$

$$\sum\!\!\!\!\!\!\int_P^B \frac{1}{(P_0^2 + p_z^2 + M_B^2)} = -\frac{1}{(4\pi)^2}\left(\frac{\Lambda^2}{|2qB|}\right)^{\epsilon}\left[\frac{1}{\epsilon}m^2 - 2\zeta^{(1,0)}\left(0,\frac{1}{2}+x\right)|qB| - J_1^B(\beta m)|qB| + \mathcal{O}(\epsilon)\right], \tag{B12}$$

$$\sum\!\!\!\!\!\!\int_{\{P\}} \frac{1}{(P_0^2 + p_z^2 + m_f^2)} = -\frac{1}{(4\pi)^2}\left(\frac{\Lambda^2}{m_f^2}\right)^{\epsilon}\left[\left(\frac{1}{\epsilon}+1\right)m_f^2 + K_1(\beta m_f)T^2 + \mathcal{O}(\epsilon)\right], \tag{B13}$$

$$\sum\!\!\!\!\!\!\int_{\{P\}}^B \frac{1}{(P_0^2 + p_z^2 + M_B^2)} = -\frac{1}{(4\pi)^2}\left(\frac{\Lambda^2}{|2q_fB|}\right)^{\epsilon}\left[\frac{1}{\epsilon}m_f^2 - 2\zeta^{(1,0)}(0,x_f)|q_fB| + K_1^B(\beta m_f)|q_fB| + \mathcal{O}(\epsilon)\right], \tag{B14}$$

where $x = m^2/2|qB|$, $x_f = m_f^2/2|q_fB|$. The bosonic and fermionic masses are $M_B = \sqrt{m^2 + |qB|(2k+1)}$ and $M_B = \sqrt{m_f^2 + |q_fB|(2k+1-s)}$, respectively. The generalized ζ function is defined by $\zeta(s,q) = \sum_{k=0}^{\infty}(q+k)^{-s}$. The thermal functions $J_n(\beta M)$, $J_n^B(\beta M)$, $K_n(\beta m_f)$, and $K_n^B(\beta m_f)$ are defined by

$$J_n(\beta m) = \frac{4e^{\gamma_E\epsilon}\Gamma(\frac{1}{2})}{\Gamma(\frac{5}{2}-n-\epsilon)}\beta^{4-2n}m^{2\epsilon}\int_0^{\infty}\frac{p^{4-2n-2\epsilon}dp}{\sqrt{p^2+m^2}}\frac{1}{e^{\beta\sqrt{p^2+m^2}}-1}, \tag{B15}$$

$$J_n^B(\beta m) = \frac{8e^{\gamma_E\epsilon}\Gamma(\frac{1}{2})}{\Gamma(\frac{3}{2}-n-\epsilon)}\beta^{2-2n}(|2qB|)^{\epsilon}\sum_{k=0}^{\infty}\int_0^{\infty}\frac{p_z^{2-2n-2\epsilon}dp_z}{\sqrt{p_z^2+M_B^2}}\frac{1}{e^{\beta\sqrt{p_z^2+M_B^2}}-1}, \tag{B16}$$

$$K_n(\beta m_f) = \frac{4e^{\gamma_E\epsilon}\Gamma(\frac{1}{2})}{\Gamma(\frac{5}{2}-n-\epsilon)}\beta^{4-2n}m_f^{2\epsilon}\int_0^\infty \frac{p^{4-2n-2\epsilon}dp}{\sqrt{p^2+m_f^2}}\frac{1}{e^{\beta\sqrt{p^2+m_f^2}}+1}, \tag{B17}$$

$$K_n^B(\beta m_f) = \frac{4e^{\gamma_E\epsilon}\Gamma(\frac{1}{2})}{\Gamma(\frac{3}{2}-n-\epsilon)}\beta^{2-2n}(|2q_fB|)^\epsilon\sum_{s=\pm1}\sum_{k=0}^\infty\int_0^\infty \frac{p_z^{2-2n-2\epsilon}dp_z}{\sqrt{p_z^2+M_B^2}}\frac{1}{e^{\beta\sqrt{p_z^2+M_B^2}}+1}. \tag{B18}$$

The sum over Matsubara frequencies is

$$T\sum_{P_0}\ln[P_0^2+\omega^2] = \omega + 2T\ln[1\pm e^{-\beta\omega}], \tag{B19}$$

where the upper sign is for fermions and the lower signs is for bosons.

APPENDIX C: SMALL AND LARGE-B EXPANSIONS

In this Appendix we list a number of small- and large-B expansions of various ζ functions. The small-x expansions of the various derivatives of the Hurwitz ζ functions are

$$\zeta^{(1,0)}(-1,x) = \zeta'(-1)+\tfrac{1}{2}x-\tfrac{1}{2}\ln(2\pi)x - x\ln x + \mathcal{O}(x^2), \tag{C1}$$

$$\zeta^{(1,0)}(-1,\tfrac{1}{2}+x) = -\tfrac{1}{2}\zeta'(-1)-\tfrac{1}{24}\ln 2-\tfrac{1}{2}x\ln 2 + \mathcal{O}(x^2), \tag{C2}$$

$$\zeta^{(1,0)}(0,x) = -\tfrac{1}{2}\ln(2\pi)-\ln x-\gamma_E x+\mathcal{O}(x^2), \tag{C3}$$

$$\zeta^{(1,0)}(0,\tfrac{1}{2}+x) = -\tfrac{1}{2}\ln 2-2x\ln 2-\gamma_E x+\mathcal{O}(x^2), \tag{C4}$$

where $\zeta'(-1) = 1/12-\ln(A)\approx -0.165\,421$ and A is the Glaisher-Kinkelin constant. The large-x expansion of the various derivatives of the Hurwitz ζ functions are

$$\zeta^{(1,0)}(-1,x) = -\frac{1}{4}x^2+\frac{1}{2}x^2\ln x-\frac{1}{2}x\ln x+\frac{1}{12}\ln x + \frac{1}{12}+\mathcal{O}\left(\frac{1}{x^2}\right), \tag{C5}$$

$$\zeta^{(1,0)}\left(-1,\frac{1}{2}+x\right) = -\frac{1}{4}x^2+\frac{1}{2}x^2\ln x-\frac{1}{24}\ln x - \frac{1}{24}+\mathcal{O}\left(\frac{1}{x^2}\right), \tag{C6}$$

$$\zeta^{(1,0)}(0,x) = x\ln x - x-\frac{1}{2}\ln x+\frac{1}{12x}+\mathcal{O}\left(\frac{1}{x^3}\right), \tag{C7}$$

$$\zeta^{(1,0)}\left(0,\frac{1}{2}+x\right) = x\ln x - x-\frac{1}{24x}+\mathcal{O}\left(\frac{1}{x^3}\right). \tag{C8}$$

APPENDIX D: PROPAGATORS IN A MAGNETIC BACKGROUND

In this Appendix, we briefly discuss the boson propagator in a constant magnetic background. Denoting the bosonic propagator in coordinate space by $\Delta(x,x')$, it satisfies the equation

$$[D_\mu D^\mu + m^2]\Delta(x,x') = \delta^4(x-x'), \tag{D1}$$

where $D_\mu = \partial_\mu + iqA_\mu^{\rm EM}$ is the covariant derivative. In the Landau gauge, we have $A_\mu^{\rm EM} = (0,0,-Bx,0)$. We next introduce the propagator $\Delta(p^0,p^3,\mathbf{x}_\perp,\mathbf{x}'_\perp)$ via the Fourier transform

$$\Delta(x,x') = \int\frac{dp^0dp^3}{(2\pi)^2}e^{-ip^0(x^0-x'^0)+ip^3(x^3-x'^3)}\Delta(p^0,p^3,\mathbf{x}_\perp,\mathbf{x}'_\perp), \tag{D2}$$

where $\mathbf{x}_\perp = (x^1,x^2)$ and $\mathbf{x}_\perp = (x'^1,x'^2)$. Inserting Eq. (D2) into Eq. (D1), we find

$$\left[-p_\parallel^2-\partial_{x^1}^2-\left(\frac{\partial}{\partial x^2}-iqBx\right)^2+m^2\right]\Delta(p^0,p^3,\mathbf{x}_\perp,\mathbf{x}'_\perp) = \delta^2(\mathbf{x}_\perp-\mathbf{x}'_\perp), \tag{D3}$$

where $p_\parallel = (p^0,p^3)$. We next need a complete set of eigenfunctions of the operator $\partial_{x^1}^2+(\partial/\partial x^2-iqBx)^2$, which are the well-known solutions involving the Hermite polynomials $H_k(x)$. The normalized wave functions are

$$\psi_{k,p^2}(\mathbf{x}_\perp) = \frac{1}{\sqrt{2\pi l}}\frac{1}{\sqrt{2^k k!\sqrt{\pi}}}H_k\left(\frac{x^1}{l}+p^2l\right)\times e^{-1/2l^2(x^1+p^2l^2)^2}e^{-is_\perp x^2p^2}, \tag{D4}$$

where $s_\perp = \mathrm{sign}(qB)$ and $l^2 = 1/|qB|$. These functions satisfy the usual orthonormality and completeness relations:

$$\int d^2x_\perp\psi^*_{k,p^2}(\mathbf{x}_\perp)\psi_{k',p'^2}(\mathbf{x}_\perp) = \delta_{kk'}\delta(p^2-p'^2), \tag{D5}$$

$$\int_{-\infty}^\infty dp^2\sum_{k=0}^\infty\psi_{k,p^2}(\mathbf{x}_\perp)\psi^*_{k,p^2}(\mathbf{x}'_\perp) = \delta^2(\mathbf{x}_\perp-\mathbf{x}'_\perp). \tag{D6}$$

Using the completeness relation (D6), the propagator can be written as

$$\Delta(p^0,p^3,\mathbf{x}_\perp,\mathbf{x}'_\perp)=\int_{-\infty}^{\infty}dp_2\sum_{k=0}^{\infty}[-p_\parallel^2+m^2+|qB|(2k+1)]^{-1}\times\psi_{k,p^2}(\mathbf{x}_\perp)\psi^*_{k,p^2}(\mathbf{x}'_\perp), \tag{D7}$$

which after some algebra can be written as

$$\begin{aligned}\Delta(p_0,p_3,\mathbf{x}_\perp,\mathbf{x}'_\perp)&=\frac{1}{2\pi l}\int_{-\infty}^{\infty}dp_2\sum_{k=0}^{\infty}[-p_\parallel^2+m^2+|qB|(2k+1)]^{-1}\frac{1}{2^k k!\sqrt{\pi}}\\&\times H_k\left(\frac{x^1}{l}+p^2 l\right)H_k\left(\frac{x'^1}{l}+p^2 l\right)\\&\times e^{-[p^2 l+(x^1+x'^1)/2l+is_\perp(x^2-x'^2)/2l]^2}e^{-(1/4l^2)(x^2-x'^2)^2}\\&\times e^{-(1/4l^2)(x^1-x'^1)^2}e^{(is_\perp/2l^2)(x^1+x'^1)(x^2-x'^2)}.\end{aligned} \tag{D8}$$

We next need the following integral:

$$\int_{-\infty}^{\infty}dx e^{-x^2}H_k(x+z)H_k(x+w)=2^k k!\sqrt{\pi}L_k(-2zw), \tag{D9}$$

where $L_k(x)$ is a Laguerre polynomial of order k. In Eq. (D8), we make the substitution $p'^2=p^2+(x^1+x'^1)/2l^2+is_\perp(x^2-x'^2)/2l^2$ and so we identify $z=(x^1-x'^1)/2l-is_\perp(x^2-x'^2)/2l$ and $w=-(x^1-x'^1)/2l-is_\perp(x^2-x'^2)/2l$. This implies that $-2zw=(\mathbf{x}_\perp-\mathbf{x}'_\perp)^2/2l^2$ and we can write

$$\begin{aligned}\Delta(p^0,p^3,\mathbf{x}_\perp,\mathbf{x}'_\perp)&=\frac{1}{2\pi l^2}\sum_{k=0}^{\infty}[-p_\parallel^2+m^2+|qB|(2k+1)]^{-1}e^{-(1/4l^2)(\mathbf{x}_\perp-\mathbf{x}'_\perp)^2}\\&\times L_k\left(\frac{(\mathbf{x}_\perp-\mathbf{x}'_\perp)^2}{2l^2}\right)e^{is_\perp\Phi(\mathbf{x}_\perp,\mathbf{x}'_\perp)},\end{aligned} \tag{D10}$$

where the so-called Schwinger phase is

$$\Phi(\mathbf{x}_\perp,\mathbf{x}'_\perp)=\frac{(x^1+x'^1)(x^2-x'^2)}{2l^2}. \tag{D11}$$

The propagator in Eq. (D10) is now a product of a translationally invariant part and the Schwinger phase. The Fourier transform $\Delta(p_\parallel,p_\perp)$ of the translationally invariant part is

$$\Delta(p_\parallel,p_\perp)=-2e^{-p_\perp^2 l^2}\sum_{k=0}^{\infty}\frac{(-1)^k}{p_\parallel^2-m^2-|qB|(2k+1)}L_k(2p_\perp^2 l^2). \tag{D12}$$

The term $p_\parallel^2-m^2-|qB|(2k+1)$ is rewritten using Schwinger's trick

$$\frac{i}{p_\parallel^2-m^2-|qB|(2k+1)}=\int_0^{\infty}ds e^{is[p_\parallel^2-m^2-|qB|(2k+1)]}. \tag{D13}$$

Using the summation formula for the generalized Laguerre polynomials $L_n^\alpha(x)$

$$\sum_{k=0}^{\infty}L_k^\alpha(x)z^k=(1-z)^{-(\alpha+1)}e^{xz/(z-1)}, \tag{D14}$$

the translationally invariant propagator can be written as

$$\Delta(p_\parallel,p_\perp)=i\int_0^{\infty}\frac{ds}{\cos(|qB|s)}\times\exp\left\{is[p_\parallel^2-m^2]-ip_\perp^2\frac{\tan(|qB|s)}{|qB|}\right\}. \tag{D15}$$

Finally, the propagator $\Delta(x,x')$ takes the form

$$\Delta(x,x')=e^{is_\perp\Phi(\mathbf{x}_\perp,\mathbf{x}'_\perp)}\int\frac{d^4p}{(2\pi)^4}e^{-ip(x-x')}\Delta(p_\parallel,p_\perp). \tag{D16}$$

REFERENCES

Agasian, N. O., and S. M. Fedorov, 2008, Phys. Lett. B **663**, 445.
Agasian, N. O., and I. A. Shushpanov, 2000, Phys. Lett. B **472**, 143.
Agasian, N. O., and I. A. Shushpanov, **2001**, J. High Energy Phys. 10, 006.
Alford, M., J. Berges, and K. Rajagopal, 2000, Nucl. Phys. **B571**, 269.
Alford, M. G., A. Schmitt, and K. Rajagopal, 2008, Rev. Mod. Phys. **80**, 1455.
Ambjørn, J., and P. Olesen, 1989a, Nucl. Phys. **B315**, 606.
Ambjørn, J., and P. Olesen, 1989b, Phys. Lett. B **218**, 67.
Andersen, J. O., 2012a, Phys. Rev. D **86**, 025020.
Andersen, J. O., **2012**b, J. High Energy Phys. 10, 005.
Andersen, J. O., W. R. Naylor, and A. Tranberg, 2014, J. High Energy Phys. 04, 187.
Andersen, J. O., W. R. Naylor, and A. Tranberg, 2015, J. High Energy Phys. 02, 042.
Andersen, J. O., and A. Tranberg, 2012, J. High Energy Phys. 08, 002.
Ayala, A., M. Loewe, A. J. Mizher, and R. Zamora, 2014, Phys. Rev. D **90**, 036001.
Ayala, A., M. Loewe, and R. Zamora, 2015, Phys. Rev. D **91**, 016002.
Bali, G. S., F. Bruckmann, M. Constantinou, M. Costa, G. Endrődi, Z. Fodor, S. D. Katz, S. Krieg, H. Panagopoulos, and A. Schaefer, 2012a, *Proc. Sci.*, Confinement 197.
Bali, G. S., F. Bruckmann, M. Constantinou, M. Costa, G. Endrődi, S. D. Katz, H. Panagopoulos, and A. Schaefer, 2012b, Phys. Rev. D **86**, 094512.
Bali, G. S., F. Bruckmann, G. Endrődi, Z. Fodor, S. D. Katz, S. Krieg, A. Schafer, and K. K. Szabo, **2012**c, J. High Energy Phys. 02, 44.
Bali, G. S., F. Bruckmann, G. Endrődi, Z. Fodor, S. D. Katz, and A. Schafer, 2012d, Phys. Rev. D **86**, 071502(R).
Banks, T., and A. Casher, 1980, Nucl. Phys. **B169**, 103.
Baym, G., D. Bödeker, and L. D. McLerran, 1996, Phys. Rev. D **53**, 662.
Bochkarev, A., and J. I. Kapusta, 1996, Phys. Rev. D **54**, 4066.
Boomsma, J. K., and D. Boer, 2009, Phys. Rev. D **80**, 034019.
Boomsma, J. K., and D. Boer, 2010, Phys. Rev. D **81**, 074005.
Bornyakov, V. G., P. V. Buividovich, N. Cundy, O. A. Kochetkov, and A. Schafer, 2014, Phys. Rev. D **90**, 034501.
Borsanyi, S., G. Endrődi, Z. Fodor, A. Jakovac, S. Krieg, C. Ratti, and K. K. Szabo, **2010**, J. High Energy Phys. 11, 077.
Bowman, E. S., and J. I. Kapusta, 2009, Phys. Rev. C **79**, 015202.

Braguta, V. V., P. V. Buividovich, T. Kalaydzhyan, S. V. Kuznetsov, and M. I. Polikarpov, 2012, Phys. At. Nucl. **75**, 488.

Braun, J., W. A. Mian, and S. Rechenberger, 2014, arXiv:1412.6025.

Brauner, T., 2010, Symmetry **2**, 609.

Brauner, T., K. Fukushima, and Y. Hidaka, 2009, Phys. Rev. D **80**, 074035.

Bruckmann, F., G. Endrődi, and T. G. Kovacs, **2013**, J. High Energy Phys. 04, 112.

Buballa, M., 2005, Phys. Rep. **407**, 205.

Buividovich, P. V., M. N. Chernodub, E. V. Luschevskaya, and M. I. Polikarpov, 2010a, Phys. Lett. B **682**, 484.

Buividovich, P. V., M. N. Chernodub, E. V. Luschevskaya, and M. I. Polikarpov, 2010b, Nucl. Phys. **B826**, 313.

Bzdak, A., and V. Skokov, 2012, Phys. Lett. B **710**, 171.

Callebaut, N., D. Dudal, and H. Verschelde, **2013**, J. High Energy Phys. 03, 033.

Chakrabarty, S., 1996, Phys. Rev. D **54**, 1306.

Chao, J., P. Chu, and M. Huang, 2013, Phys. Rev. D **88**, 054009.

Chernodub, M., 2010, Phys. Rev. D **82**, 085011.

Chernodub, M., 2011, Phys. Rev. Lett. **106**, 142003.

Chernodub, M., 2014, Phys. Rev. D **89**, 018501.

Chodos, A., R. L. Jaffe, K. Johnson, and C. B. Thorn, 1974, Phys. Rev. D **10**, 2599.

Cohen, T. D., D. A. McGady, and E. S. Werbos, 2007, Phys. Rev. C **76**, 055201.

Coleman, S., 1973, Commun. Math. Phys. **31**, 259.

Cruz, A. A., and J. O. Andersen, 2013, Phys. Rev. D **88**, 025016.

D'Elia, M., S. Mukherjee, and F. Sanfilippo, 2010, Phys. Rev. D **82**, 051501.

D'Elia, M., and F. Negro, 2011, Phys. Rev. D **83**, 114028.

De Simone, A., G. Nardini, M. Quiros, and A. Riotto, **2011**, J. Cosmol. Astropart. Phys. 10, 030.

Duncan, R. C., and C. Thompson, 1992, Astrophys. J. **392**, L9.

Ebert, D. B., and K. G. Klimenko, 1999, Phys. Rev. D **61**, 025005.

Eguchi, T., 1976, Phys. Rev. D **14**, 2755.

Einhorn, M. B., and D. R. T. Jones, **2007**, J. High Energy Phys. 04, 051.

Endrődi, G., 2013, J. High Energy Phys. 04, 23.

Endrődi, G., 2015, J. High Energy Phys. 07, 173.

Farias, R. L. S., K. P. Gomes, G. I. Krein, and M. B. Pinto, 2014, Phys. Rev. C **90**, 025203.

Fayazbakhsh, S., and N. Sadooghi, 2013, Phys. Rev. D **88**, 065030.

Fayazbakhsh, S., and N. Sadooghi, 2014, Phys. Rev. D **90**, 105030.

Ferreira, M., P. Costa, O. Lourenco, T. Frederico, and C. Providência, 2014, Phys. Rev. D **89**, 116011.

Ferreira, M., P. Costa, D. P. Menezes, C. Providência, and N. Scoccola, 2014, Phys. Rev. D **89**, 016002.

Ferreira, M., P. Costa, and C. Providência, 2014, Phys. Rev. D **90**, 016012.

Ferrer, E. J., and V. de la Incera, 2007, Phys. Rev. D **76**, 045011.

Ferrer, E. J., V. de la Incera, and C. Manuel, 2005, Phys. Rev. Lett. **95**, 152002.

Ferrer, E. J., V. de la Incera, and C. Manuel, 2006, Nucl. Phys. **B747**, 88.

Ferrer, E. J., V. de la Incera, and X. J. Wen, 2015, Phys. Rev. D **91**, 054006.

Ferrer, I., V. de la Incera, I. Portillo, and M. Quiroz, 2014, Phys. Rev. D **89**, 085034.

Fischer, C. S., A. Maas, and J. M. Pawlowski, 2009, Ann. Phys. (Amsterdam) **324**, 2408.

Ford, C., D. R. T. Jones, P. W. Stephenson, and M. B. Einhorn, 1993, Nucl. Phys. **395**, 17.

Fraga, E. S., B. W. Mintz, and J. Schaffner-Bielich, 2014, Phys. Lett. B **731**, 154.

Fraga, E. S., and Mizher, 2008, Phys. Rev. D **78**, 025016.

Fraga, E. S., J. Noronha, and L. Palhares, 2013, Phys. Rev. D **87**, 114014.

Fraga, E. S., and L. F. Palhares, 2012, Phys. Rev. D **86**, 016008.

Fukushima, K., 2004, Phys. Lett. B **591**, 277.

Fukushima, K., 2008, Phys. Rev. D **77**, 114028.

Fukushima, K., and T. Hatsuda, 2011, Rep. Prog. Phys. **74**, 014001.

Fukushima, K., and Y. Hidaka, 2013, Phys. Rev. Lett. **110**, 031601.

Fukushima, K., and J. M. Pawlowski, 2012, Phys. Rev. D **86**, 076013.

Fukushima, K., and H. J. Warringa, 2008, Phys. Rev. Lett. **100**, 032007.

Gasser, J., and H. Leutwyler, 1984, Ann. Phys. (N.Y.) **158**, 142.

Gasser, J., and H. Leutwyler, 1985, Nucl. Phys. **B250**, 465.

Gatto, R., and M. Ruggieri, 2010, Phys. Rev. D **82**, 054027.

Gatto, R., and M. Ruggieri, 2011, Phys. Rev. D **83**, 034016.

Gerber, P., and H. Leutwyler, 1989, Nucl. Phys. **B321**, 387.

Giovannini, M., and M. E. Shaposhnikov, 1998, Phys. Rev. D **57**, 199.

Gusynin, V. P., V. A. Miransky, and I. A. Shovkovy, 1994, Phys. Rev. Lett. **73**, 3499.

Gusynin, V. P., V. A. Miransky, and I. A. Shovkovy, 1995a, Phys. Rev. D **52**, 4718.

Gusynin, V. P., V. A. Miransky, and I. A. Shovkovy, 1995b, Phys. Lett. B **349**, 477.

Gusynin, V. P., V. A. Miransky, and I. A. Shovkovy, 1995c, Phys. Rev. D **52**, 4747.

Gusynin, V. P., V. A. Miransky, and I. A. Shovkovy, 1996, Nucl. Phys. **B462**, 249.

Gusynin, V. P., V. A. Miransky, and I. A. Shovkovy, 1997, Phys. Rev. D **56**, 5251.

Gusynin, V. P., V. A. Miransky, and I. A. Shovkovy, 1999, Phys. Rev. Lett. **83**, 1291.

Haas, L. M., R. Stiele, J. Braun, J. M. Pawlowski, and J. Schaffner-Bielich, 2013, Phys. Rev. D **87**, 076004.

Haber, A., F. Preis, and A. Schmitt, 2014, Phys. Rev. D **90**, 125036.

Hell, T., S. Roessner, M. Christoforetti, and W. Weise, 2009, Phys. Rev. D **79**, 014022.

Herbst, T. K., M. Mitter, J. M. Pawlowski, B.-J. Schaefer, and R. Stiele, 2014, Phys. Lett. B **731**, 248.

Herbst, T. K., J. M. Pawlowski, and B.-J. Schaefer, 2011, Phys. Lett. B **696**, 58.

Hidaka, Y., and A. Yamamoto, 2013, Phys. Rev. D **87**, 094502.

Hsu, S., and M. Schwetz, 2000, Nucl. Phys. **572**, 211.

Huber, M., and L. von Smekal, **2013**, J. High Energy Phys. 04, 149.

Huovinen, P., and P. Petreczky, 2010, Nucl. Phys. **A837**, 26.

Ilgenfritz, E.-M., M. Kalinowski, M. Muller-Preussker, B. Petersson, and A. Schreiber, 2012, Phys. Rev. D **85**, 114504.

Ilgenfritz, E.-M., B. Muller-Preussker, M. Petersson, and A. Schreiber, 2014, Phys. Rev. D **89**, 054512.

Inagaki, T., D. Kimura, and T. Murata, 2004, Prog. Theor. Phys. **111**, 371.

Johnson, K., 1975, Acta Phys. Pol. B **6**, 865 [http://www.actaphys.uj.edu.pl/].

Kajantie, K., M. Laine, J. Peisa, K. Rummukainen, and M. Shaposhnikov, 1999, Nucl. Phys. **B544**, 357.

Kajantie, K., M. Laine, K. Rummukainen, and M. Shaposhnikov, 1996, Phys. Rev. Lett. **77**, 2887.

Kajantie, K., M. Laine, K. Rummukainen, and M. Shaposhnikov, 1997, Nucl. Phys. **B493**, 413.

Kamikado, K., and T. Kanazawa, **2014**, J. High Energy Phys. 03, 009.
Kamikado, K., and T. Kanazawa, 2015a (private communication).
Kamikado, K., and T. Kanazawa, 2015b, J. High Energy Phys. 01, 129.
Kamikado, K., N. Strodthoff, L. von Smekal, and J. Wambach, 2013, Phys. Lett. B **718**, 1044.
Karsch, F., E. Laermann, and A. Peikert, 2001, Nucl. Phys. **B605**, 579.
Karsch, F., K. Redlich, and A. Tawfik, 2003, Eur. Phys. J. C **29**, 549.
Kharzeev, D. E., 2015, Annu. Rev. Nucl. Part. Sci. **65**, 193.
Kharzeev, D. E., L. D. McLerran, and H. J. Warringa, 2008, Nucl. Phys. **A803**, 227.
Klevansky, S. P., 1992, Rev. Mod. Phys. **64**, 649.
Klevansky, S. P., and R. H. Lemmer, 1989, Phys. Rev. D **39**, 3478.
Klimenko, K. G., 1991, Theor. Math. Phys. **89**, 1161.
Klimenko, K. G., 1992a, Z. Phys. C **54**, 323.
Klimenko, K. G., 1992b, Theor. Math. Phys. **90**, 1.
Klimenko, K. G., and V. C. Zhukovsky, 2008, Phys. Lett. B **665**, 352.
Kojo, T., and N. Su, 2013, Phys. Lett. B **720**, 192.
Kondo, K. I., 2010, Phys. Rev. D **82**, 065024;
Leinweiber, D. B., J. I. Skullerud, A. G. Williams, and C. Parrinello, 1999, Phys. Rev. D **60**, 094507; **61**, 079901(E) (2000).
Litim, D., 2001, Phys. Rev. D **64**, 105007.
Loewe, M., and C. Villavicencio, 2003, Phys. Rev. D **67**, 074034.
Lourenco, O., M. Dutra, A. Delfino, and M. Malheiro, 2011, Phys. Rev. D **84**, 125034.
Menezes, D. P., M. B. Pinto, S. S. Avancini, A. P. Martinez, and C. Providência, 2009, Phys. Rev. C **79**, 035807.
Miransky, V. A., and I. A. Shovkovy, 2002, Phys. Rev. D **66**, 045006.
Miransky, V. A., and I. A. Shovkovy, 2015, Phys. Rep. **576**, 1.
Mizher, A. J., M. N. Chernodub, and E. S. Fraga, 2010, Phys. Rev. D **82**, 105016.
Morris, T. R., 1994, Phys. Lett. B **329**, 241.
Mueller, N., J. Bonnet, and C. S. Fischer, 2014, Phys. Rev. D **89**, 094023.
Mueller, N., and J. M. Pawlowski, 2015, Phys. Rev. D **91**, 116010.
Nambu, Y., and G. Jona-Lasinio, 1961a, Phys. Rev. **122**, 345.
Nambu, Y., and G. Jona-Lasinio, 1961b, Phys. Rev. **124**, 246.
Nielsen, H. B., and S. Chadha, 1976, Nucl. Phys. **B105**, 445.
Nielsen, N. K., and P. Olesen, 1978, Nucl. Phys. **B144**, 376.
Noronha, J. L., and I. A. Shovkovy, 2007, Phys. Rev. D **76**, 105030.
Noronha, J. L., and I. A. Shovkovy, 2012, Phys. Rev. D **86**, 049901.
Orlovsky, V. D., and Y. A. Simonov, 2014, Phys. Rev. D **89**, 054012.
Ozaki, S., 2014, Phys. Rev. D **89**, 054022.
Pisarski, R. D., and F. Wilczek, 1984, Phys. Rev. D **29**, 338.
Rajagopal, K., and F. Wilczek, 2001, *At the frontier of particle physics*, Vol. 3 (World Scientific, Singapore), p 2061.
Ratti, C., S. Roessner, M. A. Thaler, and W. Weise, 2007, Eur. Phys. J. C **49**, 213.
Ratti, C., M. A. Thaler, and W. Weise, 2006, Phys. Rev. D **73**, 014019.
Ritus, V. I., 1978, Sov. Phys. JETP **48**, 788 [Zh. Eksp. Teor. Fiz. **75**, 1560 (1978)].
Roessner, S., C. Ratti, and W. Weise, 2007, Phys. Rev. D **75**, 034007.
Ruggieri, M., M. Tachibana, and V. Greco, **2013**, J. High Energy Phys. 07, 165.
Rummukainen, K., M. Tsypin, M. Laine, and M. Shaposhnikov, 1998, Nucl. Phys. **B532**, 283.
Sasaki, C., B. Friman, and K. Redlich, 2007, Phys. Rev. D **75**, 074013.
Scavenius, O., A. Mocsy, I. N. Mishustin, and D. H. Rischke, 2001, Phys. Rev. C **64**, 045202.
Schaefer, B.-J., J. M. Pawlowski, and J. Wambach, 2007, Phys. Rev. D **76**, 074023.
Schaefer, B.-J., M. Wagner, and J. Wambach, 2010, Phys. Rev. D **81**, 074013.
Schwinger, J., 1951, Phys. Rev. **82**, 664.
Sher, M., 1989, Phys. Rep. **179**, 273.
Shovkovy, I., 2013, Lect. Notes Phys. **871**, 13.
Shushpanov, I. A., and A. V. Smilga, 1997, Phys. Lett. B **402**, 351.
Skokov, V., 2012, Phys. Rev. D **85**, 034026.
Skokov, V., B. Friman, E. Nakano, K. Redlich, and B.-J. Schaefer, 2010, Phys. Rev. D **82**, 034029.
Skokov, V., A. Y. Illarionov, and V. Toneev, 2009, Int. J. Mod. Phys. A **24**, 5925.
Son, D. T., and M. A. Stephanov, 2001, Phys. Rev. Lett. **86**, 592.
Stephanov, M. A., 2006, *Proc. Sci.*, LAT2006 024.
Stokic, B., B. Friman, and K. Redlich, 2010, Eur. Phys. J. C **67**, 425.
Strickland, M., V. Dexheimer, and D. P. Menenez, 2012, Phys. Rev. D **86**, 125032.
Tawfik, A. N., and N. Magdy, 2014, Phys. Rev. C **90**, 015204.
't Hooft, G., 1976, Phys. Rev. D **14**, 3432.
Watanabe, H., and H. Murayama, 2014, Phys. Rev. X **4**, 031057.
Watson, P., and H. Reinhardt, 2014, Phys. Rev. D **89**, 045008.
Weinberg, S., 1979, Physica (Amsterdam) **96A**, 327.
Werbos, E., 2008, Phys. Rev. C **77**, 065202.
Wetterich, C., 1993, Phys. Lett. B **301**, 90.
Yaffe, L. G., and B. Svetitsky, 1982a, Phys. Rev. D **26**, 963.
Yaffe, L. G., and B. Svetitsky, 1982b, Nucl. Phys. **B210**, 423.
Yu, L., H. Liu, and M. Huang, 2014, Phys. Rev. D **90**, 074009.
Yu, L., J. Van Doorsselaere, and M. Huang, 2015, Phys. Rev. D **91**, 074011.
Zhang, T., T. Brauner, and D. H. Rischke, **2010**, J. High Energy Phys. 06, 064.